CONSTRUCTION AND CALIBRATION OF GASEOUS DETECTORS AT KAHVELAB AND CERN ATLAS EXPERIMENT

by

Saime Gürbüz

B.S., Physics, Boğaziçi University, 2009

B.S., Mathematics, Boğaziçi University, 2009

M.S., Physics, Boğaziçi University, 2012

Submitted to the Institute for Graduate Studies in
Science and Engineering in partial fulfillment of
the requirements for the degree of
Master of Science

Graduate Program in Physics
Boğaziçi University
2020

ACKNOWLEDGEMENTS

First of all, I would like to express my great appreciation to my thesis supervisor. He not only helped me to maintain and finish my studies, but also with his friendly, understanding and tolerant manner, provided me moral support. From him, I learned how to be a good experimental physicist. Many thanks to everyone in the KAHVELab and at CERN, who always helped me. And I owe much to my professors at Boğaziçi University during my PhD courses. Great thanks to *Mustafa*, who supported me for all of my life, especially, while writing my thesis. I wish his support and his love will always be with me. I also appreciate my family who supported me at every stage of my life. Thank you for believing in me.

This thesis is dedicated to my beloved husband,

Mustafa Gürbüz

who made my dreams possible!

ABSTRACT

CONSTRUCTION AND CALIBRATION OF GASEOUS DETECTORS AT KAHVELAB AND CERN ATLAS EXPERIMENT

Gaseous detectors detect particles that interact electromagnetically. With different geometries, they can be used for many purposes from small scale table-top experiments to high energy collider experiments. In this thesis, first the design, simulation and construction of a Delay Wire Chamber (DWC) at KAHVELab is described. Built to have the same specifications as those used at CERN beam lines, it has position resolution of 200μm and an active area of 10cm $\times$ 10cm. It has been tested with cosmic particles at KAHVELab and radioactive sources at the CERN gaseous detector laboratory, and shown to have a better gain than its counterparts at the CERN. Next, drift circle error calibration of a large collider-type gaseous detector the Transition Radiation Tracker (TRT) at ATLAS experiment is described. Drift circle errors are important for particle tracking. This calibration is performed using the pull sigma values of the drift circle error. Unlike earlier calibrations, the values are recorded in the database as a function of the mean number of the interactions per bunch. The pull sigma values approach unity as expected which validates the process. The ATLAS data and Monte Carlo comparisons are also observed to be consistent. Lastly, measurement of the $t\bar{t}V + t\bar{t}$ contamination in Z+jets control region of an ATLAS exotic analysis is presented. Z reconstruction using electrons and muons is of critical importance for many studies and make use of the data from TRT as well as the other subdetectors. The measurement is done using multivariate analysis (multilayer perceptron). The method is verified with the pseudo-data, and the measured value from the pseudo-data template fit is found to be within one sigma standard deviation of the expected value.

ÖZET

KAHVELAB VE CERN ATLAS DENEYİNDE GAZLI ALGIÇLARIN ÜRETİMİ VE KALİBRASYONU

Gazlı algıçlar elektromanyetik olarak etkileşen parçacıkları algılamak için kullanılır. Farklı geometriler ve operasyon modları ile küçük ölçekli deneylerden büyük ölçekli deneylere kadar farklı amaçlar için kullanılabilirler. Bu tezde, ilk olarak, KAHVELab'da üretilen Gecikmeli Tel Odası (GeTO)'nın tasarımı, benzetimi ve üretimi açıklanacaktır. Üretilen GeTO CERN deney hatlarında kullanılanlarla aynı özelliklere sahip. Konum çözünürlüğü 200μm ve aktif alanı 10cm $\times$ 10cm'dir. Ürettiğimiz GeTO KAHVELab'da kozmik parçacıklar ile ve CERN gazlı algıç laboratuarında radyoaktif kaynaklarla test edilmiştir. CERN'de kullanılanlardan daha iyi sonuçlar alınmıştır. Sonrasında, ATLAS deneyi Geçiş Işıması İz Sürücüsü (TRT) algıcının sürüklenme halkası hata kalibrasyonu anlatılmıştır. Sürüklenme halkası hatası vurma sınıflandırması için önemlidir. Bu kalibrasyon sürüklenme halkası hatasının pull standart sapmaları kullanılarak yapılmıştır. Öncekinden farklı olarak, kalibrasyon değerleri veri tabanına bohçanın ortalama etkileşim sayına bağlı olarak yazılmıştır. Pull standart sapma değerleri beklendiği gibi birime yaklaşmaktadır ve doğrulaması başarı ile yapılmıştır. ATLAS veri ve benzetim karşılaştırmaları doğrulama değerleri için tutarlıdır. Son olarak, ATLAS verisindeki Z+jets kontrol alanındaki $t\bar{t}V + t\bar{t}$ bulaşının ölçümü sunulacak. Bu kontrol alanları egzotik fizik çalışmaları için önemlidir. Ölçüm çoklu değişken analizi (multilayer perceptron) tekniği kullanılarak yapıldı. Bu teknik monte carlo örneklerinden oluşturulan sözde (psödo) veri ile doğrulanmıştır. Ölçülen değer beklenen değerin ve bir standart sapma aralığındadır.

TABLE OF CONTENTS

ACKNOWLEDGEMENTS iii
ABSTRACT v
ÖZET vi
LIST OF FIGURES xi
LIST OF TABLES xvi
LIST OF SYMBOLS xvii
LIST OF ACRONYMS/ABBREVIATIONS xix
1. INTRODUCTION 1
2. PHYSICS OF GASEOUS DETECTORS 3
2.1. Interaction of charged particles with matter 3
2.2. Transportation of Charged Particles in Gaseous Media 6
2.2.1. Diffusion of Electrons and Ions in Gaseous Media 7
2.2.2. Drift of Electrons and Ions in Gaseous Medium 8
2.3. Signal Creation 9
2.4. Types of Gaseous Detectors 10
2.4.1. Recombination Region 10
2.4.2. Ionization Chamber 10
2.4.3. Proportional Counter 12
2.4.4. Limited Proportionality 15
2.4.5. Geiger Muller Counter 16
2.4.6. Discharge Region 16
3. DELAY WIRE CHAMBER 17
3.1. Working Principle 17
3.2. Theoretical Calculations 20
3.3. Design 20
3.4. Simulation 23
3.5. Construction 25
3.5.1. Producing Frames 25

3.5.2. Attaching Wires 26
3.5.3. Alcohol Bath and Heat Treatment 28
3.5.4. Electronics 28
3.5.5. Placement in a Box 30
3.6. ESEM Studies of the Wires 31
3.7. Gas System 33
3.7.1. Monitoring of Gas Purity Through Humidity 35
3.8. High Voltage 36
3.9. Operation 36
4. ATLAS TRANSITION RADIATION TRACKER 40
4.1. ATLAS Detector 40
4.1.1. CERN and LHC 40
4.1.2. The ATLAS Experiment 41
4.1.3. ATLAS Detector Geometry and Track Parametrization 42
4.1.4. Inner Detector 44
4.1.5. Calorimeters 45
4.1.6. Muon Spectrometer 46
4.1.7. Magnet System 47
4.2. The TRT Detector 48
4.2.1. TRT working principle and variables. 49
4.2.2. Drift Circle Errors and Calibration 51
4.2.3. Pull distribution of TRT Drift Circle Error 54
4.3. TRT Drift Circle Error Calibration 55
4.3.1. Calibration using Pull Distributions 56
4.3.2. Drift Circle Error vs Mean Number of Interactions per Bunch Crossing 57
4.3.3. Implementation 58
4.4. Results 60
4.4.1. Change in the pull sigma values 60
4.4.2. Validation 62
5. ATLAS Z+JETS BACKGROUND CONTAMINATION MEASUREMENT US-

ING DIBOSON +X ANALYSIS FRAMEWORK 67
5.1. Object Selection 69
5.1.1. Electrons 69
5.1.2. Muons 69
5.1.3. Jets 69
5.1.4. Overlap Removal 70
5.2. Datasets and Event Selection 70
5.3. Variable distributions 75
5.4. Multivariate Analysis Techniques 76
5.5. Multi-Layer Perceptron studies 77
5.6. Pseododata studies 84
5.7. Applying Z Scale Factor 87
5.8. Combining Results 88
6. CONCLUSION 89
REFERENCES 90
APPENDIX A: DESIGN OF DWC WRITTEN IN OPENSCAD SOFTWARE 96
APPENDIX B: SIMULATION OF DWC USING GARFIELD++ SOFTWARE 99
APPENDIX C: ATLAS TRT CALIBRATION DATA SETS PACKAGES . . . 104
APPENDIX D: TMVA TRAINING CODE 105
APPENDIX E: TEMPLETE FIT USING TFRACTIONFITTER 109
APPENDIX F: DATASETS AND CUTS USED IN THE ISOSINGLET QUARK SEARCHES BACKGROUND ANALYSIS 113
F.1. Data 113
F.2. Z+Jets Background 113
F.3. SM $t\bar{t}$ and Single Top Background 114
F.4. Di-Boson Background 114
F.5. SM $t\bar{t}$ with Associated Vector Bosons Background 115
F.6. Reconstruction Cuts 115
APPENDIX G: PERMISSIONS OF THE USAGE OF FIGURES 118
G.1. CERN Resources 118
G.2. Sauli, F., Gaseous Radiation Detectors 121

G.3. Garfield++ Programming Language 126
G.4. The Trigger Chambers of the ATLAS Muon Spectrometer 127
G.5. ATLAS Transition Radiation Tracker (TRT) 134
G.6. TRT Software Twiki 141
G.7. TRT Public Results 142

LIST OF FIGURES

2.1 Energy loss of pions in Copper [1]. 4
2.2 Mean energy loss of various particles in different gaseous media [1]. 5
2.3 Stopping power vs momentum for muons in Copper [1]. 6
2.4 Density, average energy of electron-ion pairs and total energy loss of different gases [2]. 6
2.5 Electron diffusion when there is no electric or magnetic field [1]. . 7
2.6 Avalance build up around the anode wire [2]. 10
2.7 Number of ions collected vs high voltage applied for gaseous detectors [1]. 11
2.8 Proportional counter originally designed by Rutherford and Geiger. [1] 13
2.9 Photo of the first MWPC and the variables used to design a MWPC [2]. 14
2.10 Electric field of MWPC [2]. 15
3.1 Example of DWC at CERN and the placement of its anode and cathode layers [3]. 18
3.2 The readouts of the MWPC and the DWC compared [3]. 19
3.3 Signal formation in the DWC [3]. 19
3.4 The screen-shot of the code that calculates the tension limit for a DWC when only the electromagnetic constraint is considered. . . . 21
3.5 The design of the DWC drawn with the OpenSCAD software. . . 22
3.6 The model of the box of DWC with the frames drawn using the OpenSCAD software. 23
3.7 The general structure and the classes of Garfield++ [4]. 23
3.8 The geometry (Left) and electric field (Right) of DWC simulated with Garfield++. 24
3.9 Total signal obtained with Garfield++ simulations a muon of 1GeV energy moving through the DWC. 24

3.10 The template of the positions for the milling machine. 25
3.11 The design and final product of the converter PCB to be used in between cathode wires (signal) and readout connectors. 26
3.12 Photo of soldering cathode Cu/Be wires stretched with the fishing sinkers. 27
3.13 The oven and the ultrasonic alcohol bath used to treat the frames with wire. 28
3.14 The original schematics of the electronics of the DWC used at CERN [3]. 29
3.15 The design of the electronics of the DWC used at KAHVELab. . . 30
3.16 Design schematics of the AIZ-502J delay chip. 30
3.17 The DWC placed in a plastic and metal box. 31
3.18 DWC wires taped on an aliminium plate for ESEM imaging. . . . 32
3.19 The ESEM image of wires that have been subject to sparks, at 1500× magnification. The wire on the left has not been baked while the wire on the right has. 33
3.20 The ESEM image of wires before and after ultrasonic bath at 1500× magnification. The photo of the brand new wire image is placed for comparison 33
3.21 The ESEM image of wires when a force is applied (streched) or not (brand new) at 1500× magnification. 34
3.22 The ESEM image of the leftover wires that are touched with bare hands. 34
3.23 The schematics of the gas system of the DWC used at KAHVELab 35
3.24 The gas system connected to the DWC 35
3.25 The data from DHT22 obtained while testing the detector. 36
3.26 Counts vs high voltage from the cathode at the trigger treshold of 80mV. 37
3.27 Primary test with the simple electronics without the delay line and the very first signals read from the DWC: 37
3.28 DWC in the metal box and the calibration signals 38

3.29 The screen-shot of the oscilloscope for the signals of the cosmic particles. Blue and yellow: readout from either end of the detector. Green: HV applied (scaled by a factor of 1000) 38

3.30 Tests at CERN using Sr-90 and example signals observed with the oscilloscope. 39

3.31 DWC placed between two scintillators and the output signals. . . 39

4.1 Overview of the LHC and the experiments [5]. 41

4.2 A cut away computer generated image of ATLAS detector [6]. . . 42

4.3 Track parametrization in the ATLAS coordinate system [7]. 43

4.4 Schematic view of a quarter-section of the ATLAS Inner Detector showing each of the major elements with its active dimensions [8]. 45

4.5 Schematic view of ATLAS Calorimeter system [9]. 46

4.6 Schematic view of ATLAS Muon Spectrometer [10]. 47

4.7 Schematic view of ATLAS Magnet System [11] 48

4.8 Simulation of a track passing through a TRT straw and the electrons are collected by the anode [12]. 49

4.9 Example of a TRT signal and the data read [13]. 51

4.10 TRT time variables read from the straw signal [12]. 52

4.11 TRT $R(t)$ dependency for barrel and end-caps. The tracks used to populate these plots are required to have at least 6 hits in the SCT and at least 20 hits in the TRT. [14] 52

4.12 Definition of Drift Circle Error. [15] 53

4.13 Definitions of TRT hits [15]. 53

4.14 Pull distribution for the drift circle radius of a selected Ar-filled straw. 55

4.15 Pull sigma vs drift time obtained using Data 2015 (Run 276329) for Barrel and Endcap Argon straws. Drift time is divided between [0:37.5ns] with each bin 3.125ns. 56

4.16 Pull sigma vs μ for Data 2015 for Barrel and Endcap Argon straws. 57

4.17 ATLAS TRT detector gas geometry in 2015 [16]. 59

4.18 Pull Sigma vs drift time MC15. 60

4.19 Pull Sigma vs μ for MC15. 61
4.20 Pull Sigma vs drift time for Data15. 61
4.21 Pull Sigma vs μ for Data15 62
4.22 Position Residual vs Drift Time before calibration with the old μ scaling 63
4.23 Position Residual vs μ before calibration with the old μ scaling . . 63
4.24 Precision Hit fraction vs Drift Time before calibration with the old μ scaling 64
4.25 Precision hit fraction vs μ before calibration with the old μ scaling 64
4.26 Position Residual vs Drift Time after new calibration 65
4.27 Position Residual vs μ after new calibration 65
4.28 Precision Hit fraction vs Drift Time after new calibration 66
4.29 Precision hit fraction vs μ after new calibration 66
5.1 Iso-singlet quark pair decaying in the $H - Z$ channel, with the Z boson later decaying into a pair of charged leptons, and the H boson decaying into a pair of b-jets [17]. 68
5.2 Example Feynman diagrams of background processes that pass through Z+jets CR cuts in the $ZHjj$ analysis. 68
5.3 Event yields for all backgrounds after Z+jet cuts for $Z \to ee$ channel. 72
5.4 Event yields for all backgrounds after Z+jet cuts for $Z \to \mu\mu$ channel. 73
5.5 The background rejection and reciprocal of the background efficiency versus signal efficiency ("ROC curve") 77
5.6 MLP neural network layout with number of variables plus 5 hidden layers. The thichness of the line represents the weight. 78
5.7 MVA input variables for Z+jet + diboson and $t\bar{t}V + t\bar{t}$ background for $Z \to ee$. Z+jet + diboson labeled as the signal (blue) and $t\bar{t}V + t\bar{t}$ labeled as the background (red). 79

5.8 MVA input variables for Z+jet + diboson and $t\bar{t}V + t\bar{t}$ background for $Z \to \mu\mu$. Z+jet + diboson labeled as the signal (blue) and $t\bar{t}V + t\bar{t}$ labeled as the background (red). 80
5.9 Correlation matrices of the variables for Z+jet + diboson and $t\bar{t}V + t\bar{t}$ backgrounds for $Z \to ee$. 80
5.10 Correlation matrices of the variables for Z+jet + diboson and $t\bar{t}V + t\bar{t}$ backgrounds for $Z \to \mu\mu$. 81
5.11 MLP Classifier Output Distributions (test and training samples superimposed). 81
5.12 MLP output distribution for the MC background samples and ATLAS data. 82
5.13 Template fit to ATLAS data using MLP response distributions for signal (Z+jet + diboson) and background ($t\bar{t}V + t\bar{t}$). 83
5.14 Template fit on pseudodata for different contamination fractions of $t\bar{t} + t\bar{t}V$ in Z+jet CR. 85
5.15 Expected vs measured $t\bar{t} + t\bar{t}V$ fraction in Z+jet CR pseudodata 86
5.16 Z+jet MLP response before and after Z scale factor. 87
5.17 Template fit after applying the Z scale factor 87
5.18 The combined plot of MLP studies before and after Z scale factor correction, obtained with the pseudodata. 88

LIST OF TABLES

3.1 The parameters of DWC [3] 21

4.1 Track parametrization in ATLAS (values taken from [7]). 43

4.2 Parameters of inner detector (values taken from [12]). 44

4.3 Parameters of calorimeter system of ATLAS (values taken from [18], [19]). 46

4.4 Parameters of muon spectrometer of ATLAS (values taken from [20], [21]). 47

4.5 Parameters of the magnet system of ATLAS (values taken from [11]). 48

4.6 TRT time variables. 54

5.1 Selection criteria for Z+jet control region (reproduced from [17]). . 71

5.2 Z+jet CR contamination calculated from the event yields of the MC simulations. 74

5.3 Number of training and testing events for TMVA (Signal: Z+jet + diboson Background: $t\bar{t}V + t\bar{t}$). 78

5.4 Pseudodata measurements 84

F.1 Electron selection criteria. 115

F.2 Muon selection criteria. 116

F.3 Jet selection criteria. 116

F.4 b-tagging selection criteria. 117

F.5 Overlap removal criteria. 117

LIST OF SYMBOLS

N	Number of the electrons
dx	Thickness of the interaction medium
$beta$	Velocity of the particle
Z	Atomic number of the medium
A	Atomic mass
ρ	Density of the medium
$C, delta$	Correction factors
E	Energy of the particle
M	Mass of the particle
ΔE	Total energy loss
W	Average energy of the electron ion pair
D	Diffusion coefficient
T	Temperature
V	Mean velocity
λ	Mean free path
P	Pressure
$w_{+/-}$	Drift velocity of ions/electrons
E	Electric field
$\mu^{+/-}$	Mobility of ions/electrons
C	Capacitance per unit length
E_0	Electric Field
l	distance between anode and cathode
s	distance between the anode wires
a	diameter of anode
T	tension
V_0	applied voltage
Tm	critical tension of the tungsten
d_0	Transverse impact parameter

q/p	Track curvature
x	Horizontal axis
y	Vertical axis
z	Axis along beam line
z_0	Longitudonal impact parameter
p_T	Transverse momentum
ΔR	distance in $\eta - \phi$ plane
θ	Polar angle
ϕ	Azimuthal angle
η	Pseudorapidity
μ	Number of interactions per bunch cross
t_{LE}	Leading edge time
t_{TE}	Trailing edge time
t_{ToT}	Time over threshold
$t_{collision}$	ATLAS collision time relative to LHC clock
t_{ToF}	Time of Flight Time
t_{SP}	Signal Propogation Time
t_0	Time Calibration Constant
Z	Z boson
H	Higgs Boson
j	Jet
$t(\bar{t})$	(anti) top quark
μ	muon
e	electron
$D(\bar{D})$	(anti) heavy quark
V	Vector Boson
p	Proton
z_{pT}	Transverse Momentum of Z boson
$\sqrt{s}$	Total Center of Mass Energy

LIST OF ACRONYMS/ABBREVIATIONS

NTP	Normal Temperature and Pressure
DWC	Delay Wire Chamber
MWPC	Multiwire Proportional Chamber
TUBITAK	TR:Türkiye Bilimsel ve Teknolojik Araştırma Kurumu
TUBITAK	EN:The Scientific and Technological Research Council of Turkey
KAHVELab	TR:Kandilli Algıç Hızlandırıcı ve Enstrümentasyon Laboratuvarı
KAHVELab	EN:Kandilli Detector Accelarator Instrumentation Laboratary
HV	High Voltage
CAD	Computer-aided design
PCB	Printed Circuit Board
2D	2 Dimansional
CERN	European Nuclear Reasearch Center
LHC	Large Hadron Collider
ATLAS	A Toroidal LHC ApparatuS
CMS	Compact Muon Solenoid
ALICE	A Large Ion Collider Experiment
LHCb	Large Hadron Collider beauty
TRT	Transition Radiation Dedector
ID	Inner Dedector
SCT	Silicon MicroStrip Dedector
MDT	Muon Drift Tube
RPC	Resistive Plate Chamber
CSC	Cathode Strip Chamber
TGC	Thin Gap Chambers
LAr	Liquid Argon Detector
MC	Monte Carlo

TR	Transition Radiation
PID	Particle Identification
LT	Low Threshold
HT	High Threshold
LE	Leading Edge
TE	Trailing Edge
ToT	Time over Threshold
ToF	Time of Flight
DBXA	Diboson +X Analysis Framework
SM	Standard Model
CR	Control Region
VLQ	Vector Like Quark
LEP0	Highest transverse momentum lepton
LEP1	Second highest transverse momentum lepton
JET0	Highest transverse momentum jet
JET1	Second highest transverse momentum jet
MET	Missing transverse energy
MLP	Multilayer perceptron
ROC	Receiver operating characteristic
TMVA	Toolkit for Multivariate Analysis
MVA	Multivariate Analysis

1. INTRODUCTION

Gaseous detectors are used in different purposes in particle physics. With varying sizes and geometries of gaseous detectors, position measurement, energy measurement or particle identification may be achieved. Thus, they are used in different scale experiments from beam line beam profile measurement to big scale experiment tracking. Even the position resolution is not as precise as the solid state detectors, they are easy to produce and inexpensive to build and maintain.

In this thesis, first the principles and some theoretical calculations of the gaseous detectors will be explained. To understand the working principle better, the interaction between the particles and the matter, for this case gases, is expressed with Bethe-Bloch formula. Then diffusion and drift of the electrons and ions are discussed. To create a signal, avalanche effect is introduced. Finally, the types of the detectors and working principles are categorized.

Delay Wire Chamber (DWC) is a wire chamber which operates with a gas mixture of CO_2 and Argon. An anode layer of 4mm apart placed 20μm diameter gold plated tungsten wires are sandwiched between two cathode layers of 2mm apart placed 100μm Copper-Beryllium wires. With such two configuration, 2D position measurement of charged particles are achieved. With the help of a delay line between the cathode wires, the readout is taken by only very few readout channels. The DWC is used at CERN beamlines for beam profile measurements and in Kandilli Detector Accelarator and Instrumentation Laboratory (KAHVELab), a DWC with the same specification is build. The active area of the DWC is 10cm $\times$ 10cm and spatial resolution of 200μm is achieved. The design, construction and tests of the detector are explained in detail.

While the DWC is used in small scale experiments, gaseous detectors are used in many big experiments such as ATLAS experiment at CERN. Transition Radiation Detector (TRT) is outermost part of the ATLAS inner detector system. While TRT

is used to contribute to the tracking, its main purpose is particle identification. By placing transition radiation material between straws of diameter 4mm, electron/pion identification is achieved. To have good tracking and particle identification, definition of the types of hits that depends on the drift circle error very important. The calibration of the drift circle circle error is done using pull distributions. It is done separately for Argon and Xenon straws. New error are defined with respect to the mean number of interactions per bunch crossing. The calibration is implemented on the ATLAS analysis software and the change in the pull sigma values approaches to unity. Validation is done for many different TRT variables for Monte Carlo (MC) events and ATLAS detector data. In this analysis, ATLAS 2016 MC and data is used.

TRT detector and many other tracking detectors, calorimeters and muon spectrometer serves a bunch of data in ATLAS detector. Many physics scenario can be studied with this data. E6 model is one of the grand unified theories proposed by Feza Gürsey and his colleagues. E6 foresees heavy isosinglet quarks which may decay in pp→ ZHjj channel in ATLAS experiment. In this study and in other exotic studies, the contamination of the $t\bar{t}$ in Z+jets control regions should be measured accurately. Using ATLAS 2015 data and MC at $\sqrt{s} = 13TeV$ with a scaled luminosity of $139fb^{-}1$, $t\bar{t}V + t\bar{t}$ contamination in Z+jets (+diboson) control region is measured. The analysis is done using multivariate analysis with Multi-Layer Perceptron (MLP) method. Many variables are studied and 12 most effective are used. The studies are also confirmed in Pseudo data made from MC samples. It is found that the expected contamination ratio is 1 sigma range of the calculated ratio.

2. PHYSICS OF GASEOUS DETECTORS

When a particle passes through a gaseous medium, it ionizes the gas. If there is an electric field the electrons and ions, created through the ionization, do not recombine and instead they drift. With a sensing medium such as a conducting plate or a wire, we can collect these electrons and ions and this creates a signal. Any particle interacting electromagnetically, like charged particles or gamma rays can be detected with this technique. To understand the basic principles of a gaseous detector, we will first dive into the ionization of the gas, in other words, the interaction of charged particles with matter. Then the transportation of charges in the gaseous medium, i.e. drift and diffusion of electrons and ions will be discussed. Later the creation of signal and the types of gaseous detectors will be covered.

2.1. Interaction of charged particles with matter

For a particle to be detected, it must interact with the material of the detector and lose some of its energy. We need to collect this energy and convert it to electric signals. For example, charged particles interact via ionization, bremsstrahlung, Cherenkov radiation etc. Photons interact via pair production, Compton effect, etc. Hadrons are detected through nuclear interactions. Neutrinos interact via weak interactions which makes them hard to detect. For the gaseous detectors, the main interaction of particles is ionization and the average energy loss via ionization is formulated by Bethe-Bloch formula.

The energy loss of particles in a medium was first formulized by Rutherford. In a semi-clasical formulation, Rutherford calculated the energy loss due to multiple Coulomb interactions (Equation 2.5 in book [2]). We can express the the probability of a unit charge to lose energy between ϵ and $\epsilon + d\epsilon$ as in Equation 2.1.

$$\frac{d^2N}{dxd\epsilon} = K\frac{Z}{A}\frac{\rho}{\beta^2}\frac{1}{\epsilon^2} \quad \text{, where} \quad K = \frac{4\pi Ne^2}{mc^2} \tag{2.1}$$

In Equation 2.1, dx is the thickness of the interaction medium and β is the velocity of the particle. e is the charge and m is the mass of the electron. Z is the atomic number, A is the atomic mass and ρ is the density of the medium.

For intermediate velocities this expression is very useful. But for high and low velocities, we need corrections for the Rutherford formulation. For a more general formulation, we use the Bethe-Bloch formulation (Equation 2.6 in book [2]) in Equation 2.2.

$$\frac{dE}{dx} = -\rho\frac{2KZ}{A\beta^2}\{\ln\frac{2mc^2\beta^2}{I(1-\beta^2)} - \beta^2 - \frac{C}{Z} - \frac{\delta}{2}\} \tag{2.2}$$

This formula shows differential energy loss and depends on β but not on mass. $\frac{C}{Z}$ is the innershell correction while $\frac{\delta}{2}$ is the density effect correction.

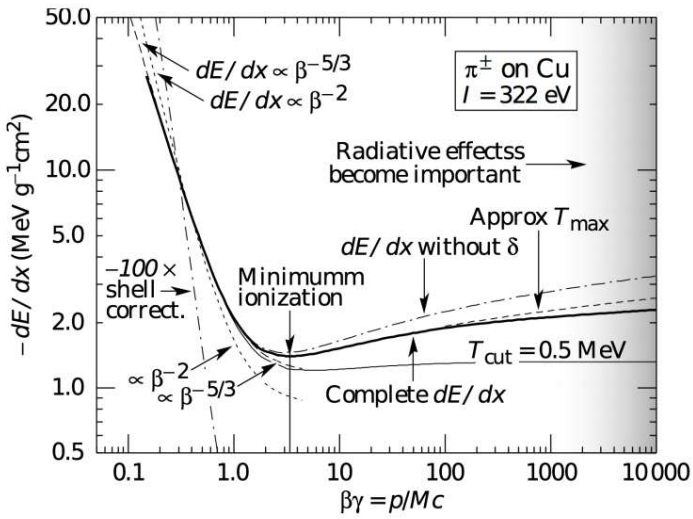

Figure 2.1: Energy loss of pions in Copper [1].

As seen from Figure 2.1, around $\beta\gamma \approx 3$, minimum ionization occurs. Particles which have corresponding energies are named minimum ionizing particles (MIP). Below the velocity that corresponds to minimum ionization, as the slower particles interact with matter more and experience electric field more, they have greater energy loss. As a result, at this region, the energy loss drops with $\beta^{\frac{-5}{2}}$. Above the minimum ionization, we see relativistic rise which goes with $\ln(\beta^2\gamma^2)$. Transverse electric field rises because

of the Lorentz transformation. This causes increase in energy loss.

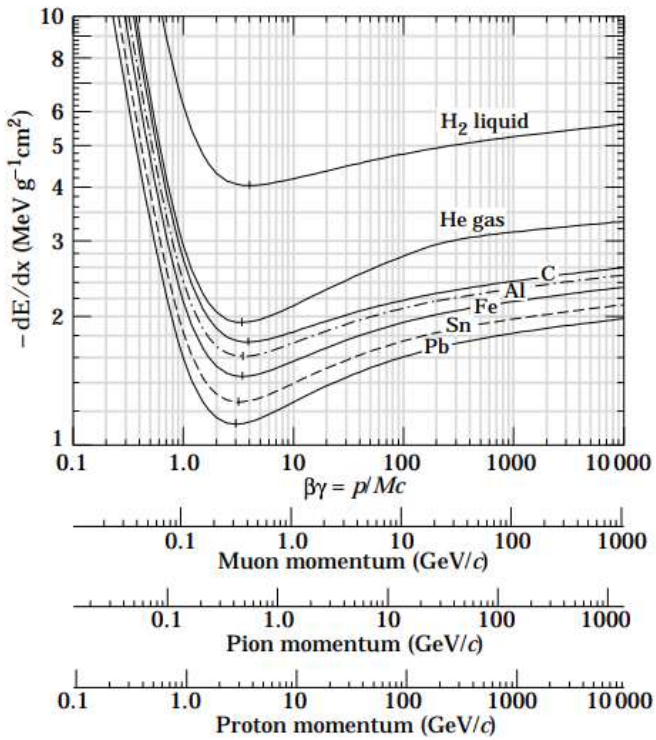

Figure 2.2: Mean energy loss of various particles in different gaseous media [1].

As the Bethe-Bloch fromula is dependent on $\frac{Z}{A}$, we have different curves for different media as can be seen from Figure 2.2. $\frac{dE}{dx}$ also depends on $\beta\gamma = \frac{p}{Mc}$ so for a given momentum, different particles have different energy losses. This fact is used to identify particles by looking at the energy loss vs momentum in detectors such as the ALICE Time Projection Chamber.

The Bethe-Bloch formula holds for energies between $0.05 < \beta\gamma < 500$ and for massive particles. For lower energies, Lindhard-Scharf and Anderson-Ziegler formulation holds. For greater energies, the radiative losses become important. These effects are included in Figure 2.3, where stopping power in Copper as a function of muon momentum is shown.

In addition to formulating the energy loss of a particle in a medium, we also need the information of how many electron-ion pairs are created in a medium. If we

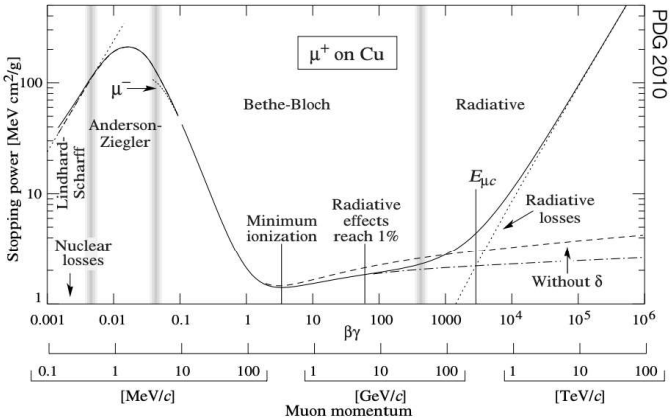

Figure 2.3: Stopping power vs momentum for muons in Copper [1].

ignore recombination and secondary processes, we can estimate the total number of electron-ion pairs as in Equation 2.3.

$$N_T = \frac{\Delta E}{W_1} \tag{2.3}$$

In Equation 2.3, ΔE is the total energy loss and W_1 is the average energy to produce an electron-ion pair. One can see the total energy loss per cm and other constants at normal temperature and pressure (NTP) in Figure 2.4.

Gas	Density mg cm^{-3}	E_x eV	E_I eV	W_I eV	$dE/dx\|_{min}$ keV cm^{-1}	N_P cm^{-1}	N_T cm^{-1}
Ne	0.839	16.7	21.6	30	1.45	13	50
Ar	1.66	11.6	15.7	25	2.53	25	106
Xe	5.495	8.4	12.1	22	6.87	41	312
CH_4	0.667	8.8	12.6	30	1.61	37	54
C_2H_6	1.26	8.2	11.5	26	2.92	48	112
iC_4H_{10}	2.49	6.5	10.6	26	5.67	90	220
CO_2	1.84	7.0	13.8	34	3.35	35	100
CF_4	3.78	10.0	16.0	54	6.38	63	120

Figure 2.4: Density, average energy of electron-ion pairs and total energy loss of different gases [2].

2.2. Transportation of Charged Particles in Gaseous Media

When an electron-ion pair is created in a medium, electrons and ions tend to diffuse if there is no electric field and they drift in case of an electric field. The diffusion

and drift velocity and the mobility of electrons and ions depend on temperature, density and pressure of the gas used.

2.2.1. Diffusion of Electrons and Ions in Gaseous Media

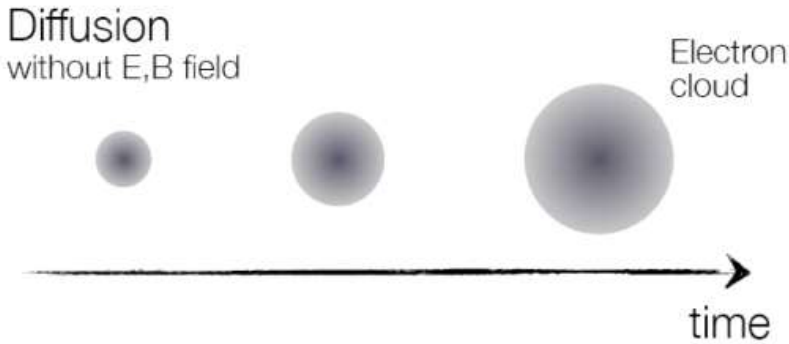

Figure 2.5: Electron diffusion when there is no electric or magnetic field [1].

For the case of the diffusion of the ions, we can formulize the motion by using Maxwell-Boltzmann statistics as the kinetic theory of gases is valid. The change in number of electrons/ions can be expressed in Equation 2.4.

$$\frac{dN}{dx} = \frac{N_0}{\sqrt{4\pi DT}} \exp(\frac{-x'}{x_i DT}) \tag{2.4}$$

In Equation 2.4, N_0 is the total number of electrons/ions, D is the diffusion coefficient, T is the temperature. This equation tells us that electrons/ions diffuse like a Gaussian in time as seen in Figure 2.5 with a width

$$\sigma(r) = \sqrt{6Dt} \tag{2.5}$$

The diffusion coefficient is defined as

$$D = \frac{1}{3}\lambda \tag{2.6}$$

In Equation 2.6, v is the mean velocity and expressed as

$$v = \sqrt{\frac{8kT}{\pi m}} \tag{2.7}$$

From Maxwell distrubution and λ is the mean free path of electrons/ions can defined as

$$\lambda = \frac{1}{\sqrt{2}} \frac{kT}{\sigma_0 P}$$

where σ_0 is the initial width of the electron-ion cloud and P is the pressure.

Putting everything together, we can finally write the diffusion coeffiecient as;

$$D = \frac{2}{3\sqrt{\pi}} \frac{1}{\sigma_0 P} \sqrt{\frac{(kT)^3}{m}} \tag{2.8}$$

Even though the electrons and ions obey the same rules for diffusion, as the mass of electrons are much more smaller than that of the ions, the diffusion coefficient of electrons is several orders higher. This leads to higher diffusion velocity for electrons.

2.2.2. Drift of Electrons and Ions in Gaseous Medium

When there is an external electric field applied to a gaseous medium, in addition to isotropic motion (diffusion), the electrons and ions are drifted along the electric field lines. Unlike diffusion in a gas, the electrons and ions behave differently in the electric field.

Average drift velocity of ions (w^+) is proportional to the electric field (E) upto very lstrong fields. This proportionality is called the mobility (μ^+):

$$\mu^+ = \frac{w^+}{E} \tag{2.9}$$

The mobility depends on the type of the gas and the type of the particle. It is also directly proportional to the temperature and inversely proportional to the pressure of the gas. There is also a relation between the diffusion coefficient and the mobility:

$$\frac{D}{\mu} = \frac{kT}{E} \tag{2.10}$$

As the mass of the electrons is very low compared to the ions, they can have their energy increased when they collide with the gas molecules. As described by Townsend, the drift velocity can be written as

$$w^{-} = k\frac{eE}{m}\tau \tag{2.11}$$

In Equation 2.11, τ is the mean time between the collisions. This formula holds except for very weak electric fields.

2.3. Signal Creation

To read the signal, the electrons or ions should be connected by the anode or cathode of the detector. Hovever before creating a signal, first the losses will be discussed.

When a particle passes through the gaseous medium, electrons and ions are created. Sometimes these electrons and ions recombine depending on the gas, recombination coefficient. Recombination does also depend on the electric field. In a detector where HV is used, recombination effect is not significant. In addition, if some electronegative gas molecules such as O_2 is used, electrons may bind to these molecules. This effect is charactezied by the electron attachment coefficient.

Most importantly, if the electrons are subject to a very high electric field, we observe the avalanche effect. Such field is created by the thin wires. One can see the schematics of the avalance formation in Figure 2.6. When an electron is close to the

wire, it gets multiplied by ionizing collisions. Electrons and ions are then laterally diffused. And the shape of droplet is formed around the wire.

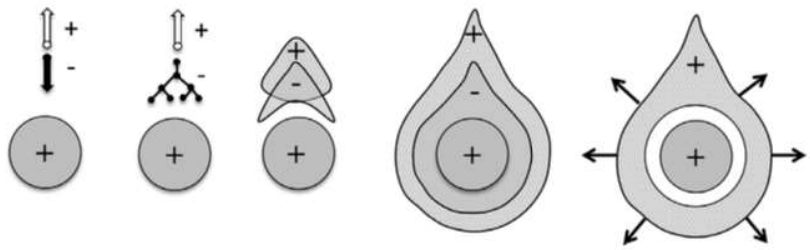

Figure 2.6: Avalance build up around the anode wire [2].

2.4. Types of Gaseous Detectors

The response of a gaseous detector changes with the voltage applied. So, one can classify gaseous detector according to the modes. To clarify these modes, we will plot the number of ions collected (i.e. signal height) vs the voltage applied.

2.4.1. Recombination Region

When the voltage applied to anode is very low, the ions and electrons drift hardly and they tend to quickly recombine. Some charges are still collected but as the recombination is very dominant, the signal is very small.

2.4.2. Ionization Chamber

When the voltage is increased such that the electrons and ions are drifted before they recombine, the detector operates as an ionization chamber. In the ionization chamber mode, gas multiplication does not occur. Independent of the voltage applied, constant number of ions may be collected. As there is no multiplication, the detector does not have any dead time, which makes this mode very useful at high radiation doses. The disadvantages of the ionization chambers are the low signal outputs and the need far sensitive preamplifier circuits with low noise. Furthermore, their operation accuracy are affected by moisture.

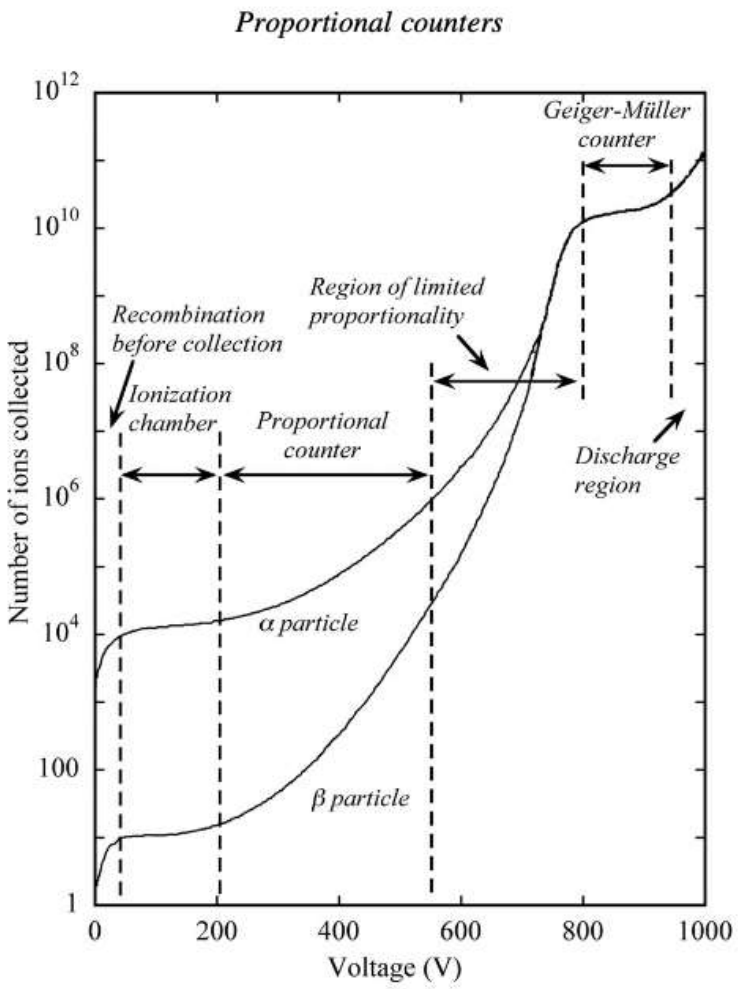

Figure 2.7: Number of ions collected vs high voltage applied for gaseous detectors [1].

Ionization chambers have different geometries. The most basic geometry is planar geometry where are the anode and cathode are planes like a parallel plate capacitor positioned in a gas tight container. When a charged particle ionizes the gas, one can measure the induced current from the anode and cathode. As the induced charge is read, the current is constant while the electrons and ions are drifting. Total induced charge depends on the spacing between the plates. As the mobility of the electrons is 102 times higher than the mobility of the ions, the electron signal is faster and greater than the ion signal. When the charges are collected by the electrodes, the signal ends. This type of detectors may have big active areas like 100cm×60cm as in the Multi-sampling ionization chamber (MUSIC II) at GSI [22].

Ionizing chambers are also used in dosimeters. It generally has a cylindrical geometry with cathods at the wall and anode in the middle. It is generally filled with air and charged from a charging point.

Ionization chambers are very useful for nuclear physics experiments running at 10-100MeV. They can measure the energy of a particle and by measuring the energy and change in the energy, particle identification may be achieved.

2.4.3. Proportional Counter

After a certain threshold value, the electric field around the anode is high enough to cause an avalanche effect and signal gets multiplied. In this region, the output current is proportional to the energy deposit. This way, it is possible to measure a particle's energy. The proportional counters can be used in large areas and can discriminite between α and β particles. However to achieve high electric field around the anode wires, very thin wires should be used, which makes the detector very delicate.

In high energy physics experiments, we see lots of examples of usage of proportional counters with cylindrical coaxial geometry. The anode is a thin wire laid in the center and the cathode is the walls of the straw as originally designed by Rutherford

and Geiger (Figure 2.8). The anode wire should be as thin as a couple of 10μm to let avalanches. Because of the avalanche there is gas amplification. For example for an argon filled detector with an anode wire thickness of 30μm and straw radius of 1cm, the gas multiplication is around 10. This means that the total charge of the signal is 10 times higher than the number of the electrons created because of the ionization. The rise time of the electron signal is in the order of ns while for the ions it is around 10ms. The proportional straw tubes are used in many big experiments such as LHCb outer straw tubes and ATLAS Transition Radiation Tracker (TRT).

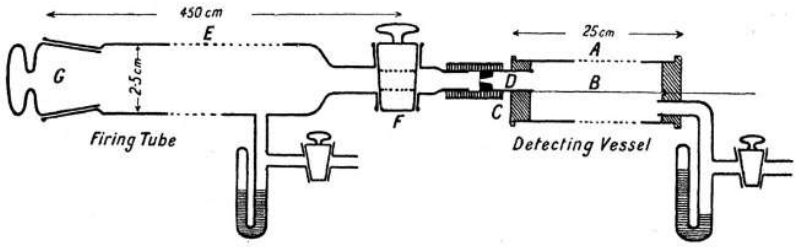

Figure 2.8: Proportional counter originally designed by Rutherford and Geiger. [1]

Another breakthrough proportional counter in high energy physics is Multi Wire Proportional Chamber (MWPC)., which was first used at CERN at 1960s. The first MWPC (Figure 2.9a) had 10cm×10cm active area which was achieved by 24 anode wires. It was invented by Georges Charpak and he won the Nobel Prize in Physics for "for his invention and development of particle detectors, in particular the multiwire proportional chamber" in 1992. Multiwire proportional chambers are constructed with thin anode wires stretched between parallel cathode planes. As the anode wires are very thin with radii around a couple of 10μm, avalanche occurs around the wire which provides a sizable signal.

The variables used to define an MWPC is summarized in Figure 2.9b. The x axis is defined to be perpendicular to the anode wires and parallel to the cathode planes. The origin is chosen to be at the center of the detector. s is the distance between anode wires. l is the distance between the neighbouring anode wires and cathode plane. Other than these variables a is the diameter of the anode wires.

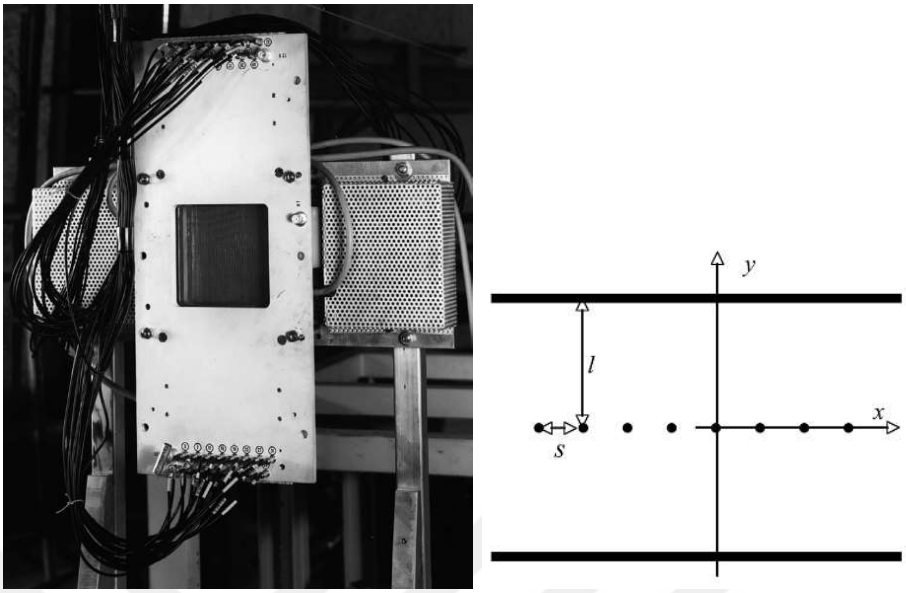

(a) First MWPC (b) Geometry and variables of MWPC

Figure 2.9: Photo of the first MWPC and the variables used to design a MWPC [2].

By using these geometric variables and electromagnetic theory, we can calculate the capacitance per unit length, the potential difference and the electric field for any point within the MWPC with Equations 2.12, 2.13, 2.14.

$$C = \frac{2\pi\epsilon_0}{\frac{\pi l}{s} - \ln\frac{2\pi a}{s}} \tag{2.12}$$

$$V(x,y) = \frac{CV_0}{4\pi\epsilon_0}\frac{2\pi l}{s} - \ln[4\sin^2(\frac{\pi x}{s}) + \sinh^2(\frac{\pi y}{s})] \tag{2.13}$$

$$E(x,y) = \frac{CV_0}{2\pi\epsilon_0}\frac{2\pi l}{s}(1+\tan^2(\frac{\pi x}{s})\tanh^2(\frac{\pi y}{s}))^{\frac{1}{2}}(\tan^2(\frac{\pi x}{s}) + \tanh^2(\frac{\pi y}{s}))^{-\frac{1}{2}} \tag{2.14}$$

In Equation 2.14, V_0 is the applied voltage. If we calculate the electric field the field lines and the equipotential lines look like in Figure 2.10a and the electric field plot with respect to the distance from the center of the wire along the x and y axes is shown in Figure 2.10b. The electric field is the highest around the anode wire and drops with $\frac{1}{r}$ further. Electric field dereases between the wires (along the x axis) and extends to a uniform field in the direction perpendicular to the wires (along the y axis). In this uniform field the electrons and ions are drifted and the avalanche happens very close to the anode wires.

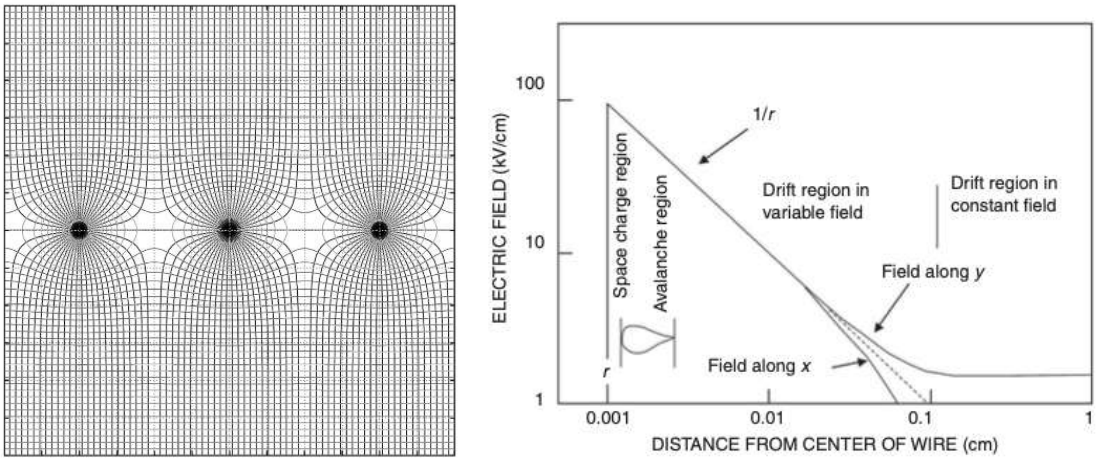

(a) Field lines and equipotentials of MWPC

(b) Field along x and y axis

Figure 2.10: Electric field of MWPC [2].

While the gain increases by using a thinner wires, the mechanical tolerance drops significantly. Because of the electrostatic forces caused by the electric field on the wires, wires tend to move and even a small displacement causes a change in the gain because of the distortion of the geometry. Furthermore, the accuracy of the position measurement depends on the distance of the anode wires. If the wires are closer the position may be measured accurately but each wire means a new readout channel and it is hard to handle too many channels. So tightly separated and thin wires are hard to operate.

There are other proportional counters such as Microstrip gas chambers, Micromegas, Gas electron multiplier (GEM) which have similar physics with different geometries and readouts. The proportional counters are used in big particle physics experiments such the ATLAS detector at CERN, on beam lines and in small laboratory experiments.

2.4.4. Limited Proportionality

When the voltage is increased more than the proportional counter mode, the proportionality can not be achieved beyond a certain limit as a result of distortions in

the electric field because of the very high avalanches around the anode. So this region is saturated at some point. As a result the output current becomes independent of the particle type, energy, etc.

2.4.5. Geiger Muller Counter

Beyond the saturation of limited proportionality, Geiger Muller counters operate. At this region, one can not identify the particle or measure its energy, but the signal size is very high which makes the output easy to read. On the other hand, as the avalanche is saturated, the dead time of the detector is highest. The Geiger Muller counters can be produced at varying sizes and they are cheap and robust.

2.4.6. Discharge Region

If the voltage applied is extremely high, the discharge region is reached. This should be avoided in the detectors as the discharges may damage the wires.

3. DELAY WIRE CHAMBER

Delay wire chamber (DWC) is a modified version of the MultiWire Proportional Chamber (MWPC) that has been discussed in the previous chapter. It is a low-cost, simply operated gaseous detector with sophisticated electronics and is used for spatial measurement of a charged particle passing through it. It has been developed by the beam instrument group at CERN. It can be operated at 100kHz with a spatial resolution of 0.2mm.

In this chapter, we will focus on the DWC constructed at Bogazici University Kandilli Detector, Accelerator and Instrumentation Laboratory (KAHVELab) with the funding of TÜBİTAK 1005 (114F467). It is a detector with an active area of 10cm×10cm and position resolution of 200μm, and is operated at around 2500kV using gas mixture of CO_2(50%) and Ar(50%).

The detector has been constructed using the KAHVELab facilities and most of the materials have been procured from local companies. It has been tested both at the KAHVELab and CERN gaseous detector laboratory and has successfully passed all the tests.

3.1. Working Principle

DWCa are today mainly used at beam lines to measure beam profile as shown in Figure 3.1a. A DWC has anode and cathode layers made of wires, unlike the MWPC, which uses wires for anode but plates for cathode. The anode layer is sandwiched between the cathode layers and the wires of different layers are placed perpendicular (Figure 3.1b). However, the voltage, electric field and physical parameters of the MWPC and DWC are essentially the same.

When a charged particle passes through the chamber, it ionizes the gas. by

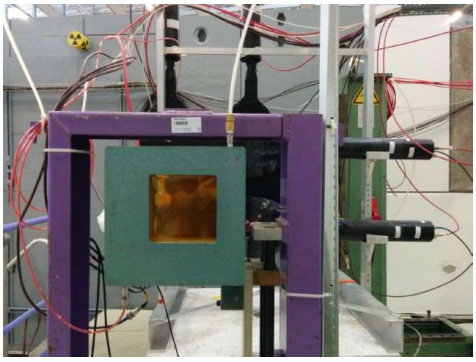

(a) DWC used at CERN beamlines

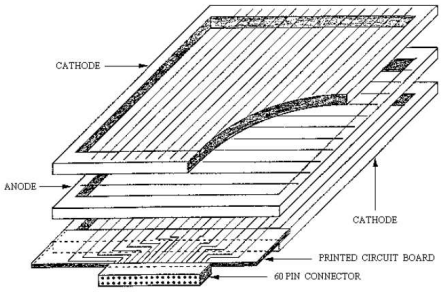

(b) Sandwiched layers of cathode and anode

Figure 3.1: Example of DWC at CERN and the placement of its anode and cathode layers [3].

applying High Voltage (HV) to the anode, an electric field is generated inside. Under the influence of the electric field, the electrons are drifted towards the anode and ions are drifted to the cathode. As the anode wire is very thin, there is a huge electric field around the anode wires and this creates avalanche ionization. The image charge of these avalanche electrons are read from the cathode layers.

In the MWPC, one has a seperate readout channel for each anode wire. However, for the DWC anode signal are directly collected together, while the signal from each cathode wire is delayed by 5ns with respect to its neighbor wire using electronics and then gets added up.Then from each end of the cathode layers, measurements are collected. This confguration decreases the number of the readout channels from the number of wires to only two readout channels for a 1D measurement and to four readout channels for a 2D measurement. The comparison of the readouts of the MWPC and DWC is depicted in Figure 3.2. For example, when the particle passes through the detector close to the upper part of the detector, the upward propogating signal experience smaller delay than the downward signal. From the time difference of the two readouts, position where the particle passes can be calculated. The signal formation in a single layer of the DWC is shown in Figure 3.3.

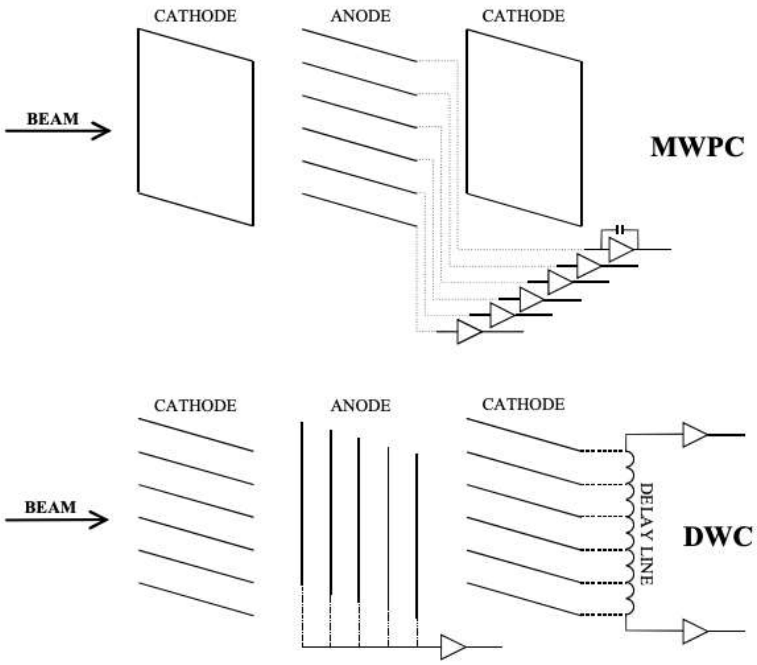

Figure 3.2: The readouts of the MWPC and the DWC compared [3].

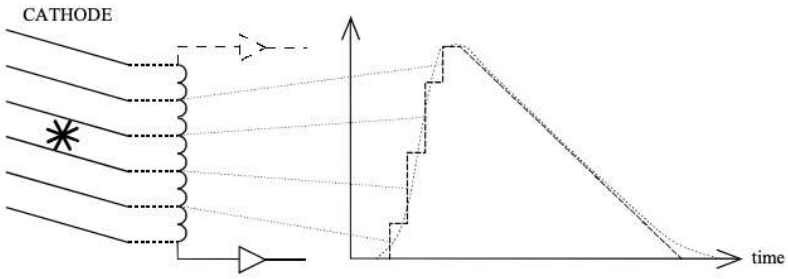

Figure 3.3: Signal formation in the DWC [3].

3.2. Theoretical Calculations

To determine technical limits of the DWC, theoretical calculations of the capacitance and the tension on the wires under this capacitance is needed. The formula for the capacitance per unit length (C) is given in Equation 3.1. As in MWPC, l is the distance between the anode and cathode layers, s is the distance between anode wires, a is the diameter of an anode wire.

$$C = \frac{2\pi\epsilon_0}{(\pi l/s) - \ln(2\pi a/s)} \tag{3.1}$$

The critical tension for the wires is calculated with the formula (Equation 8.10 of the book [2]) given in Equation 3.2. In addition to the variables defined before, V_0 is the voltage applied to the anode and L is the length of the wire.

$$T = \frac{1}{4\pi\epsilon_0}(CV_0L/s)^2 \tag{3.2}$$

Critical tension for the tungsten (T_m) is given in SI units in Equation 3.3.

$$T_m = 0.1710^6 s^2 - 0.10810^3 s + 0.05 \tag{3.3}$$

Comparing T with T_m, one can decide if it is possible to construct such any given chamber. In order to facilitate the design process, the calculations from these equations have been embedded in a C++ programme. The screen-shot of the code output can be seen in Figure 3.4. As can be seen from the results, we are able to create quite sizable chambers when we the only constraint is the tension generated because of the capacitance when a HV is applied.

3.3. Design

The design of the DWC used at CERN beam lines has been taken as a model [3]. The full list of used parameters are given in Table 3.1. With the design, position

```
Calculations for MWPC or DWC:
Please enter l value(mm): (distance between anode and cathode)
3
Please enter s value(mm): (distance between anode wires)
2
Please enter a value(um): (diameter of anode)
20
Please enter V0 value(V): (Voltage applied)
3000
Please enter L value(cm): (Length of wire)
12
Capacitance per unit length is: 7.43419 pF/m
For this configuration tension should be higher than: 0.0161017 N
i.e you need to hang  1.61017 grams

Critical tension for tungsten is: 0.514 N
You can construct such a chamber!

Maximum lenght without any support is: 67.7996 cm
To prevent wires motion in electrical field.
```

Figure 3.4: The screen-shot of the code that calculates the tension limit for a DWC when only the electromagnetic constraint is considered.

measurement with a precision of 200 μm with an active detection area of 10cm×10cm has been aimed.

Table 3.1: The parameters of DWC [3]

Variable	Value
Active Area	100mm × 100mm
Cathode Wires	100μm diameter Cu-Be wires
Spacing between Cathode Wires	2mm
Anode Wires	20μm Au plated W wires
Spacing between Anode Wires	4mm
Spacing between layers	5mm
Operating High Voltage	∼2500V
Low Voltage	bipolar ±6V
Gas Mixture	50% CO_2 %50 Ar
Maximum Beam Rate	∼10^5 particles per second
Chamber Dead Time	250ns
Gas Flux	10cm^3/second

The technical drawings have been done using OpenSCAD [23]. OpenSCAD is a free software to create 3D CAD models by simply writing a script and compiling it. The script based design process allows the user to adjust the parameters easily.

We start by designing the frames where the wires are to be attached. The frame of a layer of the DWC , created with the OpenSCAD by using the parameters on Table 3.1 can be seen in Figure 3.5a. On each frame, the places where the PCBs will be glued are designed to be etched (green etches on the figure). Holes are placed in the corners to fix the frames together through bolts. The places where the wires will be positioned by soldering are designed to be etched.

The model of the anode and cathode planes are exactly same. Anode is sandwiched between the cathode planes with a 90°. To achieve 2D position measurement, two of these cathode-anode-cathode configurations are stacked on top of, but oriented at 90° to each other. All the layers positioned in place can be seen in Figure 3.5b. The PCBs (purple in figure) are placed in etches as described.

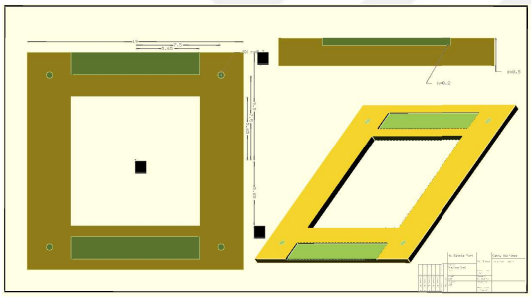

(a) One layer of DWC as seen from top view, side view and the angled view

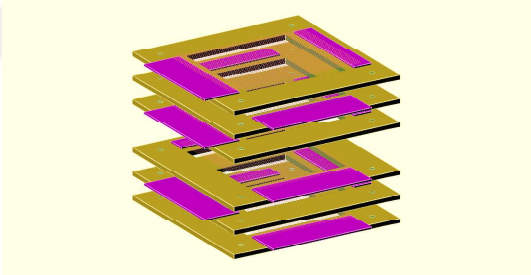

(b) All 6 layers that are needed 2D position measurement

Figure 3.5: The design of the DWC drawn with the OpenSCAD software.

A gas tight box is designed to put the detector frames in. The model of the box can seen in Figure 3.6. As seen in the top view with the blue door, gas input and outputs are placed on the opposite sides to create gas flow inside. There is a kapton window for the active area of the detector. The frames are shown in red as seen in the side and angled views. The high voltage input (red circle) and the data outputs (on black triangle) have been designed to be on the top of the detector for easier access.

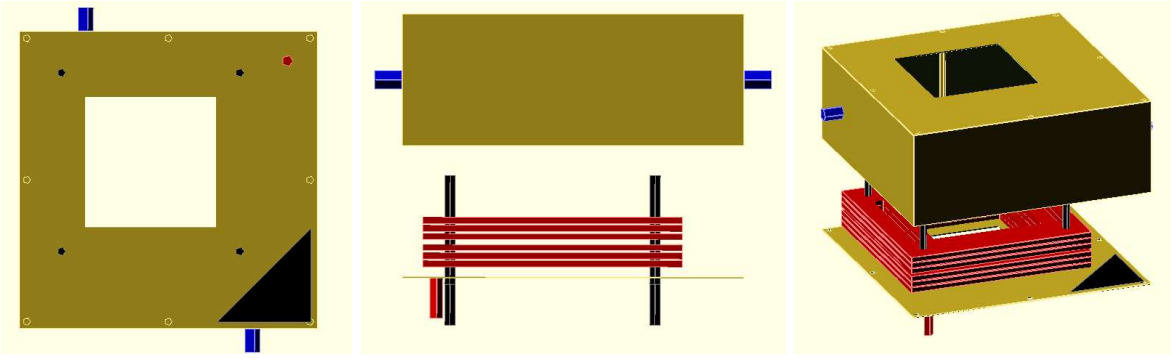

(a) Top view (b) Side view (c) Angled view

Figure 3.6: The model of the box of DWC with the frames drawn using the OpenSCAD software.

3.4. Simulation

To simulate the electric field and the signals of the delay wire chamber Garfield++ toolkit [4] is used. Garfield++ is a C++ and ROOT based simulating package. The user defines the medium (gas or semiconductor) and the geometry of the detector and track and drift properties of the particles can be simulated. The structure and the overview of its classes may be seen in Figure 3.7.

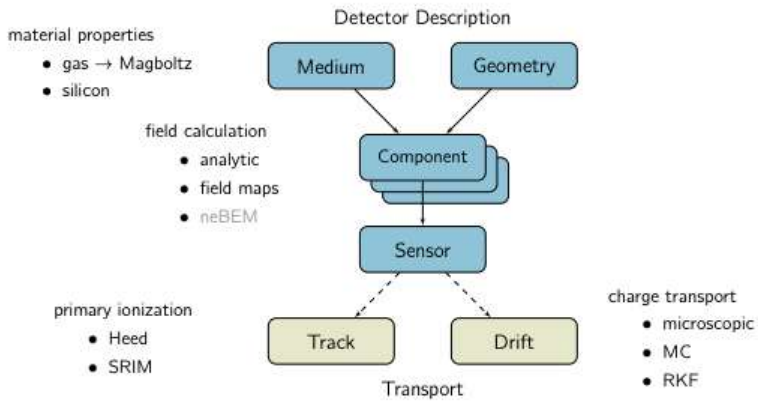

Figure 3.7: The general structure and the classes of Garfield++ [4].

To simulate DWC using Garfield++, first the parameters from Table 3.1 including the dimensions, wire radii and spacing between wires are defined. The gas is used as equal mixture of CO_2 and Ar at 1atm and room temperature. The sensors are defined

as anode and cathode wires. Voltage of 2kV is applied to the anode wires and the cathode wires are grounded. First the electric field is simulated. The defined detector geometry and the simulated electric field can be seen in Figure 3.8. As expected, close to the anode lines, we have a very high electric field which will cause avalanche and we have a rather linear electric field close to the cathode lines.

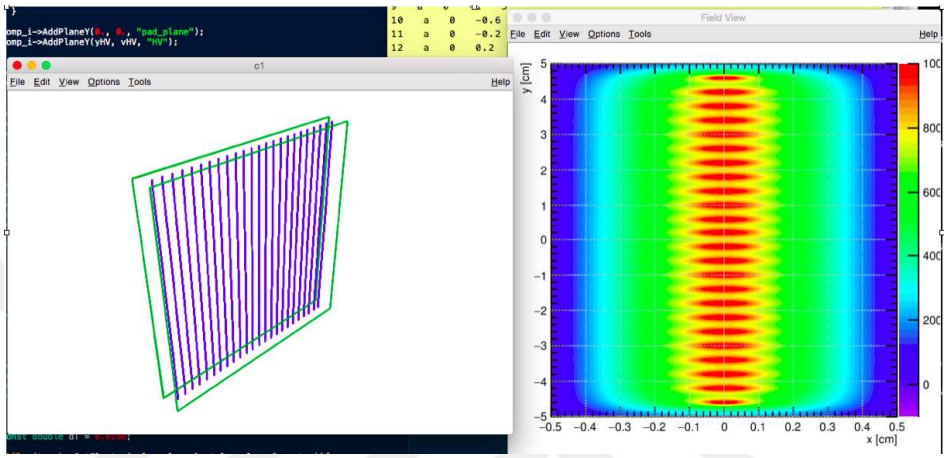

Figure 3.8: The geometry (Left) and electric field (Right) of DWC simulated with Garfield++.

Then a muon of 1GeV energy is directed inside the box and it creates electrons and ions. They are drifted through the gas to the wires. The signals collected from anode and cathode are shown in Figure 3.9.

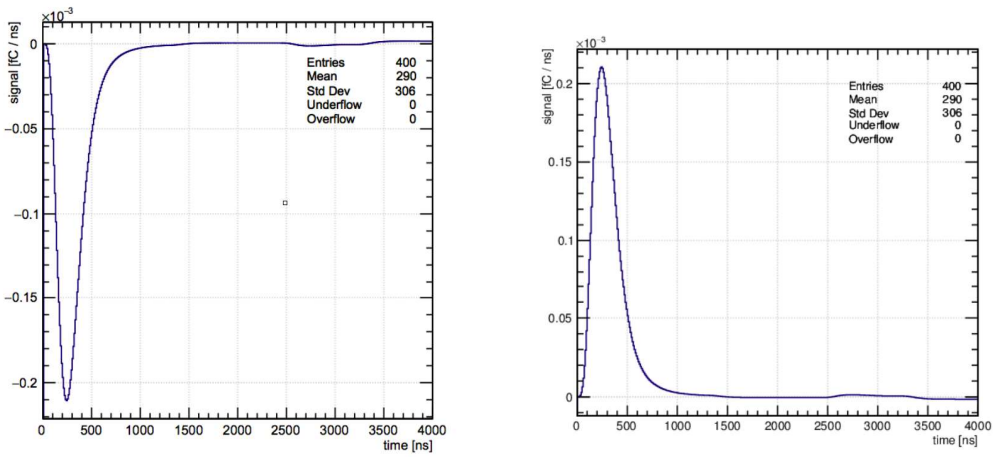

(a) Anode Signal (b) Cathode Signal

Figure 3.9: Total signal obtained with Garfield++ simulations a muon of 1GeV energy moving through the DWC.

3.5. Construction

The construction of the chamber has been entirely done at Boğaziçi University Physics Workshop and KAHVELab Workshop and Lab space. The process does not need any specialized equipment; ordinary construction power tools, milling machine, soldering station and simple repair tools are found to be sufficient. In the following sections each step of the construction is explained in detail.

3.5.1. Producing Frames

The frames of anode and cathode are made of 5mm thick FR4, which is a composite material of glass fibers and epoxy. FR4 is versatile and non-flammable but hard to manipulate. First the plates are cut with a saw mill and the detailed shaping is done using the milling machine. In the milling machine the template in Figure 3.5 is used. The holes on the corners are drilled with 6mm tip. For the rest of the work, 5mm drilling and milling tips are used. As Rockwell hardness of FR4 is 110 M scale (close to steel), diamond tips are used. After drilling the holes on the corners, the window is opened with the milling mactine, the etches for the PCBs and the etches on the back where the solders of the bottom frame of the DWC will be positioned are done. The template for positioning the milling machine can be seen in Figure 3.10.

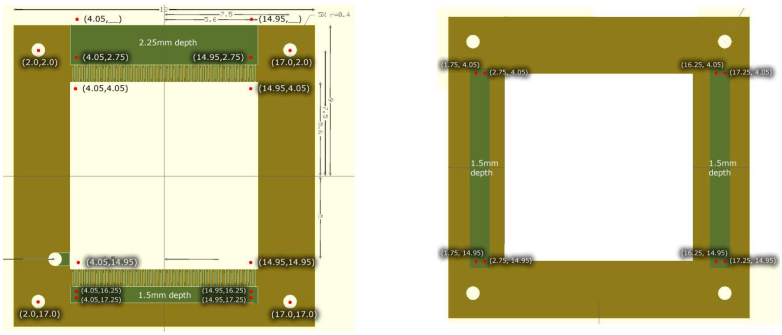

(a) Front View (b) Back View

Figure 3.10: The template of the positions for the milling machine.

The anode and cathode layers are produced identically. After the milling work is finished, the PCBs where the wires will be soldered are glued with epoxy. On one side

of the frame 2mm spaced standard proto PCB is used. On the other side, where we will read the signal, a converter to 2mm to 2.54mm is used. These converter PCBs are produced at CERN Technology Department. The design can be seen in Figure 3.11.

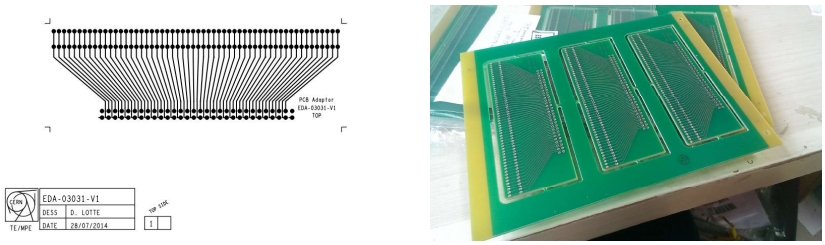

(a) Design (b) Final Product

Figure 3.11: The design and final product of the converter PCB to be used in between cathode wires (signal) and readout connectors.

For the anode all the outputs are combined together to get a single anode signal. For the cathode signal, the output from the converter PCB is transferred to the electronic circuit via flat cable.

3.5.2. Attaching Wires

After the frames have been produced and the PCBs glued, wires of cathode and anode layers are soldered to the PCBs. As high voltage is to be applied to the anode wires, the resulting electric field inside the chamber. may cause the wires to move when there is a current of signal. To prevent this, the wires should be kept tight. To keep all the wires at the same tension, fishing sinkers are first soldered to each wire, then the wire is released with the force, aligned to the PCB and soldered. While soldering latex gloves are used to prevent oiling the wires. The soldering procedure by which the wires are stretched with sinkers is shown in Figure 3.12.

For 1D measurement, we need 1 anode layer sandwiched between 2 cathode layers. To achieve 2D measurement, we have produced 2 sets of these, making in total 2 anode, 4 cathode layers. After their production all the layers produced they are aligned with the holes on the corners.

Figure 3.12: Photo of soldering cathode Cu/Be wires stretched with the fishing sinkers.

For cathode layers, copper (98%) beryllium (2%) wire with a diameter of 100μm is used. This alloy of Cu-Be is corrosion resistant and has high strength. They are placed 2mm apart. Cu98/Be2 has tensile strength in the range 500-1300MPa [24]. For this tensile strength we decided use 0.1kg fishing sinkers to stretch the wires along the frames.

For the anode layers, gold plated tungsten wires of 20μm diameter are used. In its purest form tungsten has the highest melting point which makes it suitable for use as filaments. Since high voltage is to be applied to the anode layers, we prefer to use tungsten. With the gold plating, durability is increased and soldering is improved. The tensile strength is 1920MPa [25]. While the tensile is higher than the Cu/Be as the diameter is really small, we use lighter 20g fishing sinkers. The same converter and standard proto PCBs are used in anode layers skipping every other hole so the spacing between the neighbouring wires is 4mm.

3.5.3. Alcohol Bath and Heat Treatment

After soldering the wires, all the frames are placed in a oven to be treated at 150°C for two hours. Baking is advised by the CERN gaseous detector laboratory for protecting the wires from probable damages caused by the sparks. The frames in the oven (protherma HLF200) can be seen in Figure 3.13a.

In spite of the great care taken while attaching the wires, some oil may get deposited on the wires. In this case, the signal efficiency is likely to drop. Hence as the last step the frames are treated with an ultrasonic bath in isopropyl alcohol at room temperature for an hour. The alcohol bath is shown in Figure 3.13b.

(a) Oven (b) Ultrasonic alcohol bath

Figure 3.13: The oven and the ultrasonic alcohol bath used to treat the frames with wire.

3.5.4. Electronics

The clever design of the electronics is what makes the DWC special. The delay line postpones the signal from each cathode wire by 5ns cumulatively, thus essentially encoding the positioninformationinto the time development of a single signal. While the main duty of electronics is hence epitomized in the delay line, other functions include

the collection of the anode signal, which may be used for triggering the detector, and the calibration of the detector when used with a signal generator. There are 3 calibration channels which send signals to either at ±30mm from or right at the center. The calibration signals are chosen to be at 40 mV over 50 ohms, which are read out at −80 mV output at cathodes and anodes. The operating low voltage (LV) of the electronics is ±6V. The original design of electronics of the DWC used at CERN can be seen in Figure 3.14.

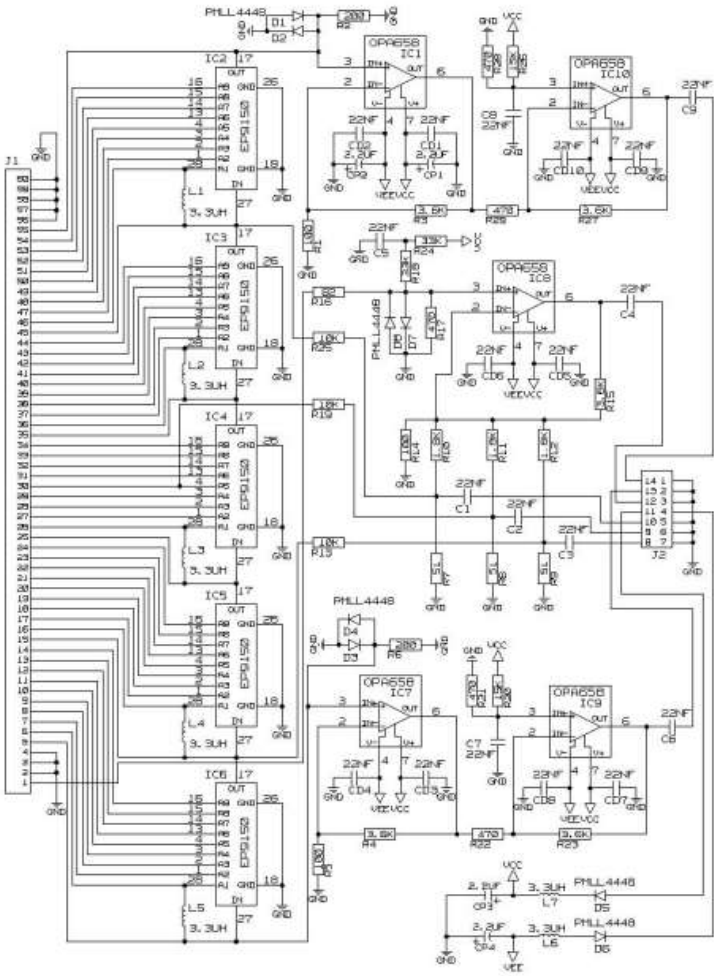

Figure 3.14: The original schematics of the electronics of the DWC used at CERN [3].

We used the same electronic elements or their substitutes as the ones seen in the CERN schematics. Our design of DWC can seen from the figure 3.15 which has the same specifications except the voltage needed to operate is ±5V. The design has been printed on a 6 layer PCB using one layer for ground, one layer for +Vcc and one layer

for −Vcc. As a Faraday cage, the circuit is placed a tin box. Further details on the electronics can be found in [26]. We used AIZ-502J delay chips to create delay between the wire. The schematics of the chip is shown in Figure 3.16.

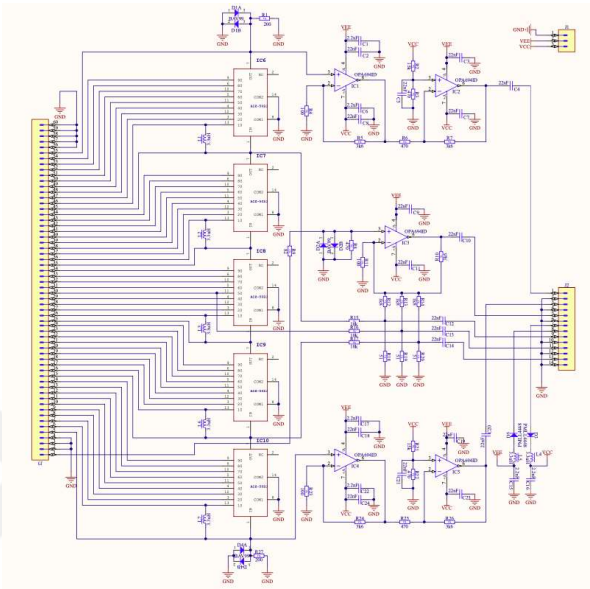

Figure 3.15: The design of the electronics of the DWC used at KAHVELab.

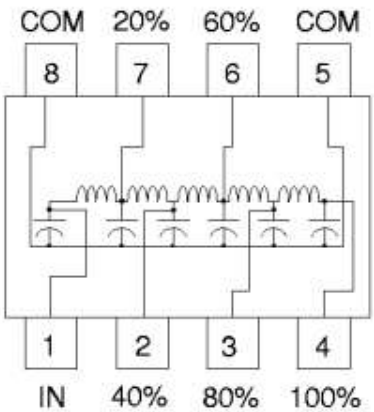

Figure 3.16: Design schematics of the AIZ-502J delay chip.

3.5.5. Placement in a Box

After all the layers and electronic cards are ready, they are all placed in a gas tight box. Two boxes have been used for the DWC. The first box was made of plastic, had dimensions of 23cm×30cm×9cm, and was humidity proof. While the plastic box was not very durable but, it was easy to adjust for the primary tests. Unfortunately, it

did not turned out to have good gas tightness and a decision was taken to move to an aluminum box with the dimensions 25cm×25cm×10cm. The metal box is more durable and serves better gas tightness. For these two boxes a window of 10cm×10cm has been opened on top and bottom faces where the active area of the detector is positioned. Kapton film at the thickness of 25μm is glued with epoxy to these windows. The gas input and outputs are placed on the opposite corners of the detector to provide good gas flow. The HV and readout channels are placed in the face where the access is easy. The pictures of the boxes with the DWC inside can be seen in Figure 3.17.

(a) Plastic box (open) (b) Plastic box (closed) (c) Plastic box on top and metal box on the below

Figure 3.17: The DWC placed in a plastic and metal box.

3.6. ESEM Studies of the Wires

After all the layers of the DWC have been constructed and the wires attached, we would like to observe the cleanness of the wires and the effect of the baking and of the alcohol bath. Thus, we have examined the wire samples in FEI-Philips XL30 Environmental Scanning Electron Microscope (ESEM) at Boğaziçi University Advance Technologies Research and Development Center Laboratory. The ESEM has a magnification of 300000× with a resolution of 5 nm at 30 kV and can scan 50×50mm area [27]. The following samples of anode and cathode wires have been imaged:

- Brand new wires taken from the spool
- Wires baked in oven (no alcohol bath)
- Wires which have been treated in the ultrasonic alcohol bath (no oven)

- Wires baked in oven and bathed in ultrasonic alcohol
- Wires taken from the spool and a spark of 400V went through
- Baked wires through which subject to a spark at 400V
- Leftover wires from the table which we touched with bare hands

These samples were taped with an aluminum band on aluminum plate of 5cm×5cm as seen in Figure 3.18. The plates were cleaned with alcohol before placing the wires.

(a) (b)

Figure 3.18: DWC wires taped on an aliminium plate for ESEM imaging.

ESEM images are taken monochromatic. The bright parts are mostly organic i.e. oily. The holes look darker in the images. First we examined the effect of baking the frames in the oven. It is expected that the wires will become resistant to spark damage when they are heated in the oven. So we applied 400V to sample wires to get a spark though the wire before and after baking. As can be seen from Figure 3.19, when the wires are baked in the oven, the sparks leave less serious damage to the wires.

The second thing we would like to observe, is the effect of the ultrasonic alcohol bath. So sample wires were imaged before and after alcohol bath. As can be seen from Figure 3.20, before the ultrasonic bath, the wires have organic compounds on them and they are cleaned after the bath. A wire after the ultrasonic bath is as clean as a brand new wire from the spool.

Another effect that we realize is that we can see the stretch marks on the wires. As can be seen from Figure 3.21, the stretch marks on the wires are visible at 1500×

magnification when we compare a wire that has been streched with the weights (than removed) and the brand new wires.

Lastly, the images of the leftover wires that are touched with bare hands as in Figure 3.22 show us the importance of using gloves and cleaning afterwards in the ultrasonic bath. There is an organic deposit (most probably oil) on the wires that have been touched with bare hands or not carefully handled.

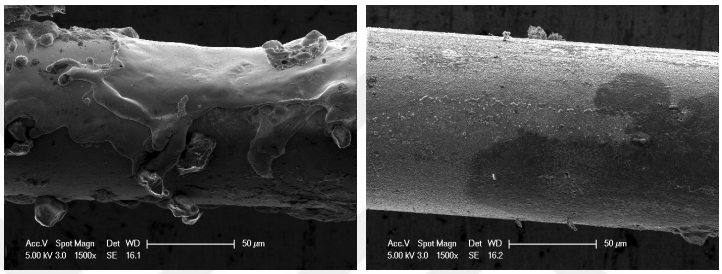

(a) Spark before the oven (b) Spark after the oven

Figure 3.19: The ESEM image of wires that have been subject to sparks, at 1500× magnification. The wire on the left has not been baked while the wire on the right has.

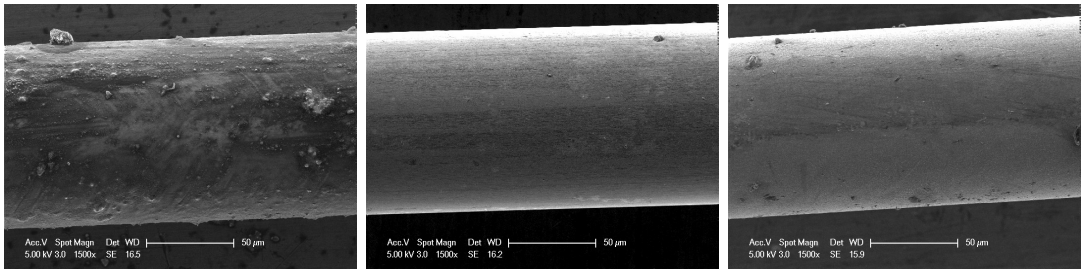

(a) Before ultrasonic alcohol bath (b) After ultrasonic alcohol bath (c) Brand new

Figure 3.20: The ESEM image of wires before and after ultrasonic bath at 1500× magnification. The photo of the brand new wire image is placed for comparison

3.7. Gas System

The mixtures of the CO_2 and Ar (50/50) are used to operate the DWC. The mixture is provided from the local companies and stored in a 10L gas tube at a pressure of 100atm. In order to circulate the gas through the detector, we need a pressure of 1atm. To decrease the pressure and observe the gas flow, the gas system seen in Figure

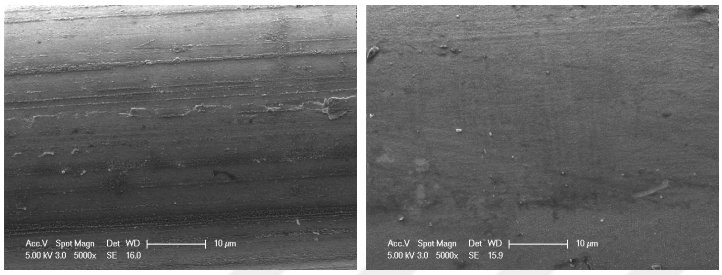

(a) Streched and baked (b) Brand new

Figure 3.21: The ESEM image of wires when a force is applied (streched) or not (brand new) at 1500× magnification.

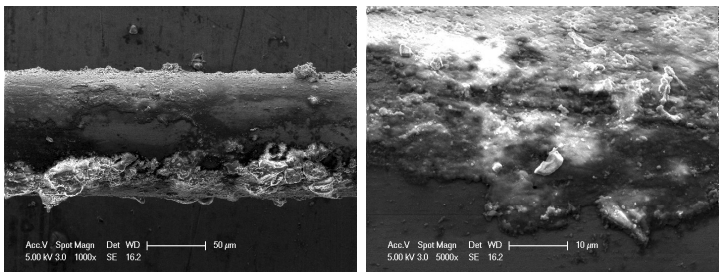

(a) 1500× magnification (b) 5000× magnification

Figure 3.22: The ESEM image of the leftover wires that are touched with bare hands.

3.23 is used. First the gas pressure is dropped to atmospheric pressure with a regulator of 0.5/1.5bar. Then to observe the flow rate of the gas a flow-meter is placed before the detector. The flow-meter can measure 0.5 - 5 L/h. For our setup we set the flow-meter around 2 L/h. Then the gas is connected to the inflow of the DWC. The outflow of the detector is connected to a bubbler to make sure that there is no significant gas leak. The gas leakage tests are done by circulating the N_2 gas trough the chamber. We expect to see a couple of bubbles every 10 seconds during the operation of the detector. When the detector set to run, the gas flow is initially adjusted to a higher level in order to flush the chamber and then the rate on the flowmeter is fixed for smooth gas flow. The DWC connected to the gas system can be seen in Figure 3.24.

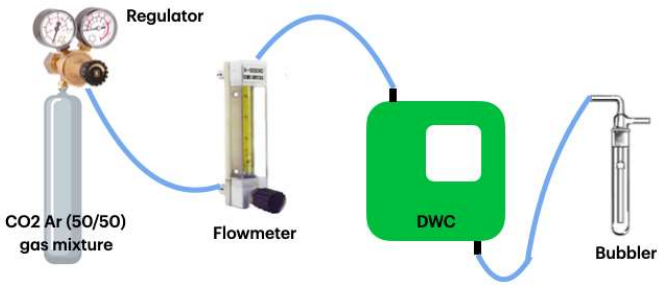

Figure 3.23: The schematics of the gas system of the DWC used at KAHVELab

Figure 3.24: The gas system connected to the DWC

3.7.1. Monitoring of Gas Purity Through Humidity

To monitor the gas flow through the chamber, a temperature and humidity module, DHT22, connected to an Arduino Uno microcontrolller board is used. This module

can be used to measure temperature between −40°C and 80°C with a 0.5°C accuracy. Relative humidity in the range 20-90% RH can also be read with the module with an accuracy 2% RH. The module is placed inside the chamber and the Arduino board is placed on the outside for an easy access. While reading the module, one can easily see the adjustments on the gas flow and see if the flow is on or off. As an example, the data obtained from the DHT22 can be seen in Figure 3.25 while testing the detector.

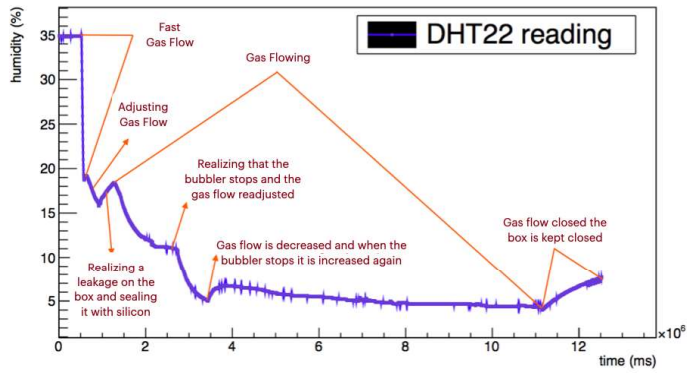

Figure 3.25: The data from DHT22 obtained while testing the detector.

3.8. High Voltage

Delay Wire Chamber relies on HV to drift and avalanche electrons. The detector is used in the Geiger region. So we need to observe a plateau in the signal vs voltage plot and set the operating voltage above the minimum value for that plateau. So we take counts from the cathode for 1 minute at different high voltages while the osciloscope trigger threshold is set to 80mV. The data are plotted in Figure 3.26. We have decided to operate the DWC above 2700V.

3.9. Operation

After all the design and the construction has been finalized, we place the frames with the wires attached in the gas tight box and connect a primative test circuit composed of a capacitor and two resistors as seen in Figure 3.27a. CO_2 Ar gas mixture is circulated and HV is applied. At this point the electronics circuit of delay line is not yet connected.

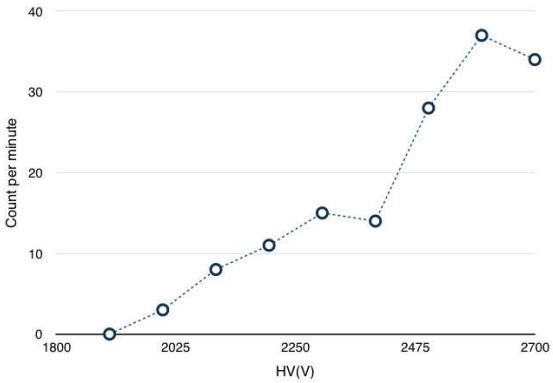

Figure 3.26: Counts vs high voltage from the cathode at the trigger treshold of 80mV.

The primary tests are conducted on follows. We wait for the humidity sensor readings to decrease and settle at a low steady value, while the bubbler is constantly operating. The gas flow is at around 0.5L/h. The HV is increased up to 3kV and no spark is observed. Then we observe anode and cathode signals beyond ±100mV as in Figure 3.27b.

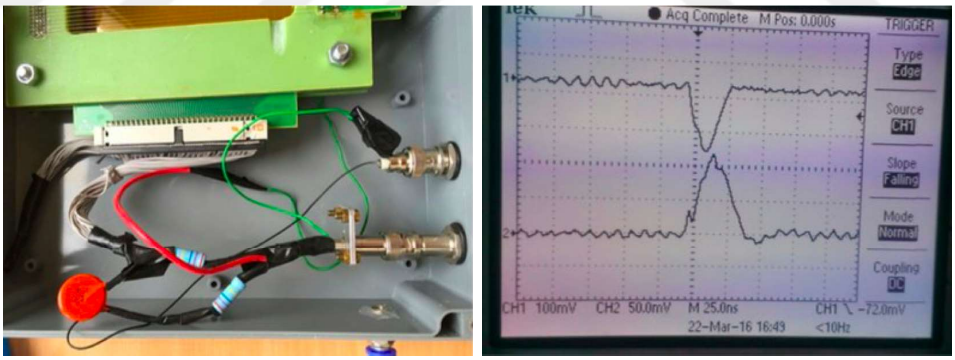

(a) Simple Readout Circuit (b) Anode and Cathode Signals

Figure 3.27: Primary test with the simple electronics without the delay line and the very first signals read from the DWC:

After the primary tests, the readout circuit with the delay line is connected to the chamber via flat cable. The circuit and the DWC are both placed in the aluminum box and outputs are connected, as in Figure 3.28. A calibration signal is applied at the center of the chamber and the output signals as in Figure 3.28c are observed. The observed signals are compatible with those expected for the calibration.

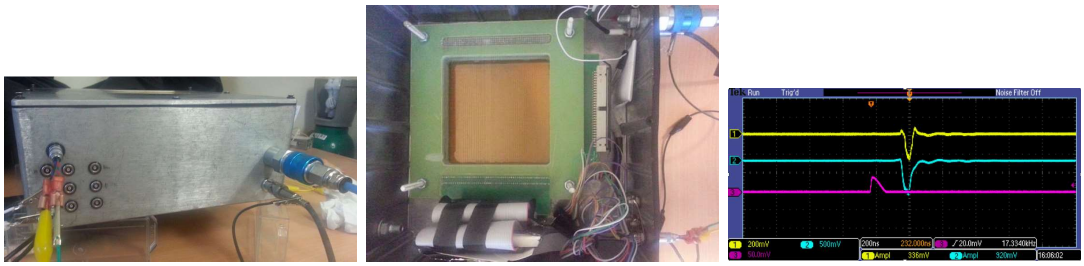

(a) Input and outputs of the metal box (b) DWC in metal box with the connections (c) Output when the calibration signal is applied at the center

Figure 3.28: DWC in the metal box and the calibration signals

Then the detector is tested with cosmic particles. The box is closed as described before and the gas flow is maintained for one hour. The trigger is set to 150mV on the oscilloscope. No signal is observed at 2500V. When the HV is increased to 3200V, a signal rate of 0.2Hz is observed. At 3500V, the signal rate reaches approximately 1.0Hz. Some of the signals observed at the oscilloscope screen can be seen in Figure 3.29. One can see that the height of the signals vary, probably because of the angle of incidence of the cosmic particles. The time difference is also varying between the two ends and is less than 250ns, an indication that the particles are passing randomly through the detector.

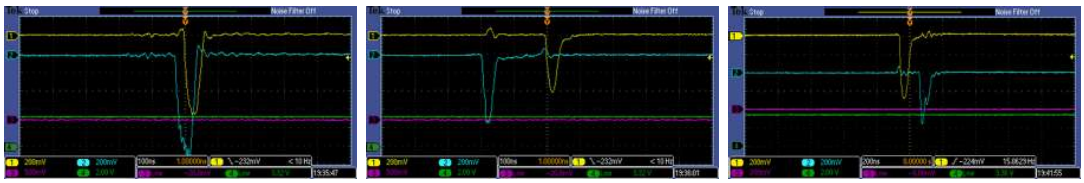

Figure 3.29: The screen-shot of the oscilloscope for the signals of the cosmic particles. Blue and yellow: readout from either end of the detector. Green: HV applied (scaled by a factor of 1000)

The DWC has also been tested at CERN Gaseous Detector Laboratory. The gas system and the readout system of CERN is used for these tests. The tests are performed with Sr-90 radioactive material with activity of 200kBq, which creates 0.546MeV electrons. The signals as seen in Figure 3.30 are compatible with the expected signals and the time difference was changing as we move the source over the chamber.

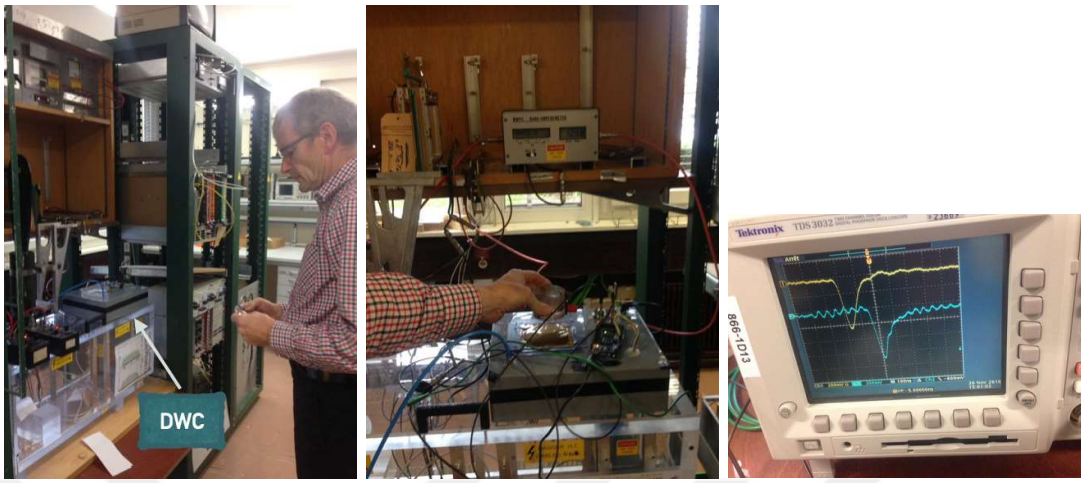

(a) DWC at the CERN Gaseous Detector Laboratory (b) Sr-90 over DWC (c) Sr-90 Signals

Figure 3.30: Tests at CERN using Sr-90 and example signals observed with the oscilloscope.

Finally, we have tested the DWC by triggering it with the scintillators at KAHVE-Lab. Two plastic scintillators are set such that a reasonable rate of coincidence is observed. Then the chamber is placed in between them as seen in Figure 3.31a. The output signals are shown in Figure 3.31b. The rate has been lower than expected but this might be because of inadequate adjustment of the thresholds.

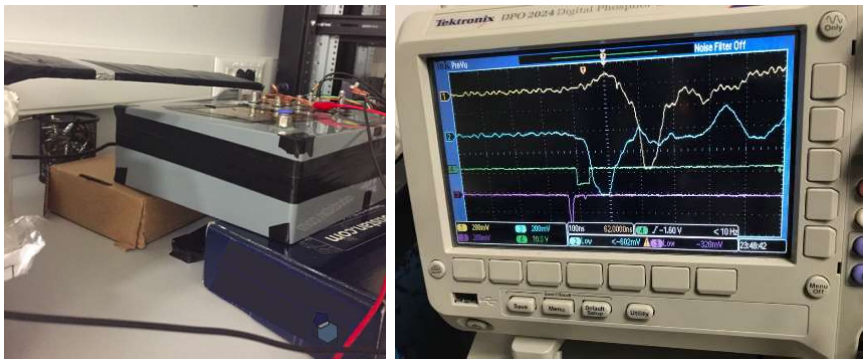

(a) DWC sandwiched between the scintillators (b) Coincidence and DWC signals

Figure 3.31: DWC placed between two scintillators and the output signals.

4. ATLAS TRANSITION RADIATION TRACKER

In addition to the spatial measurement of particles as in the DWC, gaseous detectors may also be used for particle identification. A good example of this is Transition Radiation Tracker (TRT) which is one of the subdetectors of the ATLAS experiment at CERN. It provides invaluable data used for tracking and electron identification. The detector comprises in form of tubes with radiator materials in between them to achieve transition radiation. Drift time of the particles that pass through the detector is measured and converted to drift radius. With the help of drift radius measurements tracking can be achieved.

Determination of the drift circle error has an important role in the classification of TRT hits. In this chapter, a method for calibrating drift circle errors in the TRT detector is introduced. Using pull distributions of drift radius and re-scaling drift circle errors with the sigma of the pull distributions, better calibration is achieved. The calibration is also scaled to the mean number of interaction per bunch cross, μ. In the calibration process, CERN ATLAS experiment 2015 Data and Monte Carlo (MC) simulation events are used. New errors are written on the ATLAS software database for different gas mixtures used in the TRT tubes. Data and MC results are compared for different variables and they are all found to be in good agreement.

4.1. ATLAS Detector

4.1.1. CERN and LHC

CERN stands for Conseil Européen pour la Recherche Nucléaire, the European Organization for Nuclear Research. It was founded in 1954 at the French-Swiss border. It is a multinational laboratory studying high energy physics and accelerator technologies.

Located at CERN, Large Hadron Collider (LHC) is the world's largest particle collider. It is located 50m-150m underground in a 27km circular tunnel. It housts four interaction points, at ALICE, ATLAS, CMS and LHCb experiments are situated as can be seen in Figure 4.1.

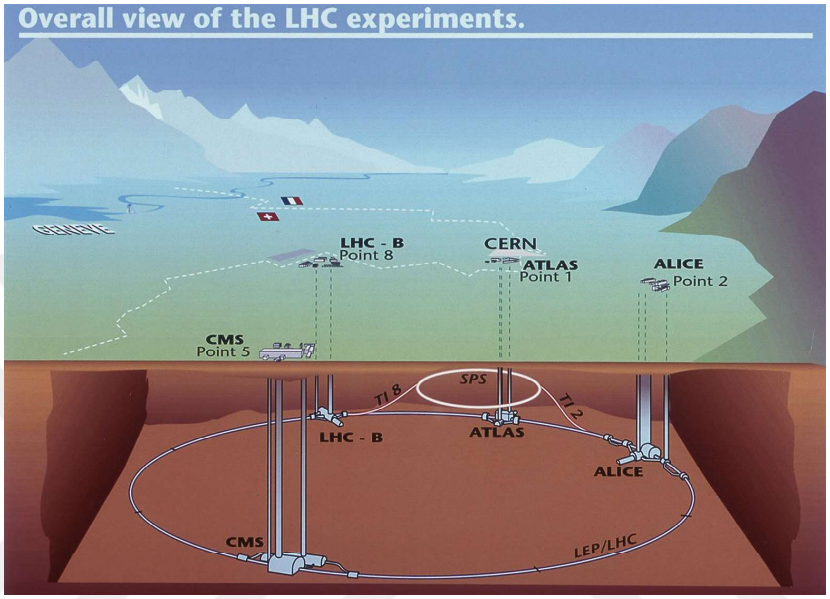

Figure 4.1: Overview of the LHC and the experiments [5].

The LHC has been designed to run at center of mass energy of 14TeV with $10^{34}\text{cm}^{-2}\text{s}^{-1}$ peak luminosity [28]. Bunches of proton or heavy ion beams cross through each other every 25ns, with an average 23 collisions per bunch cross.

4.1.2. The ATLAS Experiment

ATLAS experiment is one of the experiments at the LHC. It is a general purpose detector. Physicists are studying a wide range of toğics from the Higgs mechanism to beyond the Standart Model physics. It has dimensions of 25m×25m×44m, (Figure 4.2) and is arranged in the form of layers of detector one inside another. Different kinds of detectors, from solid state detectors to calorimeters, are used to measure position, momentum, type and energy of the particles.

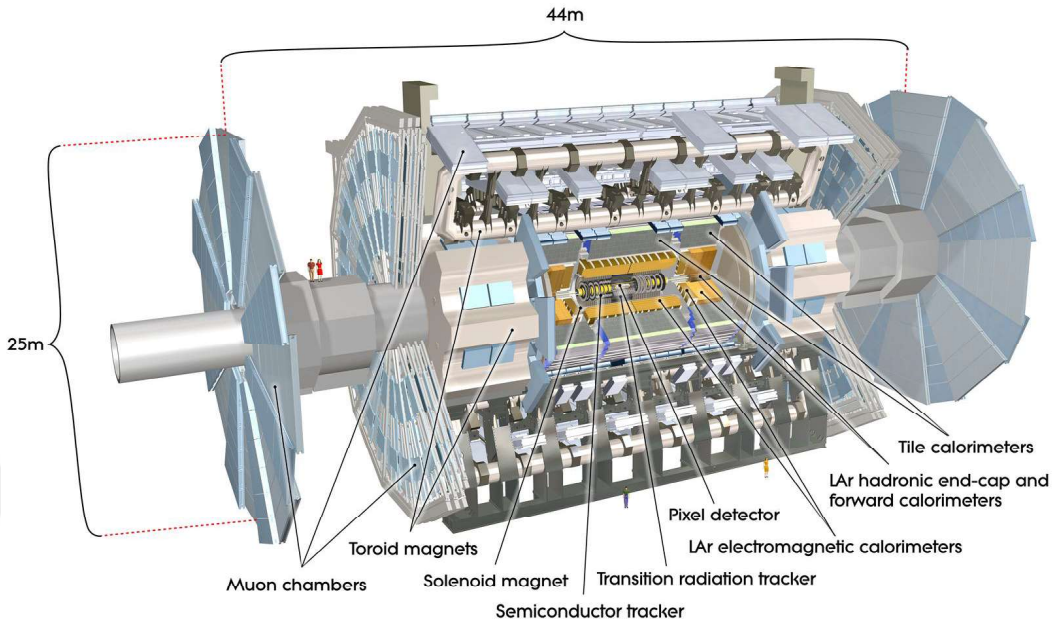

Figure 4.2: A cut away computer generated image of ATLAS detector [6].

4.1.3. ATLAS Detector Geometry and Track Parametrization

ATLAS detector is cylindrically symmetric and the origin of the coordinate system is taken to be the center of the detector. Bunches of the particles collide close to the origin. The z axis is along the beam line of LHC and with the $+z$ is taken to be clockwise along the LHC. $+z$ direction of the detector is called the A side and $-z$ direction of the detector is called the C side. $x-y$ plane is perpendicular to the beam line. $+x$ points to the center of LHC and $+y$ upward to the surface of the Earth.

Tracks are defined with 5 parameters in many collider experiments: z_0, d_0, θ, ϕ, q/p. Their geometrical depiction of the variables can be found in Figure 4.3 and the detailed definitions in Table 4.1.

Momentum of the particle is denoted by p and the projection of the momentum in the transverse plane is called transverse momentum, p_T. Transverse plane is also described in $r-\phi$ circular coordinates, where r is the distance from the beam line and ϕ is measured from the $x-$axis. Instead of polar angle, θ, pseudorapidity, η, may be

Table 4.1: Track parametrization in ATLAS (values taken from [7]).

Variable	Symbol	Definition
Longitudinal Impact Parameter	z_0	distance from interaction point to origin along z-direction
Transverse Impact Parameter	d_0	distance in $x-y$ plane from interaction point to the beam axis
Polar Angle	θ	Track angle with the z-axis
Azimuthal Angle	ϕ	Track angle in the $x-y$ plane
Track curvature	q/p	Curvature of the track

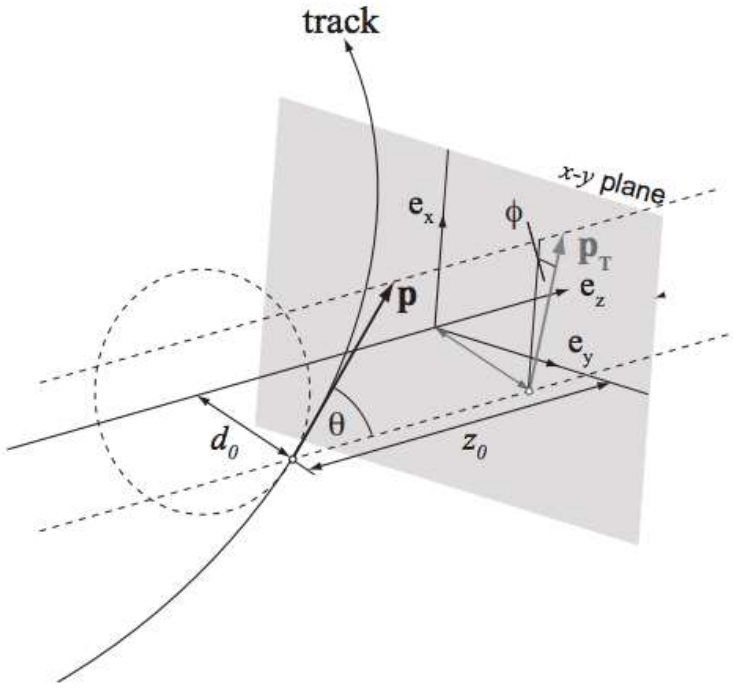

Figure 4.3: Track parametrization in the ATLAS coordinate system [7].

used as defined in Equation 4.1:

$$\eta = -\ln(\tan(\frac{\theta}{2})) \tag{4.1}$$

In the $\eta - \phi$ plane, distance ΔR is defined as in Equation 4.2.

$$\Delta R = \sqrt{\Delta\eta^2 + \Delta\phi^2} \tag{4.2}$$

4.1.4. Inner Detector

Inner detector (ID) is located at the core of the ATLAS Detector. It is composed of semiconductor and gaseous tracking detectors. Reconstruction of the vertices and the tracks particularly from primary particles is achieved with high efficiency. For example, the muon reconstruction efficiency is greater than 99%. ID also contributes to e, μ, γ identification when combined with information gathered from the calorimeter and muon system. ID provides signatures for short lived particle decay vertices. All of the inner detector section is contained in a solenoid magnet with field of $2T$. Inner detector of the ATLAS experiment has 3 main sections:

- **Pixel detector** : Pixel semiconductor detector provides space points of the particles close to the interaction point with high precision measurement and high granularity.
- **SCT detector** : Silicon MicroStrip (SCT) detector provides 4 precision measurements per track in the intermediate radial range. The space points of the SCT and Pixel detector can be used in measurements of momentum, impact parameter, vertex position and pattern recognition.
- **TRT detector** : Unlike Pixel and SCT, Transition Radiation Tracker (TRT) is a gaseous straw detector. TRT typically provides 36 measurements per track. With the help of the radiators between straws which cause transition radiation, TRT is capable of electron identification.

Table 4.2: Parameters of inner detector (values taken from [12]).

	Layer	Radii	Resolution (μm)	η coverage
Pixel	1 removable barrel layer	4cm	$R\phi = 12$, $z = 66$	± 2.5
	2 barrel layers	11cm,14cm	$R\phi = 12$, $z = 66$	± 1.7
	4 end-cap disks on each side	between 11cm-20cm	$R\phi = 12$, $z = 66$	$1.7 - 2.5$
SCT	4 barrel layers	30cm, 37cm, 45cm, 52cm	$R\phi = 16$, $z = 580$	± 1.4
	9 end-cap wheels on each side		$R\phi = 16$, $R = 580$	$1.4 - 2.5$
TRT	50000 Axial Barrel Straws	between 56cm-106cm	170 per straw	± 0.62
	120000 Radial End-cap Straws	between 64cm-100cm	170 per straw	$1.1 - 1.7$
	36 straws per track			

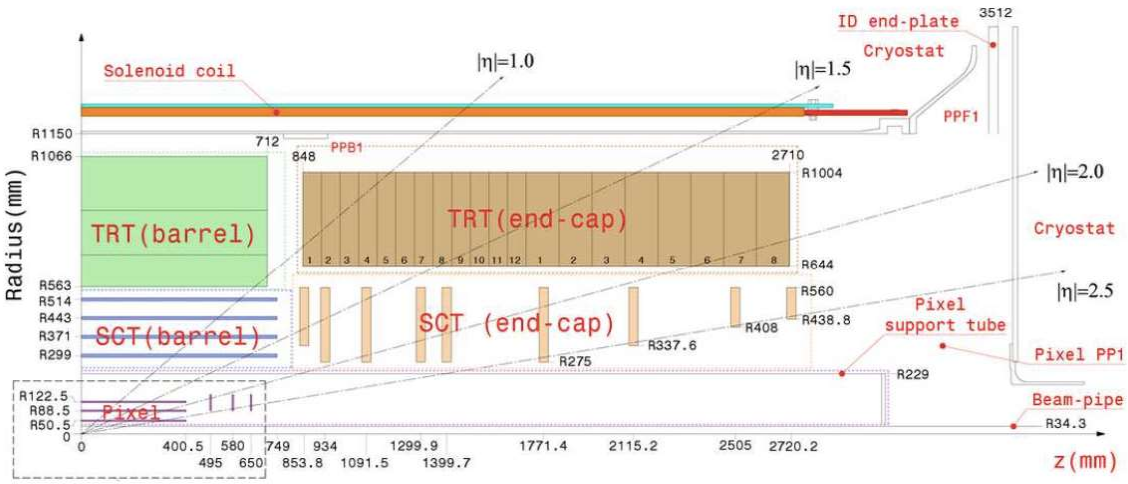

Figure 4.4: Schematic view of a quarter-section of the ATLAS Inner Detector showing each of the major elements with its active dimensions [8].

The dimensions and the configuration of the ID is sketched in Figure 4.4. The subcomponents with the radii, resolutions and the η coverrages of the each subdetector of ID is presented in Table 4.2.

4.1.5. Calorimeters

ATLAS Calorimeter system is used to determine the energy of the particles. Two types of calorimeters are used:

- **Liquid Argon Calorimeter** : Liquid Argon (LAr) Calorimeter uses liquid argon at $-183°$C as active medium. Energy resolution for electrons is 0.7% for high energies [18].
- **Tile Calorimeter** : Tile hadronic calorimeter is the central hadronic calorimeter. It is made of tiles of plastic scintillator and steel. It is a sampling calorimeter. Enery resolution of pions with energy between 16-30 GeV at SPS test beam is 6% [18].

The Schematic view of the calorimeter system is presented in Figure 4.5 while the geometry and the specifications of the subcalorimeters are summarized in Table 4.3.

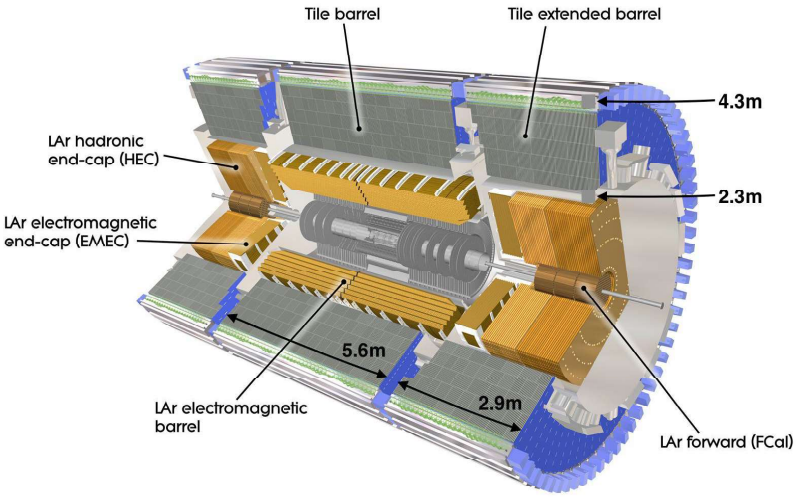

Figure 4.5: Schematic view of ATLAS Calorimeter system [9].

Table 4.3: Parameters of calorimeter system of ATLAS (values taken from [18], [19]).

	Layer	Absorber	number of layers	η coverage
LArCalo	Electromagnetic(EM)	Pb	3 layers+presampler	± 3.2
	Hadronic Endcap(HEC)	Cu	4 layers	$1.5 - 3.2$
	Forward (FCAL)	Cu or W	1EM + 2 hadronic layers	$3.1 - 4.9$
TileCalo	3 longitudinal layers	iron plates	3 longitudinal layers	± 1.7

4.1.6. Muon Spectrometer

The muon spectrometer is the outermost part of the ATLAS detector [20]. Muons pass through the inner detector and calorimeter system and are detected by the muon spectrometer. It has two main purposes; tracking of the muons in the magnetic field of the toroid magnet and triggering. In total, there are 4000 muon chambers and 4 different technologies of gaseous detectors are used as seen in Table 4.4.

MDT and CSC are used for momentum measurement and tracking of the muons. Designed momentum resolution is $\Delta p_T/p_T < 10^{-4} \times p/\text{GeV}$ for $p_T > 300\text{GeV}$. With the bending power of the ATLAS toroids, 3 points measurements are performed and momentum can be calculated using the curvature of the muon tracks.

RPC and TGC detectors are used for triggering and 2nd coordinate measurements. To achieve triggering, the bunch crossing identification has to be faster than the LHC bunch spacing of 25ns. With the measurement of the second coordinate, trigger with a well defined p_T is achieved.

Table 4.4: Parameters of muon spectrometer of ATLAS (values taken from [20], [21]).

		function	η coverage	# of chambers	Resolution
Muon Drift Tube	MDT	tracking	$\|\eta\| < 2.7$	1150	80μm position resolution
Cathode Strip Chamber	CSC	tracking	$2.0 < \|\eta\| < 2.7$	32	60μm position resolution
Resistive Plate Chamber	RPC	trigger	$\|\eta\| < 1.05$	544	1.5ns time resolution
Thin Gap Chambers	TGC	trigger	$1.05 < \|\eta\| < 2.7$	3588	$> 99\%$ efficiency for 25ns gate

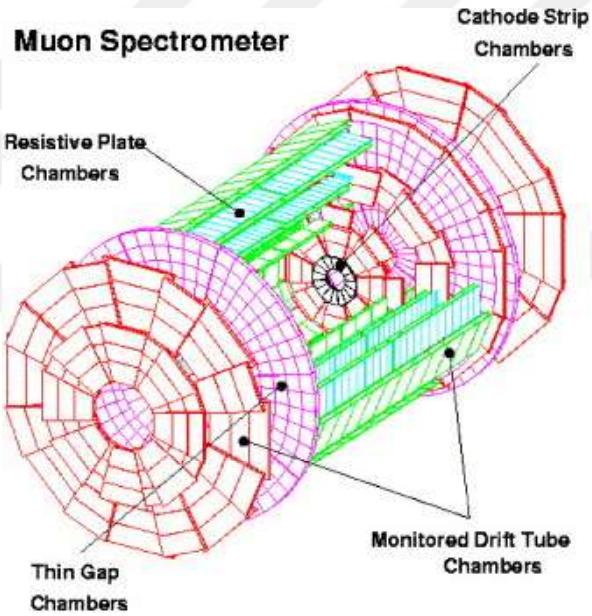

Figure 4.6: Schematic view of ATLAS Muon Spectrometer [10].

4.1.7. Magnet System

ATLAS magnet system provides magnetic field to bend charged particles to achieve measurement of momentum. It has 4 sections: a central solenoid, a barrel toroid and two end-cap toroids as can be seen in Figure 4.7 [11]. As a conductor, combinations of NbTi/Cu/Al are used. These are superconductor magnets with a cooling system down to 4.5K. Magnet parameters may be found in Table 4.5.

Table 4.5: Parameters of the magnet system of ATLAS (values taken from [11]).

	Inner diameter (m)	Outer diameter (m)	Axial Length(m)	Number of Coils	Peak Field (T)
Central Solenoid	2.44	2.63	5.3	1	2.6
Barrel Toroid	9.4	20.1	25.3	8	3.9
Endcap Toroids	1.65	10.7	5	8	4.1

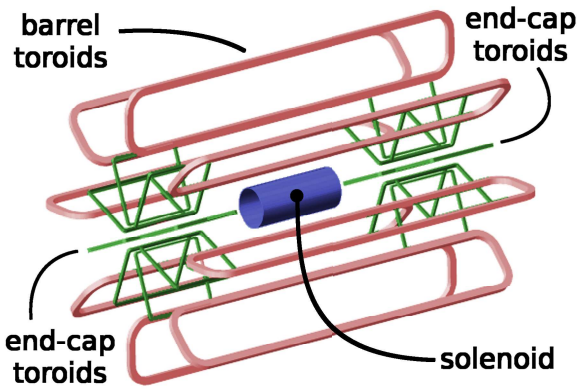

Figure 4.7: Schematic view of ATLAS Magnet System [11]

4.2. The TRT Detector

The TRT detector is the outermost component of the ATLAS Inner Detector as seen in Figure 4.4. It covers $|\eta| \leq 2$. It has three main parts, one barrel and two endcaps.

The TRT consists of over 350,000 Kapton straws with each straw having an outer radius of 2 mm and a central wire with a diameter of 31μm. Tube walls are made from alimunium coated kapton with the thickness of 20μm.

The straw walls of TRT are kept at negative high voltage around -1.5kV and central anode wires are grounded. Gas mixture of CO_2 ,O_2 and Ar or Xe is used. Gas gain is around 2500.

Straws in the barrel region are oriented parallel to the beam axis and covers

$|\eta| < 1$, 56cm $< r <$ 106cm and $|z| <$ 71cm. There are two endcap regions where straws are radially aligned with respect to the beam pipe covering $0.8 < |\eta| < 2$, 64cm $< r <$ 100cm and 84cm $< |z| <$ 271cm. End-cap straws are read from one end and barrel straws are read from two ends.

The main purposes of the TRT detector are tracking and electron-pion identification. It has a single hit design resolution of 130 μm. For a charged particle with $|\eta| \leq 2$ and $p_T \geq 0.5$GeV/c the detector gives on average 30 two dimensional space points. The TRT also contributes to particle identification making use of the transition radiation left by particles when they transverse different dielectric media [8]. Electrons with p_T greater than 5GeV/c can be separated from charged hadrons.

4.2.1. TRT working principle and variables.

When a particle passes through a TRT straw, it ionizes the gas inside. Because of the electric field created by the high voltage, electrons are drifted to the central anode wire and because of the magnetic field, they also bend. In Figure 4.8, the simulation of a track that pass through a TRT straw can be seen.

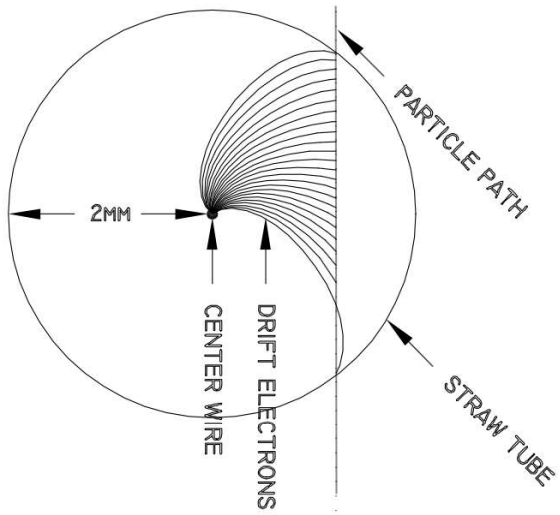

Figure 4.8: Simulation of a track passing through a TRT straw and the electrons are collected by the anode [12].

As mentioned before transition radiation (TR) is a form of electromagnetic radiation generated when particles pass through inhomogenious medium. Electrons and charged hadrons passing through TRT, create TR photons in x-ray region. Hovewer as the charged hadrons have greater mass, they emit less radiaon. The x-ray photons created by the radiating electrons can be detected. This helps to discriminate electrons from charged hadrons. If the signal from the straw is above a preset high threshold value, this means that there are TR photons in addition to the drifted electrons caused by the particles passing through.

The released electrons are collected from the anode of a TRT straw, 2 adjustable thresholds are set for characterizing and digitizing a signal: low threshold (LT) and high threshold (HT). HT is expected when transition radiation happens. An example signal and data read can be seen in Figure 4.9.

For each TRT straw the signal is read into a 27 bit word every 75ns. This corresponds to 3 ATLAS clock. Each word consists of 3 set of 9-bits. First 8 least significant bits give the signal amplitude with respect to low threshold. It is read in 25ns/8 = 3.125ns time intervals. If the LT is met then the bin is set to 1 and if the signal is below LT then the bit is set back to 0. These 8 bits are used for measuring drift time and used for tracking. 9th bit is set to 1 if the signal exceeds high threshold at some points in 25ns interval. This bit information is used for particle identification (PID).

As the bunch spacing decreased to 25ns in LHC, to keep data rate at acceptable level, 23 bits are transfered per straw by simply disregarding last 4 bits. Also a validity gate is introduced by which the signal is restricted to a certain time interval and only the middle HT bits are read. Data is compressed with Huffman lossless compression algorithm.

The time variables that can be extracted from the signal can seen in Figure 4.10. The definitions of the variables may be found in Table 4.6.

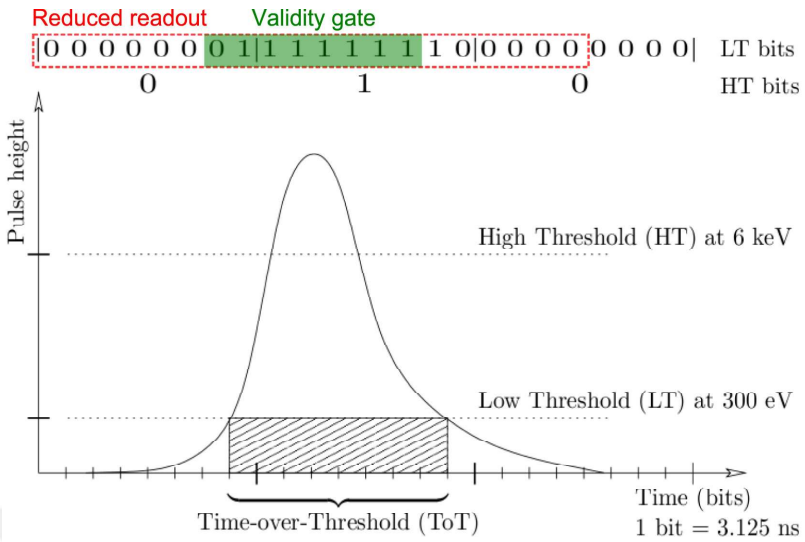

Figure 4.9: Example of a TRT signal and the data read [13].

4.2.2. Drift Circle Errors and Calibration

In the TRT, basically the drift time of particles is measured. The time difference between the signal taken from the TRT straw and the ATLAS internal clock is the TRT drift time. Measuring the drift time pricely and assuming that the drift velocity of the electrons are well known, we can calculate the drift radius, i.e. the closest distance between the track and the anode wire. The relation between the drift time and drift radius relation can be best understood by studying the $R(t)$ relation. As seen from Figure 4.11, if we plot drift time versus track to wire distance, we can fit a third degree polynomial to $R(t)$ and obtain the drift radius.

Using drift radius and the error on it, TRT hits are categorized into one of four types [15], in Figure 4.13:

- **Precision hit:** A hit with a measured drift radius within $\mp 2\sigma$ of the fitted track. A precision hit may be recognized by checking if the error on radius is less than 1.15 mm.
- **Tube hit:** A hit that is inside the straw wall but not precise. For all tube hits, a drift radius is assigned to be zero and error is assigned to be 1.15 mm. Tube

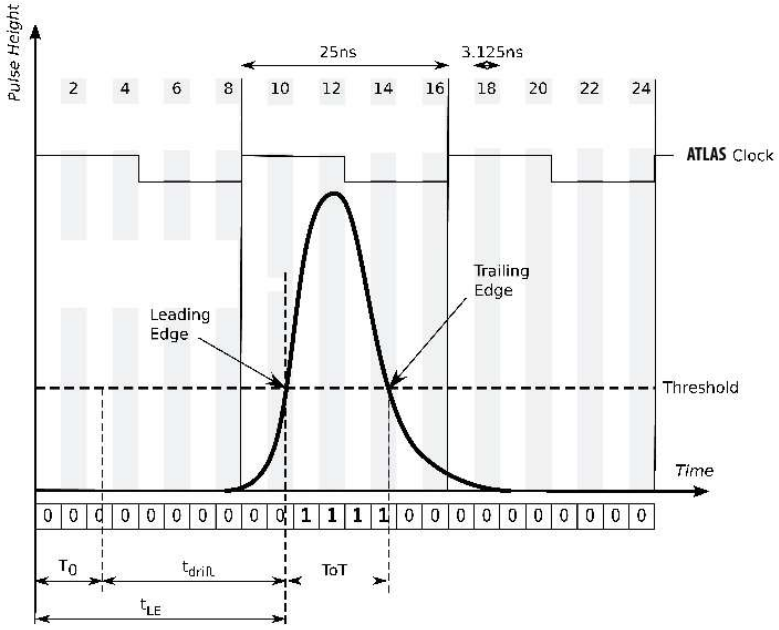

Figure 4.10: TRT time variables read from the straw signal [12].

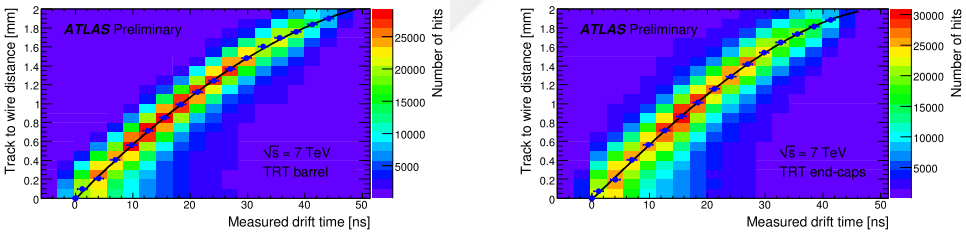

(a) Barrel (b) Endcap

Figure 4.11: TRT $R(t)$ dependency for barrel and end-caps. The tracks used to populate these plots are required to have at least 6 hits in the SCT and at least 20 hits in the TRT. [14]

hits are used in pattern recognition and in track fitting.

- **Outlier:** A hit on track for which the fitted track passes 100 μm or further from the straw wall. For all outlier hits, a drift radius is assigned to be zero and error is assigned to be 1.15 mm. Outliers are used only in pattern recognition.
- **Hole:** Straws crossed by a fitted track but with no hit.

While constructing the track, precision hits contribute more than the tube hits and the outlier hits and holes do not contribute. Hence, it is important to correctly

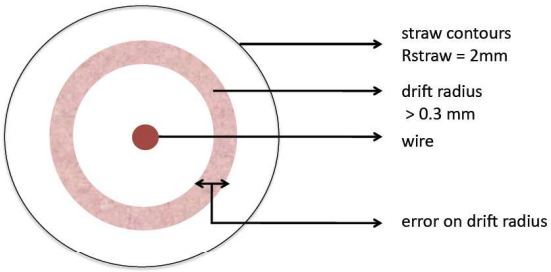

Figure 4.12: Definition of Drift Circle Error. [15]

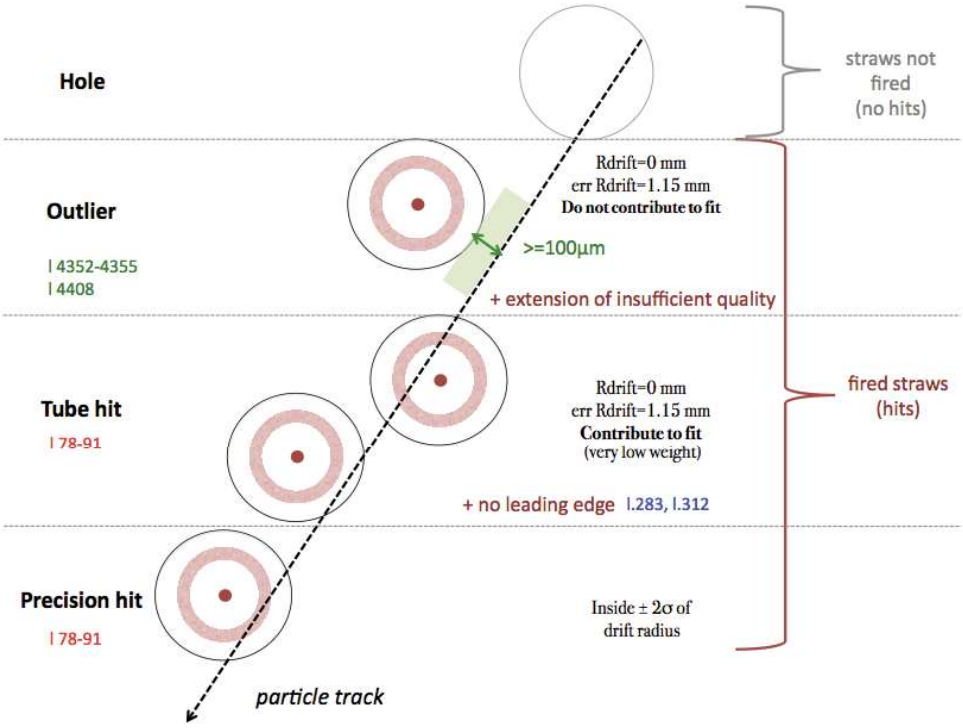

Figure 4.13: Definitions of TRT hits [15].

Table 4.6: TRT time variables.

Variable	Symbol	Definition
Leading Edge Time	t_{LE}	First transition from 0 to 1. Electrons drifting produced in the cluster of the closest approach
Trailing Edge Time	t_{TE}	First transition from 1 to 0. Electrons drifting from cluster produced far away from wire
Time over threshold	t_{ToT}	$t_{ToT} = t_{TE} - t_{LE}$. Related to the ionization power of the charged particles
Collision Time	$t_{collision}$	Time for collision with respect to the LHC clock. (Systematical effect)
Time of Flight	t_{ToF}	Time that pass for particles to reach the straw from the interaction point (Systematical effect).
Signal Propogation Time	t_{SP}	Delay in readout system
Electron drift time	t	$t = t_{LE} - (t_{collision} - t_{ToF} + t_{SP})$. Related to drift radius i.e. distance from the wire to the track of the particle
Calibration Constant	T_0	With respect to the ATLAS Time

identify the type of a hit. To determine the type, a correct determination of the error on the drift circle radius is critical. Any miscalibration may lead to a misselection of the type of a hit which will result in an error in the track reconstruction and so in physics analyses.

4.2.3. Pull distribution of TRT Drift Circle Error

TRT drift circle error calibration is performed based on the pull distribution of the drift radius. The pull distribution is commonly used to check an experimental technique when we know the true value for a set of measurements. In the TRT detector, the true value of the drift circle may be obtained from the track reconstruction. So for

this case, the pull is defined as:

$$\text{Pull} = (r - r_{track})/\sigma_r \tag{4.3}$$

where r is the drift radius, r_{track} is the track to wire distance of the hit, and σ_r is the expected value of the error of the drift radius.

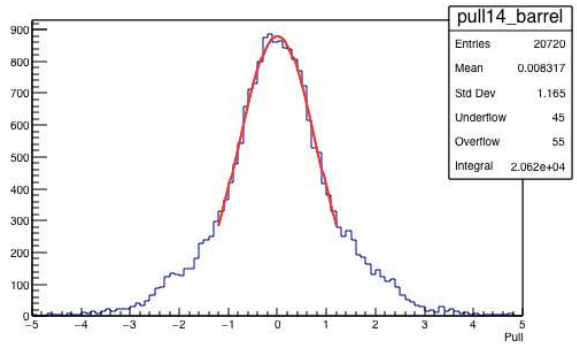

Figure 4.14: Pull distribution for the drift circle radius of a selected Ar-filled straw.

Ideally, we expect the pull distribution to be Gaussian centered at zero with unit standard deviation. If there is a problem with the measurement or the setting of the errors:

- Mean different than 0 implies bias in measurement.
- If $\sigma < 1$, the expected value of σ_r has been overestimated.
- If $\sigma > 1$, the expected value of σ_r has been underestimated.

4.3. TRT Drift Circle Error Calibration

As described in Section 4.2, drift circle error calibration is an important issue for the assignment of TRT hit types hence it changes the selection of TRT hits in analyses. In this section, the calibration procedure is described in detail.

4.3.1. Calibration using Pull Distributions

A new method for TRT drift circle error has been introduced by [8]. The pull value is defined in accordance with the previous section as;

$$Pull = \frac{\Delta r}{\delta r} \tag{4.4}$$

Δr is the position residual of the hit and δr corresponds to the error on residual. For unbiased evaluation of the residual error:

$$\delta r = \sqrt{\delta r_{hit}^2 + \delta r_{track}^2} \tag{4.5}$$

If the errors associated with hits and tracks are set correctly this pull distribution is expected to be a Gaussian with a width of 1. If not, the error may be underestimated or overestimated as explained before.

For example, if we plot drift time versus the pull sigma, in a perfectly calibrated detector, we expect the pull sigma to be equal to 1 for all values of the drift time. But as seen from the Figure 4.15, the pull sigma values is far from unity for almost all bins of the drift time.

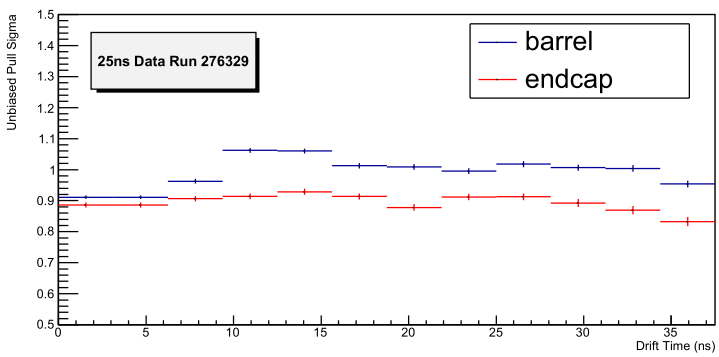

Figure 4.15: Pull sigma vs drift time obtained using Data 2015 (Run 276329) for Barrel and Endcap Argon straws. Drift time is divided between [0:37.5ns] with each bin 3.125ns.

In order to fix the error definition, an iterative calibration method is used. First, the pull for each bin is computed as:

$$Pull^i = \frac{\Delta r}{\sqrt{\delta r_{hit}^{i2} + \delta r_{track}^2}} \tag{4.6}$$

Here, δr_{hit}^i is the residual error for the time bin i used in reconstruction. Then, the hit error of the time bin is updated as:

$$\delta r_{hit}^{i\prime} = \delta r_{hit}^i \times \sigma(Pull^i) \tag{4.7}$$

For good calibration, this operation is performed multiple times. After each iteration, the pull sigma values approach unity more.

4.3.2. Drift Circle Error vs Mean Number of Interactions per Bunch Crossing

Prior to this calibration procedure, drift circle errors were kept as a function of drift time in the database and were being scaled by the same parameter independant of the mean number of interactions per bunch crossing (μ). But as can be seen from Figure 4.16, the pull sigma values do not seem to be 1 for all μ values.

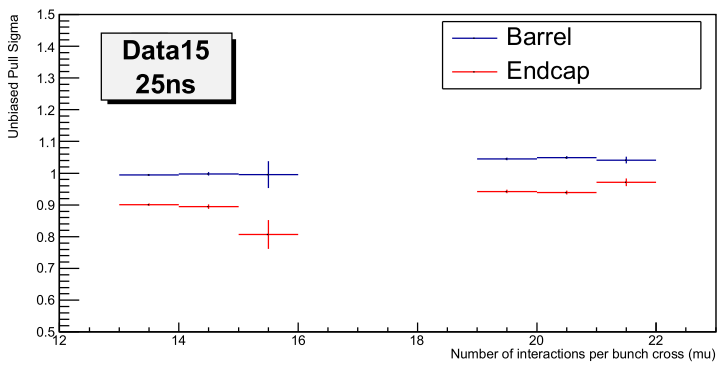

Figure 4.16: Pull sigma vs μ for Data 2015 for Barrel and Endcap Argon straws.

To adress this issue, in the database, drift circle errors for each drift time bin has

been parametrized by a first order polynomial function. This calibration is performed for MC15 and Data15 MinBias Stream (25 ns). For Xenon and Argon Straws and for Barrel and Endcap, calibrations are performed separately and then they are combined. Parametrization is performed by:

$$Error^i_{new} = Error^i_0 + Slope^i \times \mu \tag{4.8}$$

where $Error^i_0$ is the error value for μ equals to zero and $Slope^i$ is the slope for i^{th} drift time bin. New errors may be calculated using these parameters which is labeled as $Error^i_{new}$

The Monte Carlo simulation samples used for the study are inelastic minimum bias samples generated with Pythia 8 using the MSTW 2008 parton distribution functions. The 13 TeV data samples come into two sets, one for $\mu = 10 - 15$, another for $\mu = 15 - 20$. The technical details of the samples can be found in Appendix.

Hits are selected from tracks satisfying the following requirements::

- $|\eta| < 2$
- $|d_0| < 2$cm
- $p_T > 2000$MeV

Calibration has been performed for time range of [0ns:50ns] divided into 16 bins of 3.125ns.

4.3.3. Implementation

The ATLAS TRT detector uses Xenon in most of the straws and Argon in some straws in the 2015 detector configuration. The gas configuration of the 2015 geometry can be seen in Figure 4.17. So to select the gas following criteria are used:

- Argon:
  - Barrel layer 0
  - Endcap (side C) layer 3
  - Endcap (side A) layer 5
- Xenon: all other straws.

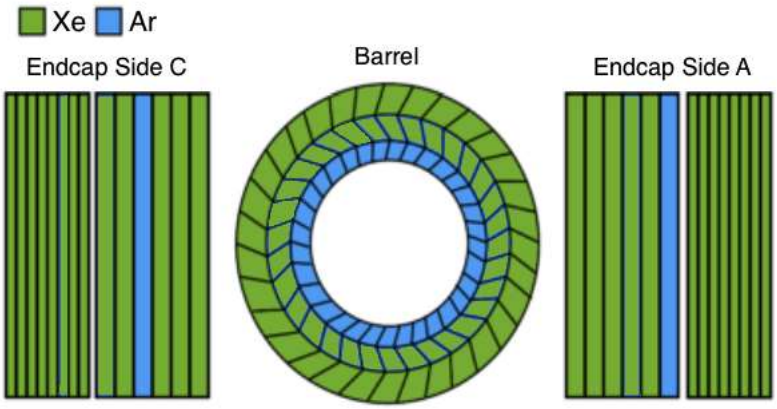

Figure 4.17: ATLAS TRT detector gas geometry in 2015 [16].

To perform the calibration Athena Release 20.1.6.4 is used. The packages used are given in the Appendix.

Furthermore, the following changes are made:

- Validity gate opened (switched off).
- μ variable added.
- Calibration output format fixed.

The calibration output files have a new file format, where the $R(t)$ relation, $R(t)$ errors and $R(t)$ slopes are included. $R(t)$ errors are the errors while $\mu = 0$ and $R(t)$ slopes gives the error correlations with respect to μ values. They are calculated for each gas separately and then combined. MC and Data calibrations are done separately for different μ ranges and then they are compared.

4.4. Results

Results and the validation plots can be seen in the following sections.

4.4.1. Change in the pull sigma values

As can be seen from Figures 4.18, 4.19, 4.20, 4.21 the pull sigma values come closer to unity after the drift circle error calibration has been performed.

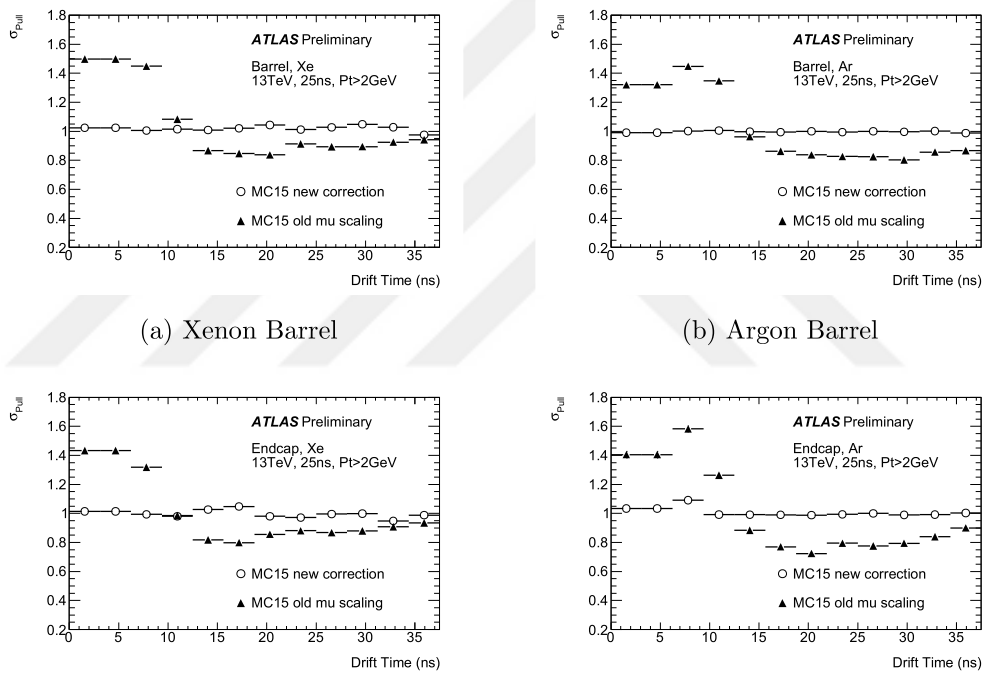

(a) Xenon Barrel (b) Argon Barrel

(c) Xenon Endcap (d) Argon Endcap

Figure 4.18: Pull Sigma vs drift time MC15.

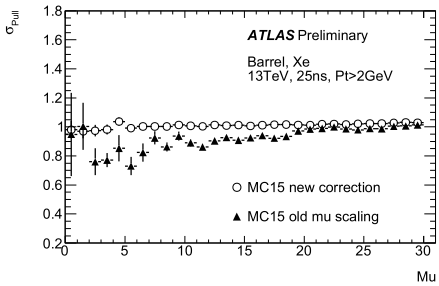

(a) Xenon Barrel

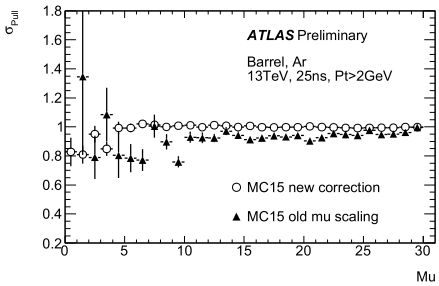

(b) Argon Barrel

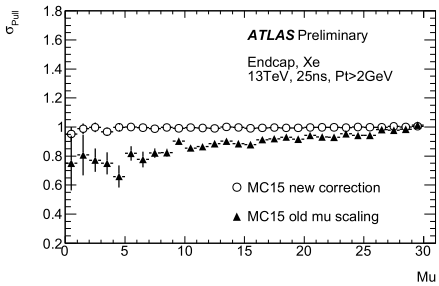

(c) Xenon Endcap

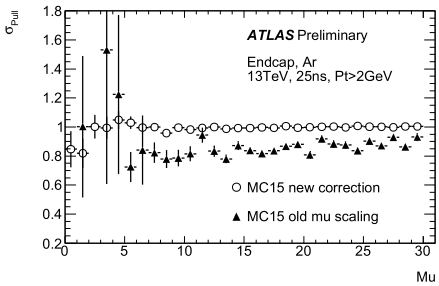

(d) Argon Endcap

Figure 4.19: Pull Sigma vs μ for MC15.

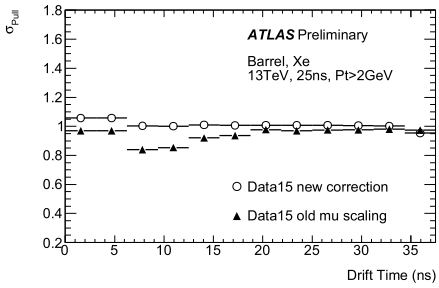

(a) Xenon Barrel

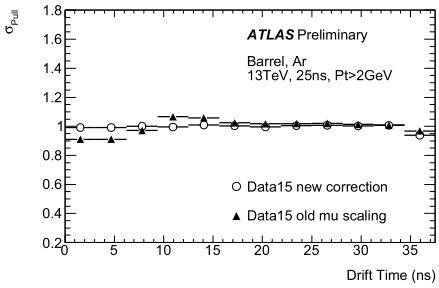

(b) Argon Barrel

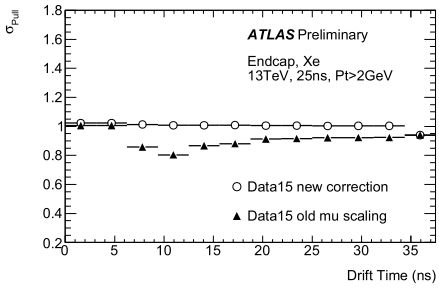

(c) Xenon Endcap

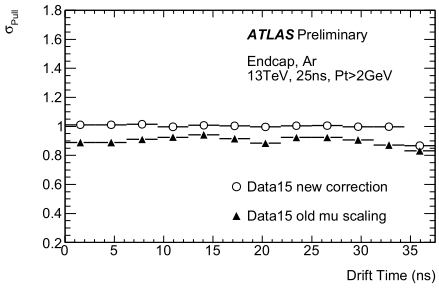

(d) Argon Endcap

Figure 4.20: Pull Sigma vs drift time for Data15.

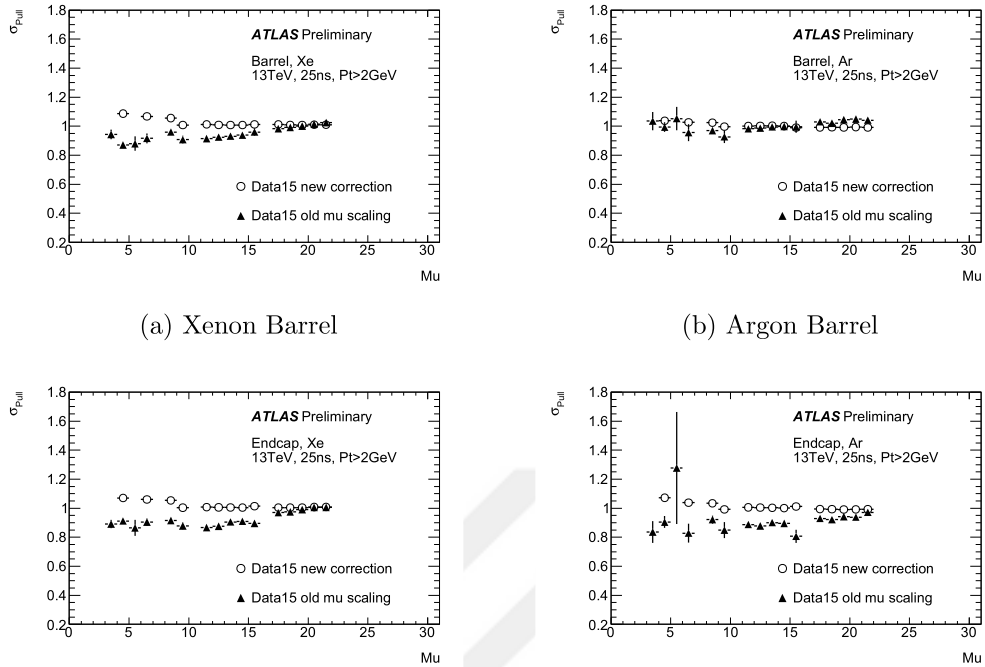

(a) Xenon Barrel (b) Argon Barrel

(c) Xenon Endcap (d) Argon Endcap

Figure 4.21: Pull Sigma vs μ for Data15

4.4.2. Validation

In this section, a comparison of Data15 and MC15 will be presented before and after the Drift Circle Error calibration with respect to μ has been applied.

Before the new calibration without μ scaling, one can see the comparison of position residual vs drift time in Figure 4.22 and position residual vs μ in Figure 4.23. Also precision hit fraction vs drift time and μ can be seen in Figure 4.24 and 4.25 respectively.

After the calibration, position residual vs drift time and μ in Figures 4.26, 4.27 and precision hit fraction vs drift time and μ in Figures 4.28, 4.29 are presented.

As can be seen from the figures, Data and Monte Carlo are consistent after calibration.

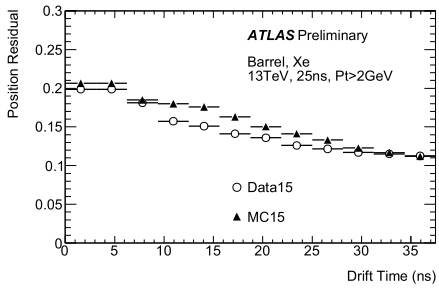

(a) Xenon Barrel

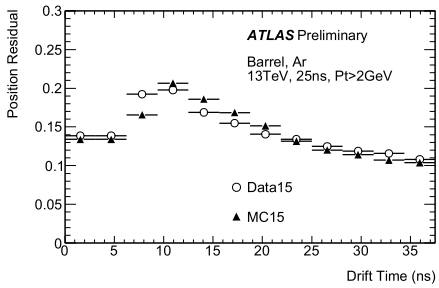

(b) Argon Barrel

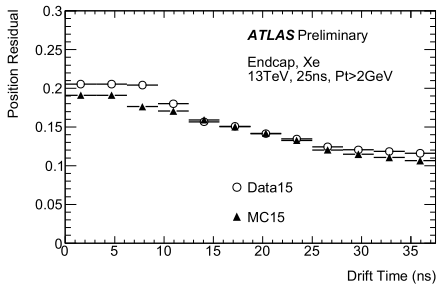

(c) Xenon Endcap

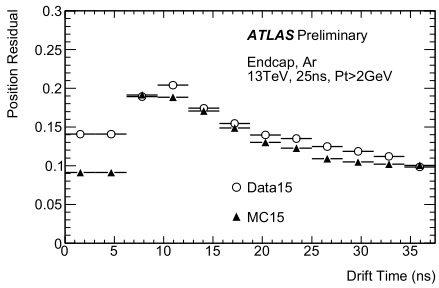

(d) Argon Endcap

Figure 4.22: Position Residual vs Drift Time before calibration with the old μ scaling

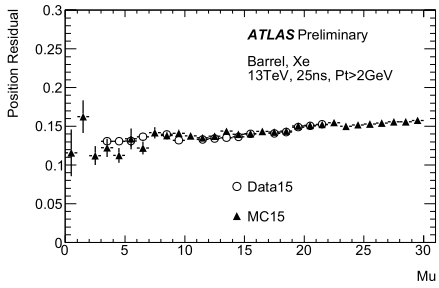

(a) Xenon Barrel

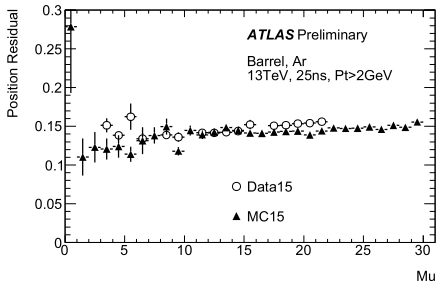

(b) Argon Barrel

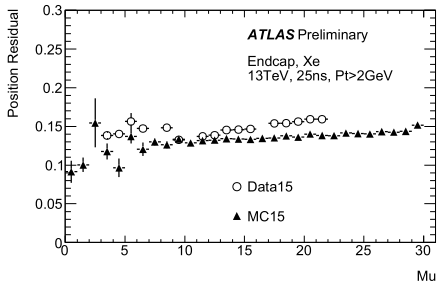

(c) Xenon Endcap

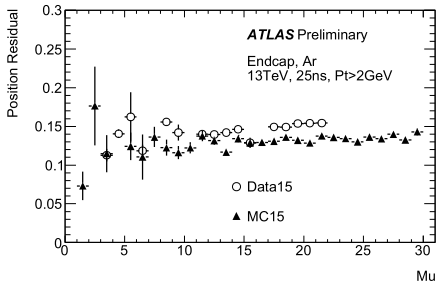

(d) Argon Endcap

Figure 4.23: Position Residual vs μ before calibration with the old μ scaling

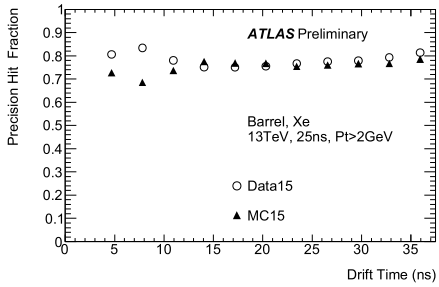

(a) Xenon Barrel

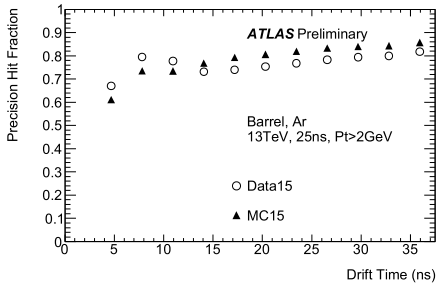

(b) Argon Barrel

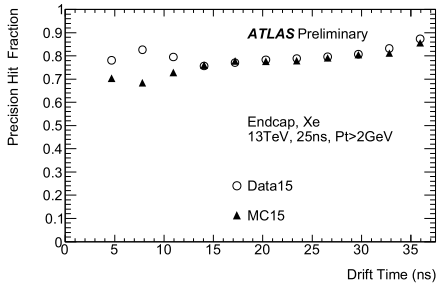

(c) Xenon Endcap

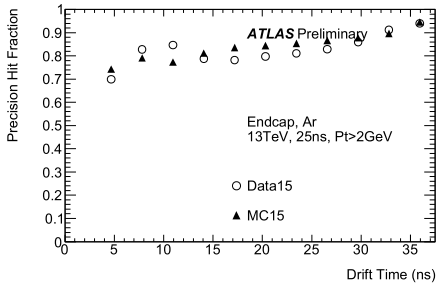

(d) Argon Endcap

Figure 4.24: Precision Hit fraction vs Drift Time before calibration with the old μ scaling

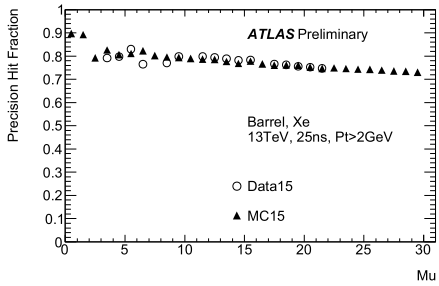

(a) Xenon Barrel

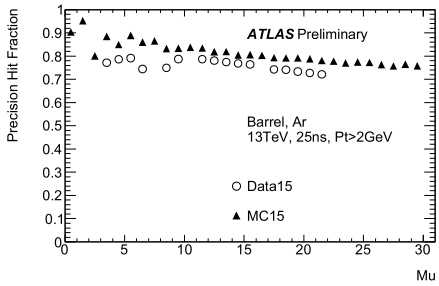

(b) Argon Barrel

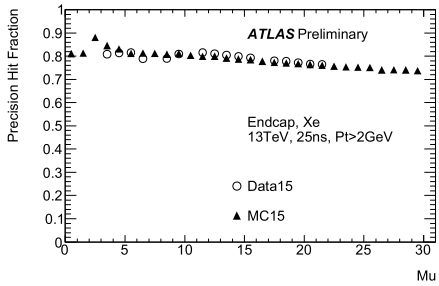

(c) Xenon Endcap

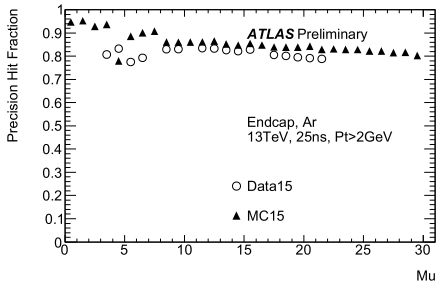

(d) Argon Endcap

Figure 4.25: Precision hit fraction vs μ before calibration with the old μ scaling

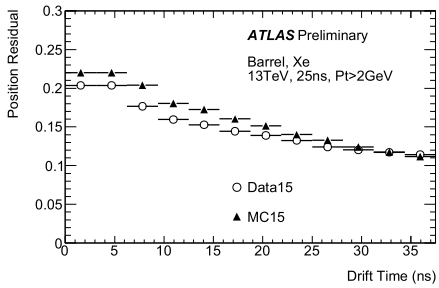

(a) Xenon Barrel

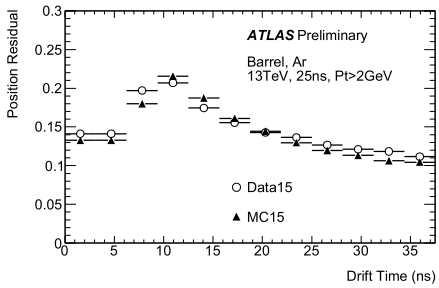

(b) Argon Barrel

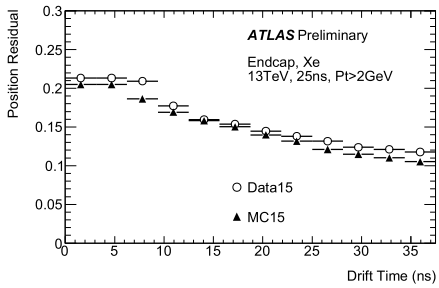

(c) Xenon Endcap

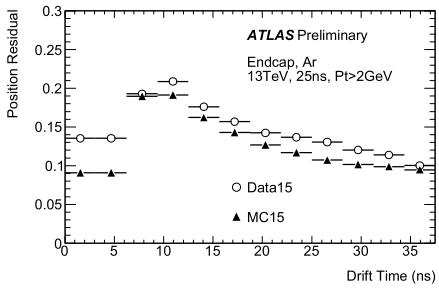

(d) Argon Endcap

Figure 4.26: Position Residual vs Drift Time after new calibration

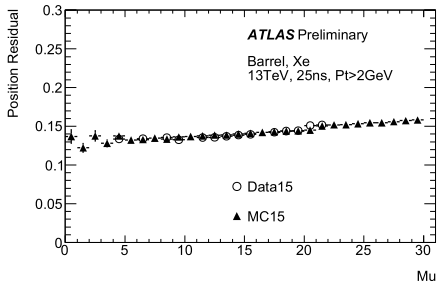

(a) Xenon Barrel

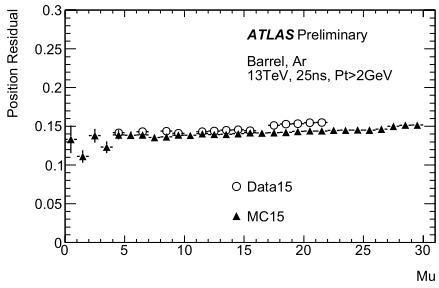

(b) Argon Barrel

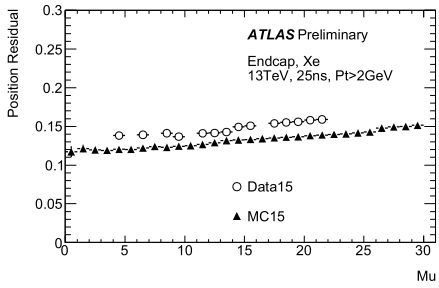

(c) Xenon Endcap

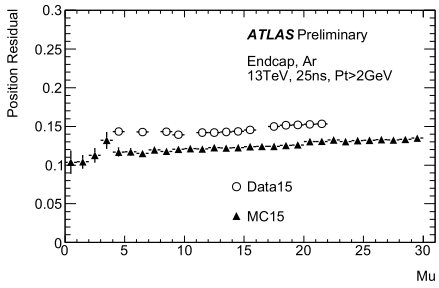

(d) Argon Endcap

Figure 4.27: Position Residual vs μ after new calibration

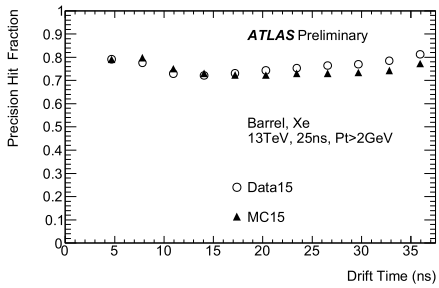

(a) Xenon Barrel

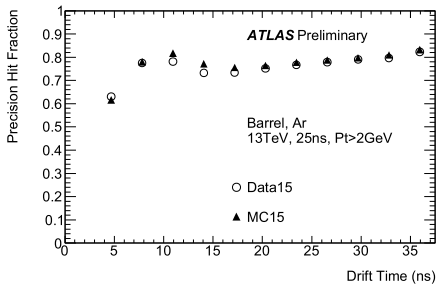

(b) Argon Barrel

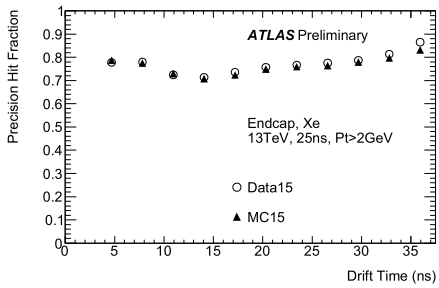

(c) Xenon Endcap

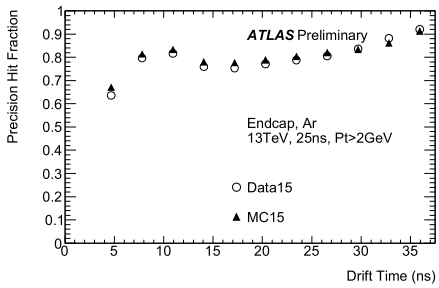

(d) Argon Endcap

Figure 4.28: Precision Hit fraction vs Drift Time after new calibration

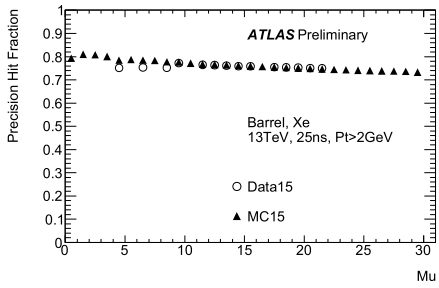

(a) Xenon Barrel

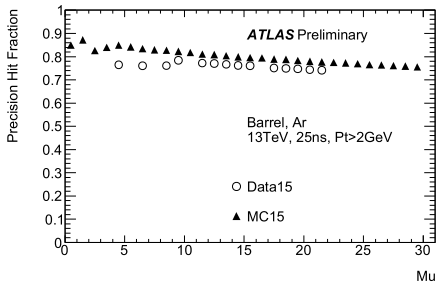

(b) Argon Barrel

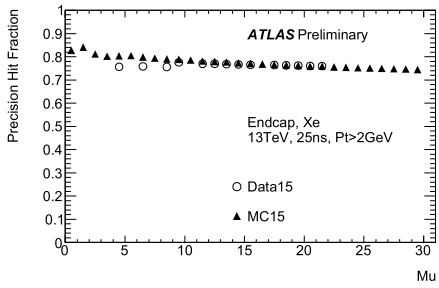

(c) Xenon Endcap

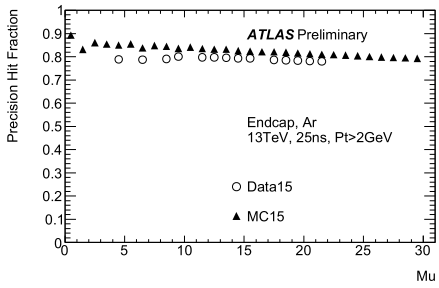

(d) Argon Endcap

Figure 4.29: Precision hit fraction vs μ after new calibration

5. ATLAS Z+JETS BACKGROUND CONTAMINATION MEASUREMENT USING DIBOSON +X ANALYSIS FRAMEWORK

Grand unification theories like the E6 model, proposed by Feza Gursey and his colleagues [29, 30], foresee heavy isosinglet quarks. Such exotic quarks can be pair-produced in the LHC and decay into the $ZHjj$ final state as in Figure 5.1. In order to identify their signals, it is vital to characterize and subtract the Standard Model(SM) backgrounds. The dominant backgrounds are from SM processes that have a Z boson in the final state and defining Controm Regions (CR) to measure and calibrate the background Monte Carlo (MC) simulations is important.

In this chapter, measurement of the fraction of $t\bar{t}V$ + $t\bar{t}$ contamination in the Z+jet control region of the $pp \rightarrow ZjHj$ analysis will be described. The measurement is done in ATLAS data using multivariate analysis techniques. Many variables such as P_T^Z and the number of b-tagged jets, which have different distributions for $t\bar{t}V$ and Z+jet samples, are used. The multivariate analysis methods are trained and tested using MC simulations and contamination percentage is measured in data taken by ATLAS detector at 2015 at $\sqrt{s} = 13$TeV with scaled to total integrated luminosity of $139\,\mathrm{fb}^{-1}$.

The dominant processes that may satisfy Z+jet CR cuts are shown in Figure 5.2.

The example of interactions that may pass after applying Z+jet CR cuts of relevant Monte Carlo (MC) samples are shown in Figure 5.2.

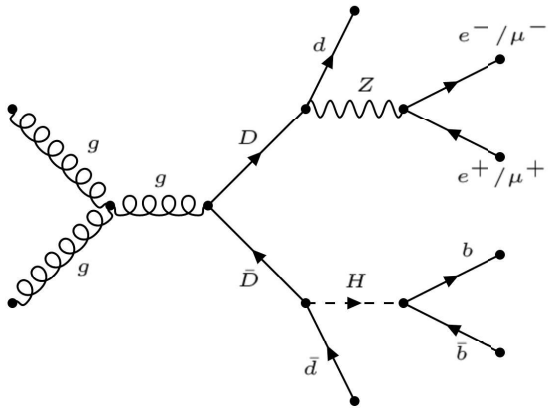

Figure 5.1: Iso-singlet quark pair decaying in the $H - Z$ channel, with the Z boson later decaying into a pair of charged leptons, and the H boson decaying into a pair of b-jets [17].

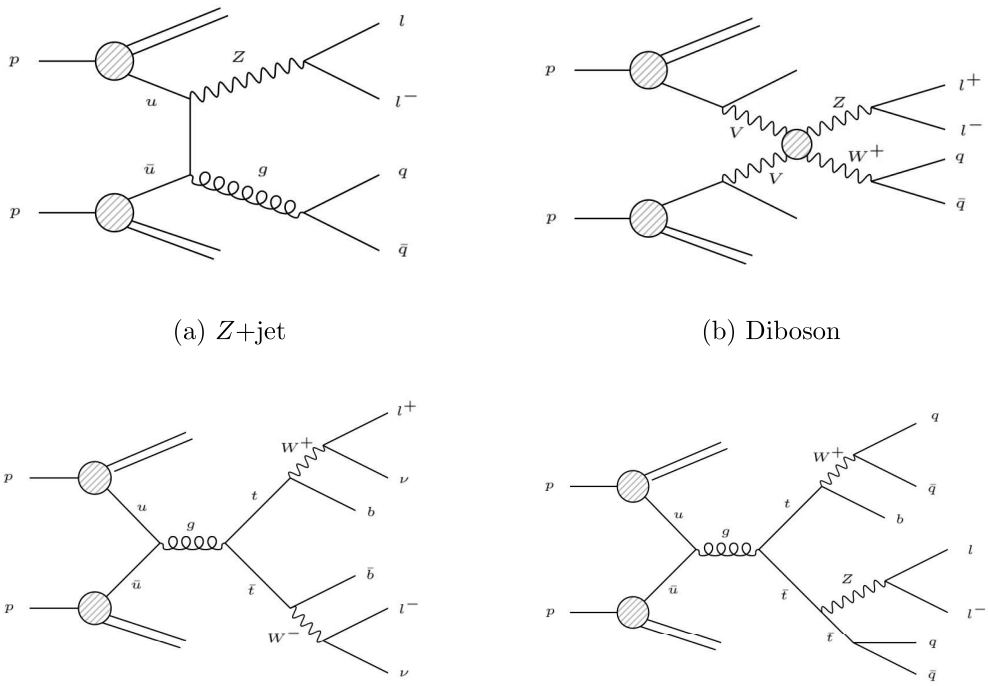

(a) Z+jet

(b) Diboson

(c) $t\bar{t}$

(d) $t\bar{t}V$

Figure 5.2: Example Feynman diagrams of background processes that pass through Z+jets CR cuts in the $ZHjj$ analysis.

5.1. Object Selection

The signals taken from the ATLAS detector are used to reconstruct objects of electron, muon and jets. These objects later form bosons, quarks and leptons in the analysis. In this analysis object identification criteria of the ATLAS VLQ analysis group [31] is used.

5.1.1. Electrons

The electrons are constructed if there is a signal on the electromagnetic calorimeter with a track in the inner detector matching. They are selected so that they do not fall in to barrel endcap transition region, so the pseudorapidity, η, range of electrons are either $|\eta| < 1.37$ or $1.52 < |\eta| < 2.47$. Minimum required transverse momentum is 28GeV [32–34]. Additionally, only the electron candidates originating from the primary vertex are selected . The full criteria list can be seen in Appendix F.

5.1.2. Muons

Muons are reconstructed from the signals of the muon spectrometer combined with the inner detector tracks. They should have transverse momentum of at least 28GeV with $|\eta| < 2.5$. Like electrons, they are required to originate from the primary vertex [35]. The full criteria list can be seen in Appendix F.

5.1.3. Jets

Small-R jets are constructed using anti-kt algorithm [36]. Anti-kt alogorithm is run with with the radius parameter of 0.4 and the clusters are selected [37, 38]. For the jets with $|\eta| < 2.5$, the requirement is $p_T > 25$GeV and for $2.5 < |\eta| < 4.5$, $p_T > 35$GeV. The full criteria list can be seen in Appendix F [36–42].

Anti-kt algorith is also run with the radius parameter of 1.0 and small-R jets are

reclustered. Furthermore, jets are b tagged.

5.1.4. Overlap Removal

To prevent labelling the same signal for the different objects at the same time, overlap removal is defined. For example, if a muon has a signal in the calorimeter and shares an ID track with an electron it is removed. After this step, electrons sharing an ID track with a muon is removed. Jets are removed against electron or muons if they satify predefined ΔR criteria. The full criteria list of the overlap removal can be seen in Appendix F.

5.2. Datasets and Event Selection

We are studying the contamination of the Z+jet control region of the $D\bar{D}$ analsis in the $HjZj$ channel. Using the objects described in Section 5.1, datasets and cut flow of the pair-produced heavy quarks decaying to $HjZj$ channel search [17] is used.

ATLAS detector data at $\sqrt{s} = 13$TeV with integrated luminosity of $139\,\mathrm{fb}^{-1}$ are used in the analysis. For the background Z+jet, $t\bar{t}$, diboson and $t\bar{t}$ associated with vector boson MC samples are used. These samples are generated using Sherpa 2.2.1, POWHEG-BOX, MC@NLO and MAGRAPH as can be seen in Appendix F.

The simulated background samples of the Z+jets, $t\bar{t}$, diboson and $t\bar{t}V$ samples are processed with the Z+jets cuts defined in Table 5.1 using the dbxA analysis framework. The analysis is done separately for $Z \to ee$ and $Z \to \mu\mu$ regions.

After the cuts, we can determine the contribution of the other MC samples to the Z+jets CR. The efficiencies after applying Z+jet CR cuts are shown in Figures 5.3, 5.4. The expected contribution of backgrounds can be seen in Table 5.2. These fractions are calculated using final weights after all cuts in the efficiency plots of the Figures 5.3, 5.4.

Table 5.1: Selection criteria for Z+jet control region (reproduced from [17]).

#	Cut	Explanation
0	ALL	Initial count with weights
1	nLEP ≥ 1	At least 1 electron or 1 muon
2	nLEP $= 2$	Exactly 2 leptons
3	qll $= 0$	Opposite sign and same flavor
4	LEPsf	Include lepton scale factor
5	$p_T^{ll} \geq 200$ GeV	2 lepton P_T
6	nJET ≥ 2	At least 2 Jets
7	SumHTJET ≥ 300 GeV	the scalar sum of the P_T of jets
8	nLJET ≥ 1	Number of reclustered jets
9	$m_{ll} \leq 400\,\text{GeV}$	Two lepton mass cut
10	nBJET ≥ 2	At least 2 b-tagged Jets
11	m_{ll} veto	$\lvert m_{ll} - m_Z \rvert > 10$ GeV and $\lvert m_{ll} \rvert > 50$ GeV
12	SumHTJET < 1050 GeV	the scalar sum of the pT of jets
13	$\chi^2 < 15$	reject event if no combination with total $\chi^2 < 15$ can be found
15	≥ 1 b-tagged Higgs daughter jet	At least one of the Higgs candidate's daughters should be b-tagged

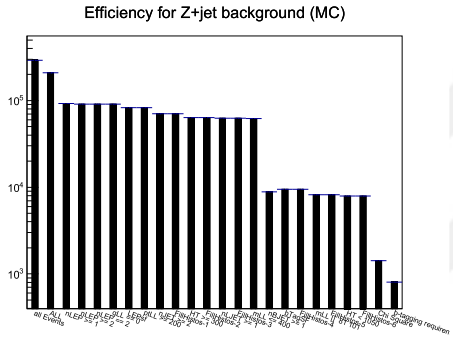

(a) Z+jet

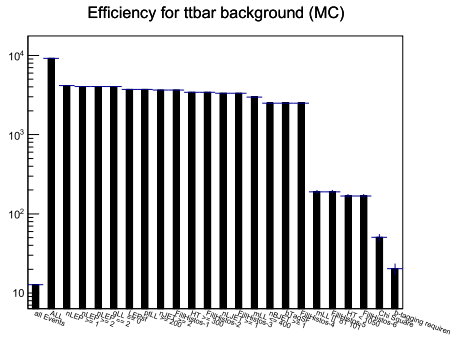

(b) $t\bar{t}$

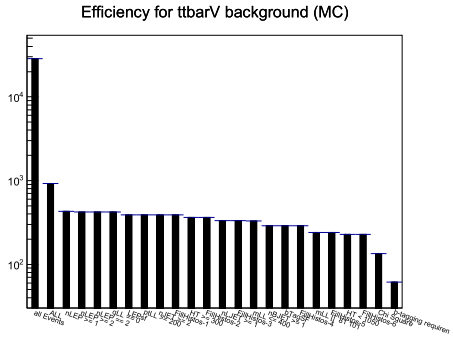

(c) $t\bar{t}V$

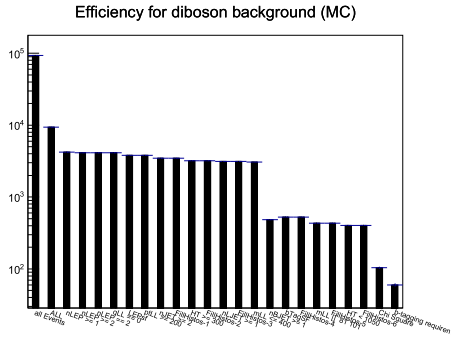

(d) diboson

Figure 5.3: Event yields for all backgrounds after Z+jet cuts for $Z \to ee$ channel.

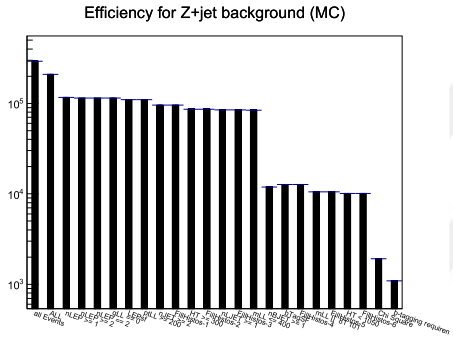

(a) Z+jet

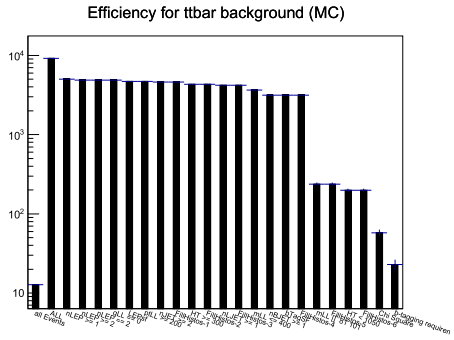

(b) $t\bar{t}$

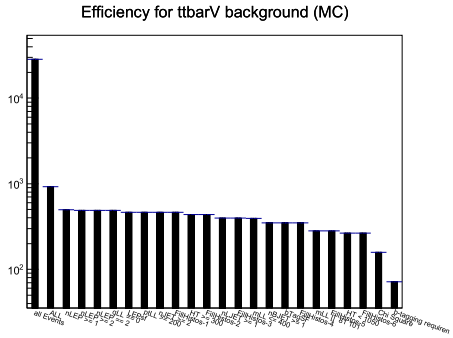

(c) $t\bar{t}V$

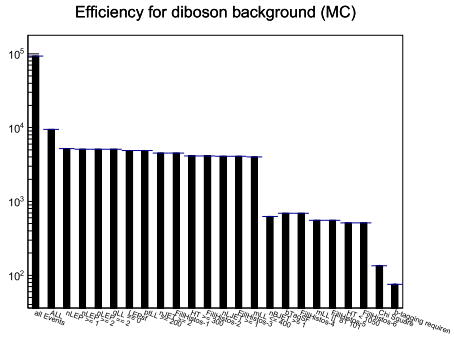

(d) diboson

Figure 5.4: Event yields for all backgrounds after Z+jet cuts for $Z \to \mu\mu$ channel.

Table 5.2: Z+jet CR contamination calculated from the event yields of the MC simulations.

Z+jet CR contamination				
	$Z \to ee$ channel		$Z \to \mu\mu$ channel	
Region	Total weight	Percentage	Total weight	Percentage
Z+jet	806.1	84.55	1088.7	85.98
diboson	59.9	6.28	75.1	5.93
$t\bar{t}$	20.2	2.12	22.9	1.81
$t\bar{t}V$	61.2	6.42	71.8	5.67
single top	1.0	0.10	3.18	0.25
signal	5.01	0.52	4.49	0.35
total	953.41	100.00	1266.17	100.00

The signal and single top processes are ignored in this analysis as the yields are low and their percentage contributions are less than 1%. We expect $t\bar{t}$ + $t\bar{t}V$ contamination in Z+jets CR region to be 8.64% (7.48%) for the $Z \to ee$ ($Z \to \mu\mu$) channel.

5.3. Variable distributions

To discriminate $t\bar{t}V$+$t\bar{t}$ events from Z+jet control region multivariate analysis methods are used. The variables studied are:

- P_T, mass, η of highest P_T (LEP0) and Second highest P_T (LEP1) lepton,
- P_T, mass, η of highest P_T (JET0) and Second highest P_T (JET1) jet
- Z (LEP0 + LEP1) mass, P_T, η, ϕ
- P_T and mass of dijet (i.e. LEP0 + LEP1)
- Angular distance, η difference and ϕ difference between LEP0 and LEP1
- Angular distance of Z to LEP0, LEP1, JET0, JET1, closest jet, closest b tagged jet and dijet
- Angular distance of LEP0 to JET0, closest jet and closest b tagged jet
- P_T and mass of reclustered jets
- Angular distance between Z and reclustered jets
- P_T, mass, η and angular distance to Z of far dijet (all possible combinations of jets are tested and the fartest to the Z is selected)
- P_T, mass, η, angular distance to Z of highest P_T dijet (all possible combinations of jets are tested and the highest P_T is selected)
- P_T, mass, η and angular distance to Z of highest η jet
- Missing Transverse Energy (MET)
- Number of b tagged jets
- Number of jet
- Number of reclustered jets

These variables have been studied with TMVA [43], using the Multilayer Perceptron method. As the Monte Carlo statistics is limited to train with too many variables, the most effective variables that create most separation between signal (Z+jet + diboson) and background ($t\bar{t}V$+$t\bar{t}$) are selected. These are:

- MET = Missing transverse energy
- $m^{jj(highestp_T)}$ = Mass of hightest P_T dijet among all combinations of jet couples
- n_{b-tag} = Number of b-tagged jets
- ${p_T}^{j0}$ = Transverse momentum of of highest P_T jet
- ${p_T}^{j(high\eta)}$ = Transverse momentum of highest η jet
- m_{joj1} = Mass of dijet constructed by highest P_T and second highest P_T jets
- $m^{j(high\eta)}$ = Mass of highest η jet
- ${p_T}^{Z}$ = Transverse momentum of Z
- ${p_T}^{l0}$ = Transverse momentum of highest P_T lepton
- $m^{jj(farZ)}$ = Mass of dijet (any two combination of jets) that is farest to Z
- η^Z = η of Z
- ${p_T}^{l1}$ = Transverse momentum of second highest P_T lepton

5.4. Multivariate Analysis Techniques

Using the variables, different Multivariate Analysis Techniques [44] are studied. Some of the methos studied are:

- Boosted Decision Trees (BDT)
- Multi-Layer Perceptron (Neural Network) (MLP) [45]
- Fisher discriminants (linear discriminant analysis)
- Likelihood classification (naive Bayes) with Spline PDF parametrisation
- PCA-transformed likelihood
- K-Nearest Neighbour classifier (KNN)
- H-Matrix (chi2-squared) method

The background rejection versus signal efficiency ("ROC curve") and reciprocal of background efficiency versus signal efficiency of the methods studied are shown in Figure 5.5. As can be seen from the ROC curves, BDT and MLP classifiers seem promising. As the distributions of the MLP method are more suitable for template fit, we continue our study using the MLP method.

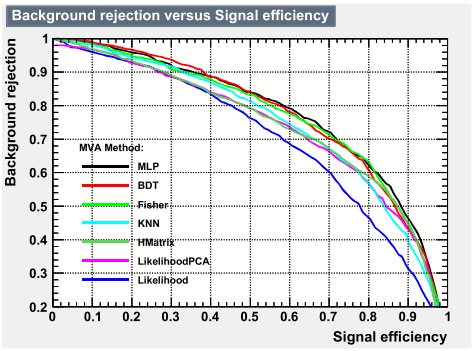

(a) The background rejection vs signal efficiency

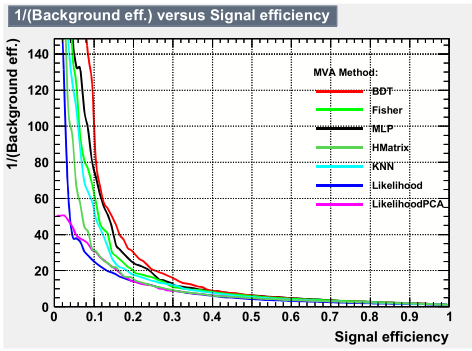

(b) Reciprocal of the background rejection vs signal efficiency

Figure 5.5: The background rejection and reciprocal of the background efficiency versus signal efficiency ("ROC curve")

5.5. Multi-Layer Perceptron studies

Multi-Layer perceptron (MLP) is a class of feedforward Artificial Neural Network (ANN). In an ANN, there are neurons whose output can take a value between 0 and 1. The input neurons are the variables from Section 5.3 and the output neurons give the probability if the event belongs to the signal (Z+jet + diboson) or background ($t\bar{t}$ + $t\bar{t}V$) regions. There are hidden layers inbetween and the neurons and these layers are connected with weights. In this analysis Toolkit for Multivariate Analysis (TMVA) [43] is used. The neural network layout can be seen from the Figure 5.6. While training the MLP classifier, Monte Carlo (MC) samples are used. Then, the weights are applied on the ATLAS data. The classifier output of the data is then fitted with a combination of the Z+jet + diboson and $t\bar{t}V$ + $t\bar{t}$ output using a template method.

The distributions of the selected input variables for signal and background regions can be seen from Figure 5.7 for the $Z \to ee$ and from Figure 5.8 for the $Z \to \mu\mu$ channel. The correlation matrices of the variables are presented in Figure 5.9 for $Z \to ee$ and the Figure 5.10 for $Z \to \mu\mu$ channel.

In our analysis, we used 5000 signal events and 5000 background events, randomly selected and normalized with the number of events for our training. Total number of

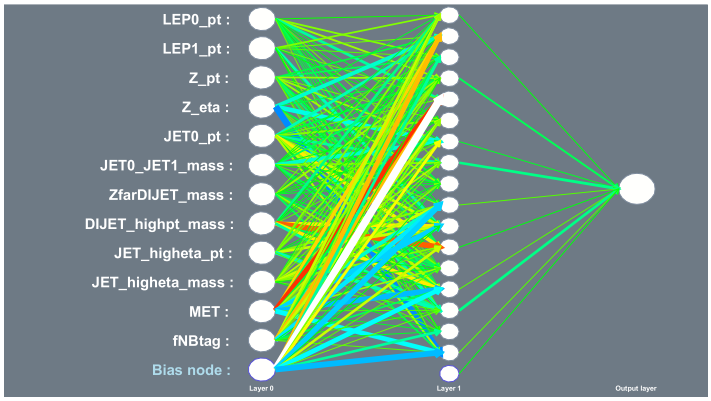

Figure 5.6: MLP neural network layout with number of variables plus 5 hidden layers. The thichness of the line represents the weight.

training and testing events are presented in Table 5.3. Neuron type of *tanh* is used with hidden layers as many as the number of input variables plus five. The classifier output distributions of the test and training samples are presented in Figure 5.11.

Table 5.3: Number of training and testing events for TMVA (Signal: Z+jet + diboson Background: $t\bar{t}V + t\bar{t}$).

for $Z \to ee$ channel			
Signal		Background	
Training Events	Testing Events	Training Events	Testing Events
5000	5246	5000	16285
Total = 10246		Total = 21285	
for $Z \to \mu\mu$ channel			
Signal		Background	
Training Events	Testing Events	Training Events	Testing Events
5000	8448	5000	24275
Total = 13488		Total = 29275	

After the training, the MLP output weights are weights are obtained for all MC samples and ATLAS data. The distributions may be seen in Figure 5.12. TMVA output gathered by the $t\bar{t}$ and $t\bar{t}V$ are very similar and the distributions of the diboson

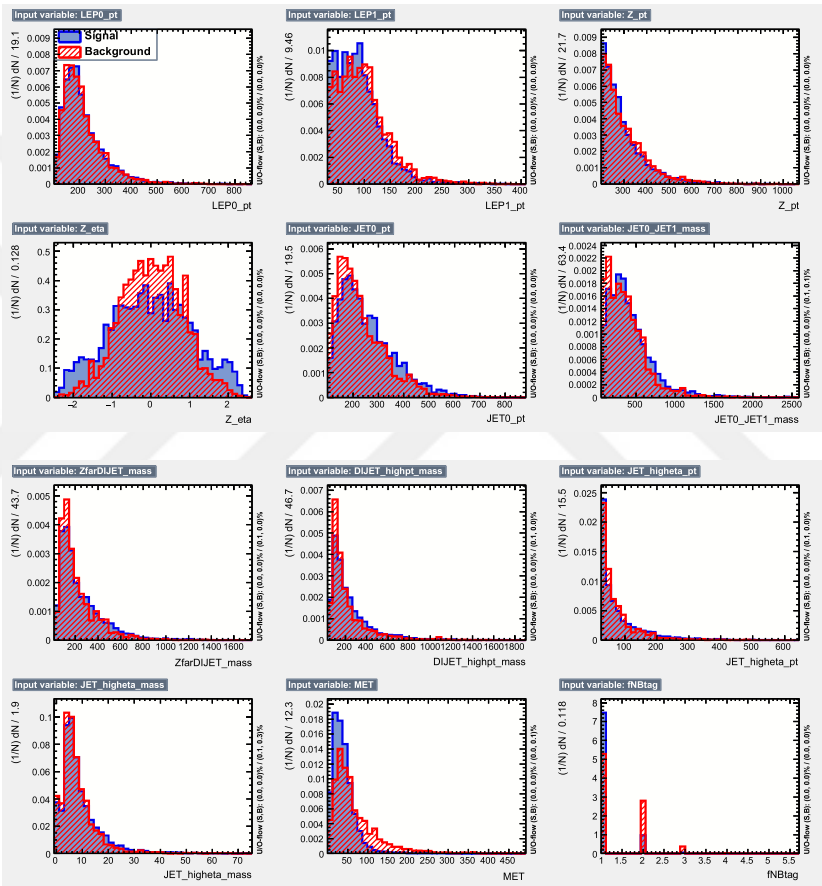

Figure 5.7: MVA input variables for Z+jet + diboson and $t\bar{t}V$ + $t\bar{t}$ background for $Z \to ee$. Z+jet + diboson labeled as the signal (blue) and $t\bar{t}V$ + $t\bar{t}$ labeled as the background (red).

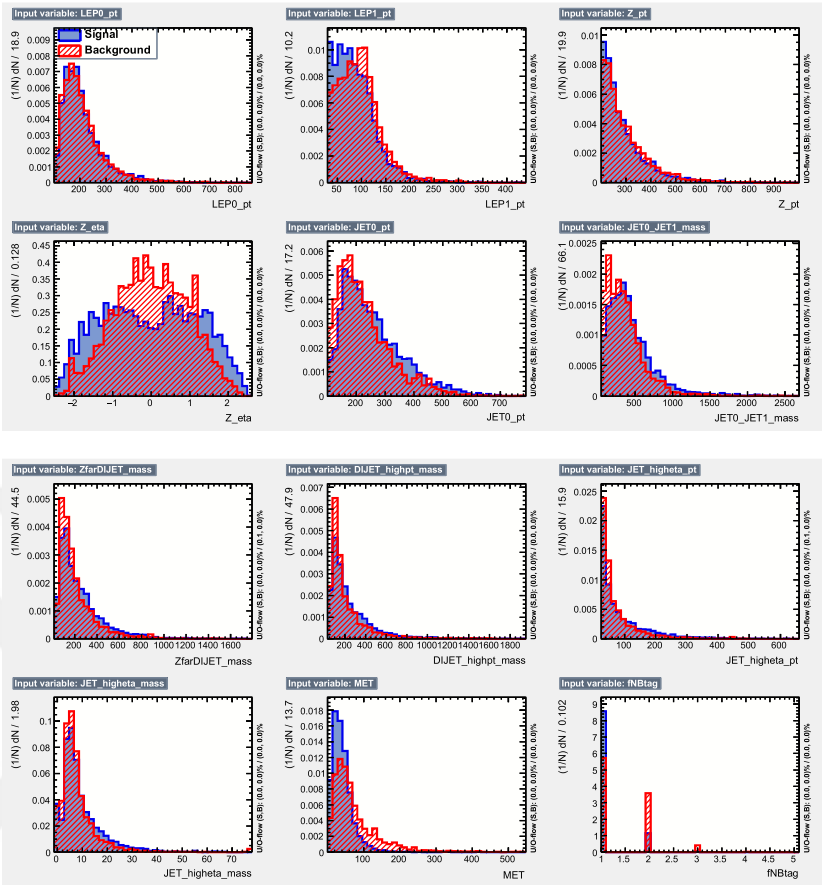

Figure 5.8: MVA input variables for Z+jet + diboson and $t\bar{t}V$ + $t\bar{t}$ background for $Z \to \mu\mu$. Z+jet + diboson labeled as the signal (blue) and $t\bar{t}V$ + $t\bar{t}$ labeled as the background (red).

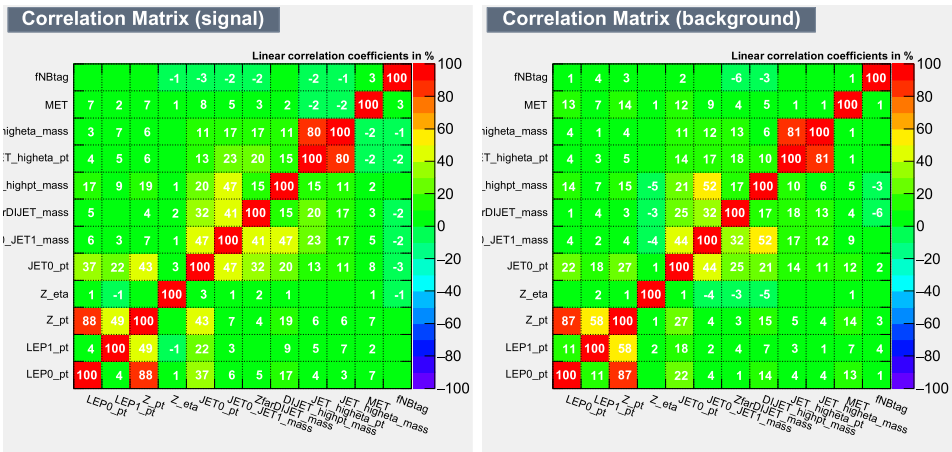

(a) Z+jet + diboson (b) $t\bar{t}V$ + $t\bar{t}$

Figure 5.9: Correlation matrices of the variables for Z+jet + diboson and $t\bar{t}V$ + $t\bar{t}$ backgrounds for $Z \to ee$.

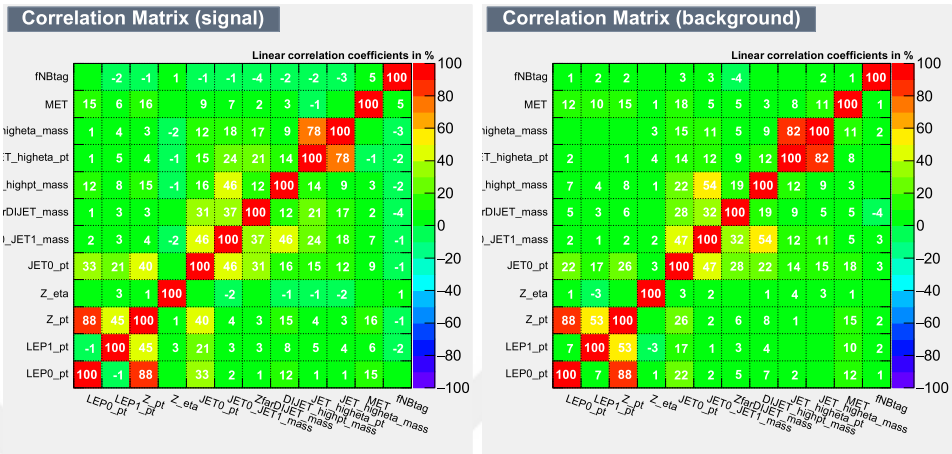

(a) Z+jet + diboson (b) $t\bar{t}V + t\bar{t}$

Figure 5.10: Correlation matrices of the variables for Z+jet + diboson and $t\bar{t}V + t\bar{t}$ backgrounds for $Z \to \mu\mu$.

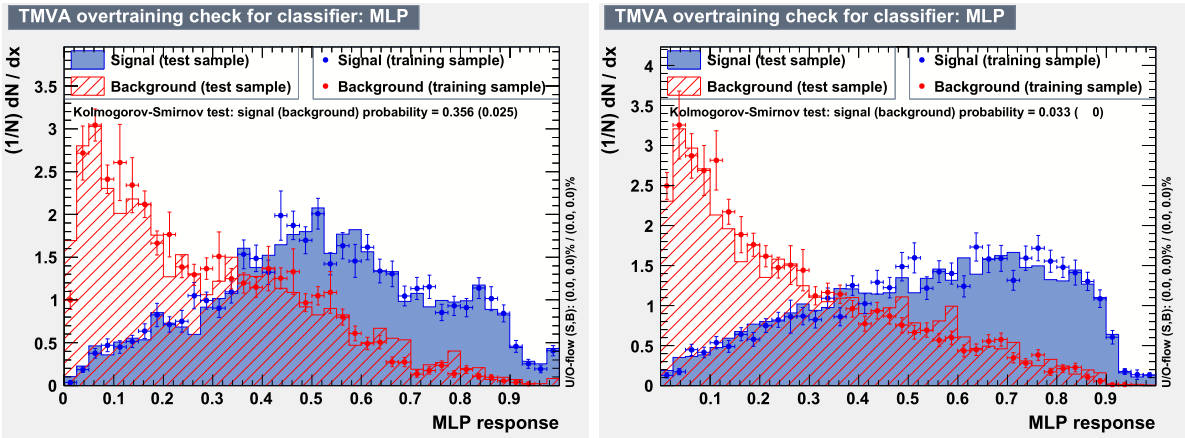

(a) $Z \to ee$ (b) $Z \to \mu\mu$

Figure 5.11: MLP Classifier Output Distributions (test and training samples superimposed).

and Z+jet are similar as expected. So combining Z+jet with the diboson sample and $t\bar{t}V$ with the $t\bar{t}$ sample helps us on the template fit.

Then by using TFractionFitter class of ROOT [46] a template fit is applied to data, see Figure 5.13. As calculated from the fit, $t\bar{t} + t\bar{t}V$ contamination of the Z+jet CR region is found to be $(8.4 \pm 4.1)\%$ (0.03σ away from the MC expected value of 8.64%) for $z \to ee$ region and $(7.4 \pm 3.0)\%$ (0.04σ away from the MC expected value of 7.48%) for $z \to \mu\mu$ region.

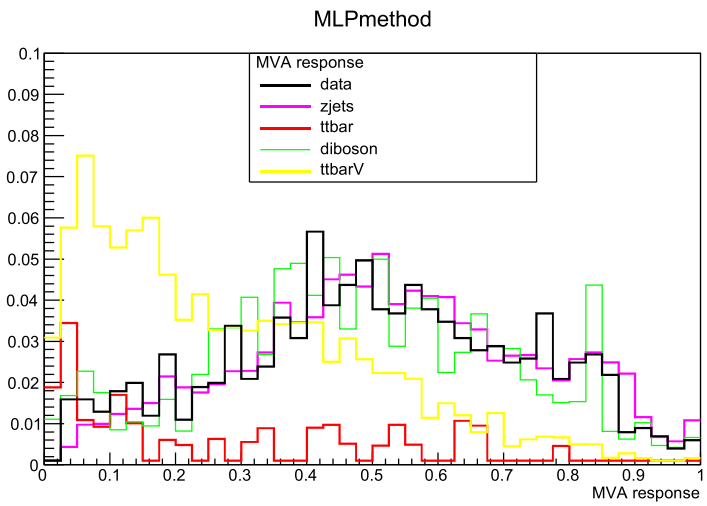

(a) $Z \to ee$

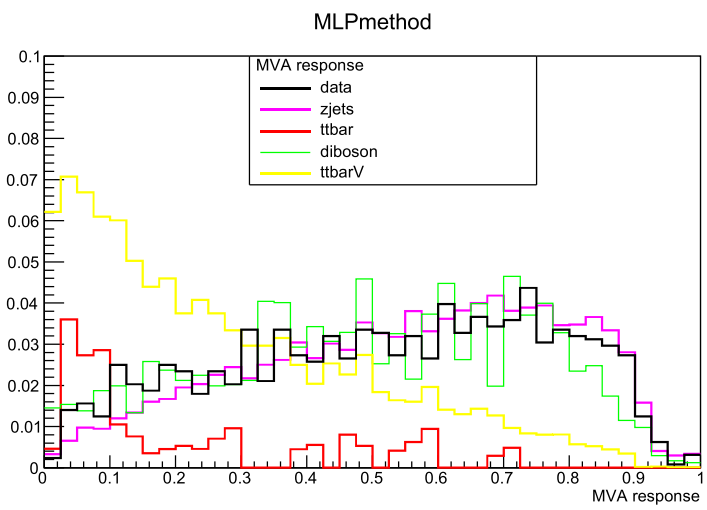

(b) $Z \to \mu\mu$

Figure 5.12: MLP output distribution for the MC background samples and ATLAS data.

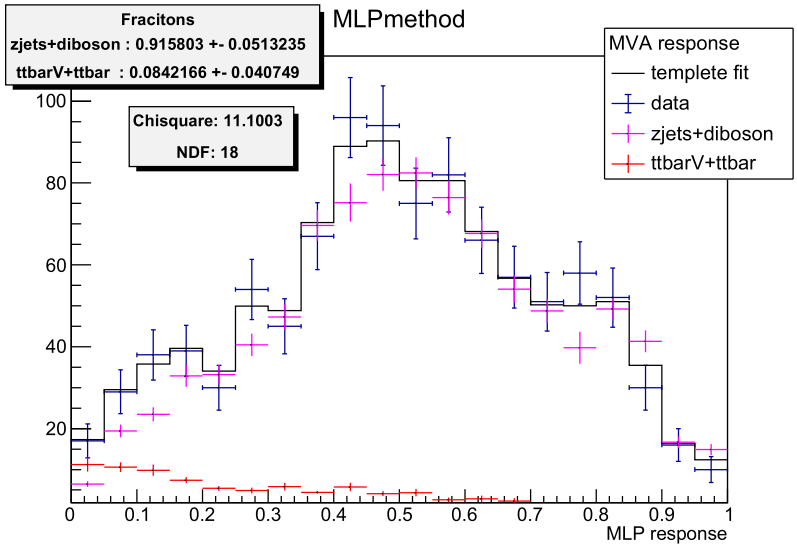

(a) $Z \to ee$

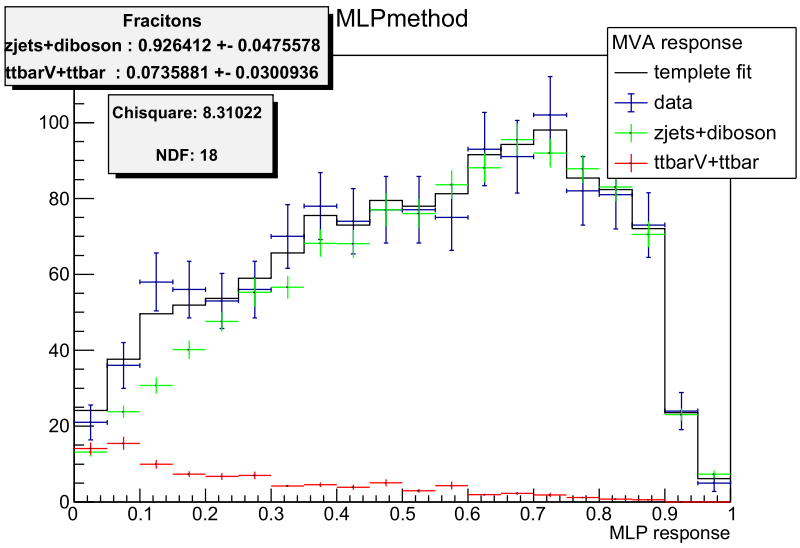

(b) $Z \to \mu\mu$

Figure 5.13: Template fit to ATLAS data using MLP response distributions for signal (Z+jet + diboson) and background ($t\bar{t}V$ + $t\bar{t}$).

5.6. Pseododata studies

To test the method that we have used, we have created sets of pseudo-data and applied the same method on them. To create background pseudo-data sets, we selected rendom events in $t\bar{t} + t\bar{t}V$ Monte Carlo until the total weight is at some desired weight (different contaminations of ratios are studied). Then this background pseudodata is added to Z+jet (+ diboson) MC. The pseudodata studies are performed on only $Z \to ee$ channel so the MLP response from Figure 5.11a is used in template fit. Using TFractionFitter and the template histograms, the fraction of $t\bar{t} + t\bar{t}V$ in Z+jet CR is calculated. The template fit for pseudodata sets with different contaminations can be seen in Figure 5.14. All the expected and calculated ratios are presented in Table 5.4. When we put the data in plot (see Figure 5.15) and perform the first degree linear fit, we find the equation $y = (0.93 \pm 0.26)x - 0.00 \pm 0.02$ in aggrement with the $y = x$ line that would point to an unbiased measurement of the contamination fraction.

Table 5.4: Pseudodata measurements

Constructed Pseudodata		Calculated $t\bar{t} + t\bar{t}V$ fraction using template fit		
Signal Weight	Background weight	Expected Fraction	Measured Fraction	$\sigma_{measured}$
866	10	0.0114	0.0113	0.0261
866	20	0.0226	0.0195	0.0272
866	30	0.0335	0.0298	0.0284
866	40	0.0442	0.0432	0.0298
866	50	0.0546	0.0487	0.0305
866	60	0.0658	0.0579	0.03164
866	70	0.0748	0.0715	0.0330
866	80	0.0846	0.0764	0.0341
866	90	0.0941	0.0860	0.0348
866	100	0.1035	0.0948	0.0362
866	110	0.1127	0.1044	0.0372
866	120	0.1217	0.1165	0.0384

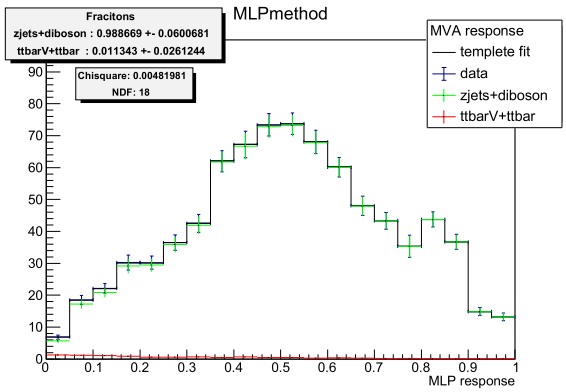

(a) 1.14%

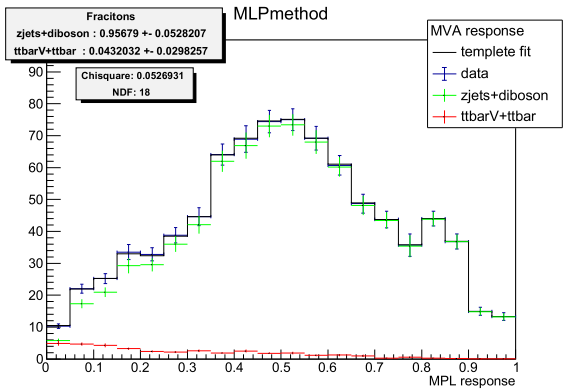

(b) 4.41%

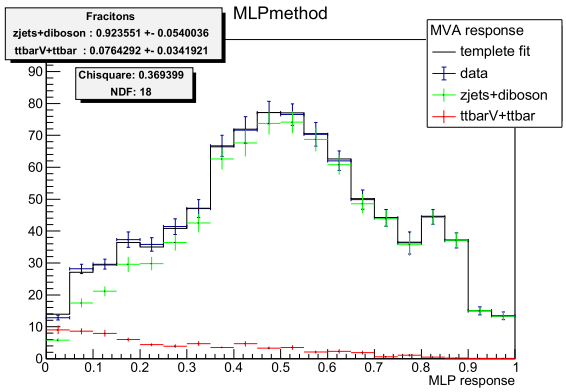

(c) 8.46%

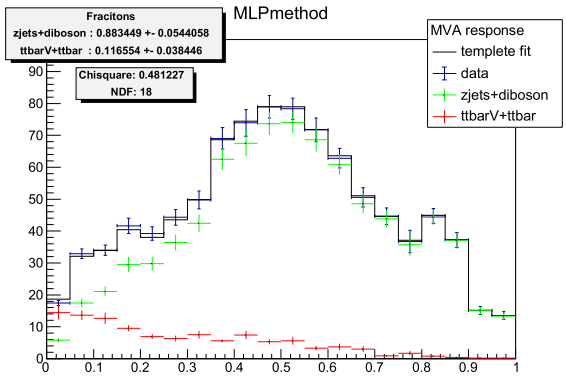

(d) 12.17%

Figure 5.14: Template fit on pseudodata for different contamination fractions of $t\bar{t}$ + $t\bar{t}V$ in Z+jet CR.

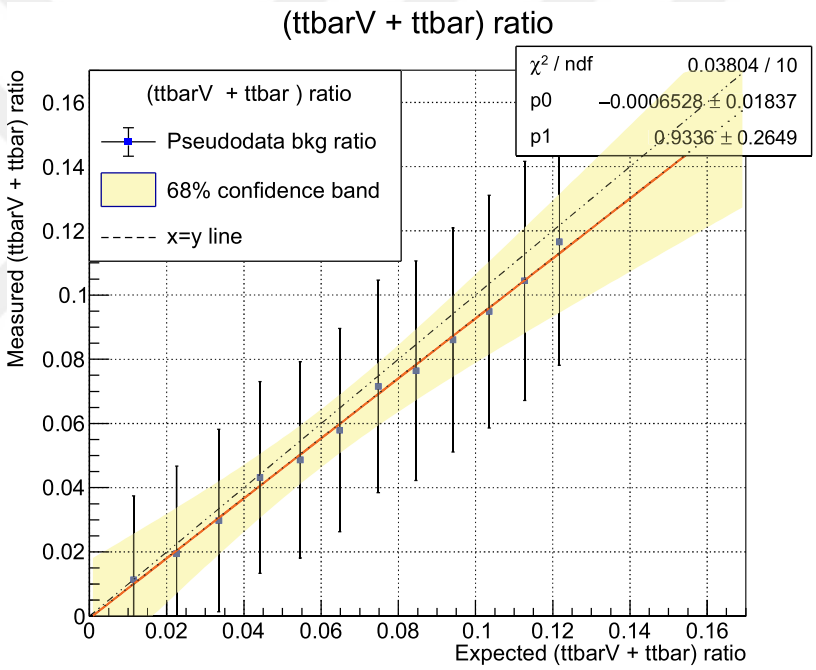

Figure 5.15: Expected vs measured $t\bar{t} + t\bar{t}V$ fraction in Z+jet CR pseudodata

5.7. Applying Z Scale Factor

Z scale factors are the multiplicative correction factors that are applied to the Z+jets MC samples in the signal region of the $HjZj$ analysis as a function of the dijet mass in each event. In order to validate our procedures, we apply them also in the CR and observe their effects on the MLP response. As seen in Figure 5.16, the Z+jets MLP distributions do not change much. The new template fit results after the application of the Z+jet scale factors can be seen in Figure 5.17.

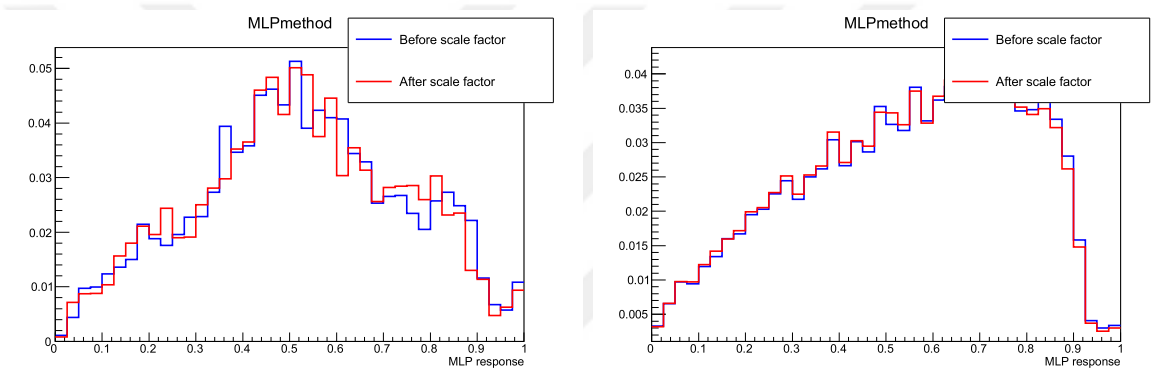

(a) $Z \to ee$ (b) $Z \to \mu\mu$

Figure 5.16: Z+jet MLP response before and after Z scale factor.

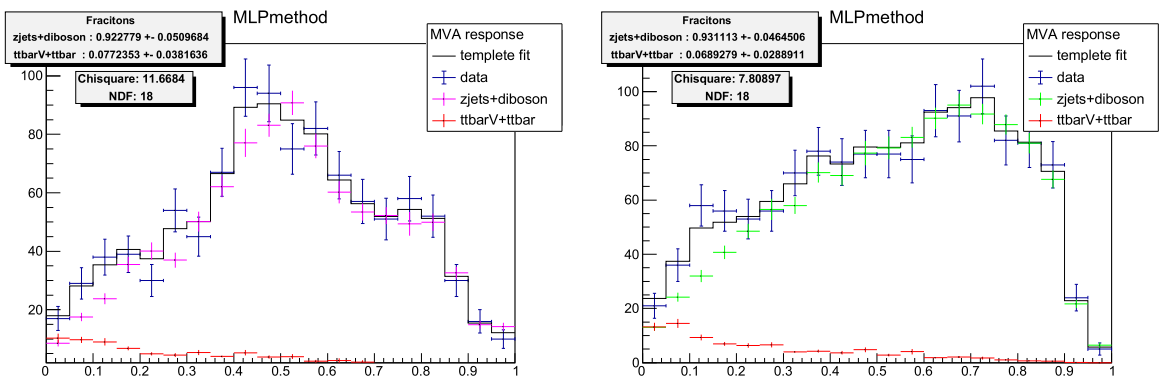

(a) $Z \to ee$ (b) $Z \to \mu\mu$

Figure 5.17: Template fit after applying the Z scale factor

5.8. Combining Results

The combined plot of MLP studies before and after Z scale factor correction with the pseudodata are shown in Figure 5.18. As seen from the figure, the calculated $t\bar{t}$ + $t\bar{t}V$ ratio in Z+jet CR is close to the expected value and within the 1 sigma of the pseusodata fit.

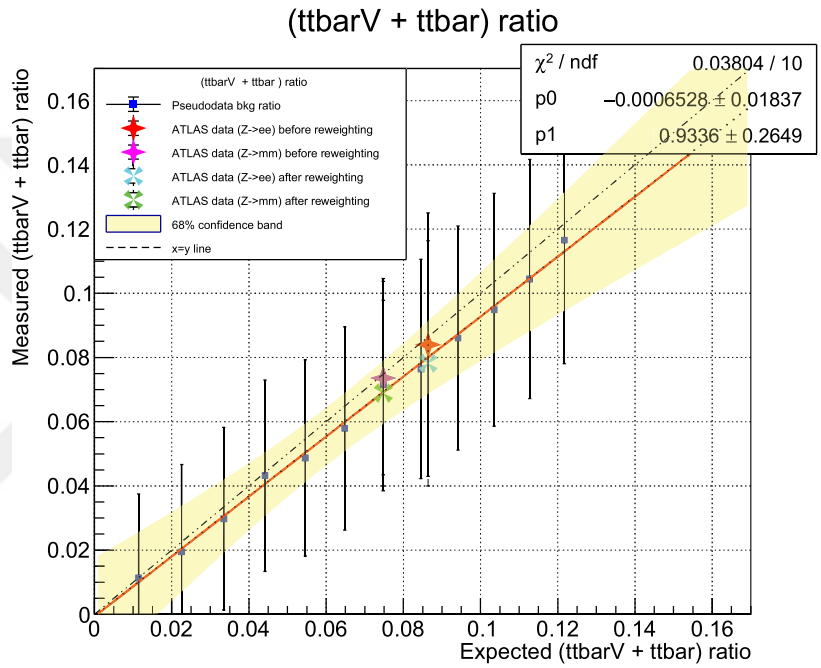

Figure 5.18: The combined plot of MLP studies before and after Z scale factor correction, obtained with the pseudodata.

6. CONCLUSION

This thesis presents three lines of interrelated works that pertains to gaseous particle detectors and their applications. These studies are supplementary to each other, from design to construction, from calibration to data analysis, a full spectrum of tasks have been succesfully caried out.

Delay Wire Chambers have been used at CERN beamlines for many years. Turkey's first DWC has designed, simulated and constructed at KAHVELab using the same specifications as the ones at CERN. The materials have mostly been procured from local companies. Machining and electronics have been done in our local workshop. The DWC has been tested at the CERN gaseous detector lab and with the cosmics in KAHVELab. It has passed all the tests successfully, even providing higher gain than the CERN DWCs.

The TRT detector drift circle error calibration has been done using the 2015 ATLAS Data and Monte Carlo. The calibration relies on extracting pull sigma values and has been perfprmed as a function of mean number of interactions per bunch crossing. The calibration values for Xenon and Argon straw values have been calculated separately. When the data and MC are reprocessed with the new calibration, the pull sigma values with respect to drift circle error approach unity as desired. The validation has been checked as a function of many variables such as position residual and precision hit fraction vs drift circle error and mean number of interaction per bunch crossing. The ATLAS data and MC are observed to be consistent in all validation plots.

$t\bar{t}V + t\bar{t}$ contamination in Z+jets CR of the $pp \rightarrow DD \rightarrow HjZj$ analysis using the ATLAS data has been measured using the multivariate analysis method known as Multi Layer Perceptron. Using a templete fit method to the pseudo data, which is itselfconstituted from the MC samples, the calculated value of the contamination ratio falls within one sigma range of the fit.

REFERENCES

1. Tanabashi, M. *et al.*, *Review of Particle Physics*, 2018, `http://cds.cern.ch/record/2636832?ln=en`.

2. Sauli, F., *Gaseous Radiation Detectors: Fundamentals and Applications*, Cambridge Monographs on Particle Physics, Nuclear Physics and Cosmology, Cambridge University Press, 2014.

3. Spanggaard, J., *Delay Wire Chambers A Users Guide*, Tech. Rep. SL-Note-98-023-BI, CERN, Geneva, Mar 1998, `http://cds.cern.ch/record/702443`.

4. Schindler, H., *Garfield++ User Guide*, 2020 (accessed in June 25, 2020), `https://garfieldpp.web.cern.ch/garfieldpp/documentation/UserGuide.pdf`.

5. AC Team, *The four main LHC experiments*, 1999, `http://cds.cern.ch/record/40525`.

6. Pequenao, J., *Computer generated image of the whole ATLAS detector*, 2008, `https://cds.cern.ch/record/1095924`.

7. Cornelissen, T. G. *et al.*, "Updates of the ATLAS Tracking Event Data Model (Release 13)", , No. ATL-SOFT-PUB-2007-003. ATL-COM-SOFT-2007-008, Jun 2007, `http://cds.cern.ch/record/1038095`.

8. Alonso, A., O. Smirnova and A. Torsten, *Transition Radiation Tracker calibration, searches beyond the Standard Model and multiparticle correlations in ATLAS*, Ph.D. Thesis, Lund U., Apr 2012, `https://cds.cern.ch/record/1452211`, Presented 20 May 2012.

9. Pequenao, J., *Computer Generated image of the ATLAS calorimeter*, 2008, `https://cds.cern.ch/record/1095927`.

10. Aloisio, A. *et al.*, "The trigger chambers of the ATLAS muon spectrometer: production and tests", *Nuclear Instruments and Methods in Physics Research Section A: Accelerators, Spectrometers, Detectors and Associated Equipment*, Vol. 535, No. 1, pp. 265 – 271, 2004, `http://www.sciencedirect.com/science/article/pii/S0168900204016511`, proceedings of the 10th International Vienna Conference on Instrumentation.

11. ATLAS Collaboration, *ATLAS magnet system: Technical Design Report, 1*, Technical Design Report ATLAS, CERN, Geneva, 1997, `http://cds.cern.ch/record/338080`.

12. Haywood, S., L. Rossi, R. Nickerson and A. Romaniouk, *ATLAS inner detector: Technical Design Report 1*, Technical Design Report ATLAS, CERN, Geneva, 1997, `https://cds.cern.ch/record/331063`.

13. Mindur, B., "ATLAS Transition Radiation Tracker (TRT): Straw tubes for tracking and particle identification at the Large Hadron Collider", *Nuclear Instruments and Methods in Physics Research Section A: Accelerators, Spectrometers, Detectors and Associated Equipment*, Vol. 845, pp. 257 – 261, 2017, `http://www.sciencedirect.com/science/article/pii/S0168900216301905`, proceedings of the Vienna Conference on Instrumentation.

14. TRT Collaboration, *TRT RT dependency for the TRT barrel and end-caps*, 2017, `https://twiki.cern.ch/twiki/bin/view/AtlasPublic/TRTPublicResults`, accessed in April 2017.

15. TRT Collaboration, *Trt Software Definitions*, 2017, `https://twiki.cern.ch/twiki/bin/viewauth/Atlas/TrtSoftwareDefinitions`, accessed in April 2017.

16. TRT Collaboration, *Tracking Properties of ATLAS TRT*, 2017, `https://cds.cern.ch/record/2223513/files/ATL-INDET-SLIDE-2016-794.pdf`,

accessed in April 2017.

17. ATLAS Colloboration, *Search for pair-produced heavy quarks decaying to HjZj at $\sqrt{s}$ = 13 TeV with the ATLAS detector*, 2020.

18. Airapetian, A. *et al.*, *ATLAS calorimeter performance Technical Design Report*, 1996.

19. Rossetti, V., "Performance of the ATLAS Calorimeters and Commissioning for LHC Run-2", , Jul 2015, `https://cds.cern.ch/record/2037117`.

20. *ATLAS muon spectrometer: Technical Design Report*, Technical Design Report ATLAS, CERN, Geneva, 1997, `http://cds.cern.ch/record/331068`.

21. Jochem, S., *The atlas muon spectrometer : commissioning and tracking*, Ph.D. Thesis, University of Twente, 2009.

22. Sumikama, T. *et al.*, "Energy-control and novel particle-identification methods combined with range in a multi-sampling ionization chamber for experiments using slowed-down RI beams", *Nuclear Instruments and Methods in Physics Research Section A: Accelerators, Spectrometers, Detectors and Associated Equipment*, Vol. 986, p. 164687, 2021, `https://www.sciencedirect.com/science/article/pii/S0168900220310846`.

23. Kintel, M., *The webpage of OpenSCAD*, 2019 (accessed in June 23, 2020), `https://www.openscad.org/`.

24. Goodfellow Group, *Specifications of Copper (98) Be(2)*, 2020 (accessed in June 27, 2020), `http://www.goodfellow.com/E/Copper-Beryllium.html`.

25. Goodfellow Group, *Specifications of Tungsten*, 2020 (accessed in June 27, 2020), `http://www.goodfellow.com/E/Tungsten.html`.

26. Istemihan, Z. *et al.*, "Design, simulation and construction of a Wire Chamber electronics", *AIP Conf. Proc.*, Vol. 1815, No. 1, p. 130005, 2017.

27. Bogazici University Advance Technologies Research and Development Center Laboratory, *FEI-Philips XL30 Environmental Scanning Electron Microscope with Field Emission Gun*, 2020 (accessed in June 27, 2020), `https://arge.boun.edu.tr/en/esem`.

28. Brüning, O. S., P. Collier, P. Lebrun, S. Myers, R. Ostojic, J. Poole and P. Proudlock, *LHC Design Report*, CERN Yellow Reports: Monographs, CERN, Geneva, 2004, `https://cds.cern.ch/record/782076`.

29. Gursey, F., P. Ramond and P. Sikivie, "A Universal Gauge Theory Model Based on E6", *Phys. Lett. B*, Vol. 60, pp. 177–180, 1976.

30. Gursey, F. and M. Serdaroglu, "Basic Fermion Masses and Mixings in the $E(6)$ Model", *Lett. Nuovo Cim.*, Vol. 21, p. 28, 1978.

31. Vale, T., "Search for pair-production of vector-like quarks in final states with at least one Z boson decaying into a pair of electrons or muons in pp collision data collected with the ATLAS detector at $\sqrt{s} = 13$ TeV", *11th International Workshop on Top Quark Physics*, 12 2018.

32. Aad, G. *et al.*, "Electron reconstruction and identification efficiency measurements with the ATLAS detector using the 2011 LHC proton-proton collision data", *Eur. Phys. J. C*, Vol. 74, No. 7, p. 2941, 2014.

33. Aaboud, M. *et al.*, "Electron efficiency measurements with the ATLAS detector using 2012 LHC proton–proton collision data", *Eur. Phys. J. C*, Vol. 77, No. 3, p. 195, 2017.

34. Aaboud, M. *et al.*, "Electron and photon energy calibration with the ATLAS detector using 2015–2016 LHC proton-proton collision data", *JINST*, Vol. 14, No. 03,

p. P03017, 2019.

35. Aad, G. *et al.*, "Muon reconstruction performance of the ATLAS detector in proton–proton collision data at $\sqrt{s}$ =13 TeV", *Eur. Phys. J. C*, Vol. 76, No. 5, p. 292, 2016.

36. Cacciari, M., G. P. Salam and G. Soyez, "The anti-k_t jet clustering algorithm", *JHEP*, Vol. 04, p. 063, 2008.

37. Aad, G. *et al.*, "Topological cell clustering in the ATLAS calorimeters and its performance in LHC Run 1", *Eur. Phys. J. C*, Vol. 77, p. 490, 2017.

38. ATLAS Collaboration, *Properties of Jets and Inputs to Jet Reconstruction and Calibration with the ATLAS Detector Using Proton-Proton Collisions at* $\sqrt{s} = 13$ *TeV*, 2015.

39. Aad, G. *et al.*, "Jet energy measurement and its systematic uncertainty in proton-proton collisions at $\sqrt{s}$ = 7 TeV with the ATLAS detector", *Eur. Phys. J. C*, Vol. 75, p. 17, 2015.

40. Aad, G. *et al.*, *Jet Calibration and Systematic Uncertainties for Jets Reconstructed in the ATLAS Detector at* $\sqrt{s}$ = 13 *TeV*, 2015, `https://cds.cern.ch/record/2037613`.

41. Aad, G. *et al.*, "Performance of pile-up mitigation techniques for jets in *pp* collisions at $\sqrt{s} = 8$ TeV using the ATLAS detector", *Eur. Phys. J. C*, Vol. 76, No. 11, p. 581, 2016.

42. Di Bello, F. A., "Optimisation of the ATLAS *b*-tagging algorithms for the 2017-2018 LHC data-taking", *PoS*, Vol. EPS-HEP2017, p. 733, 2017.

43. Hoecker, A., P. Speckmayer, J. Stelzer, J. Therhaag, E. von Toerne and H. Voss, "TMVA: Toolkit for Multivariate Data Analysis", *PoS*, Vol. ACAT, p. 040, 2007.

44. Vencatasawmy, C., "Principles of Multivariate Analysis: A User's Perspective by W. J. Krzanowski", *Journal of the Royal Statistical Society. Series D (The Statistician)*, Vol. 51, 01 2002.

45. Sieniutycz, S., "Chapter 4 - Complex systems of neural networks", S. Sieniutycz (Editor), *Complexity and Complex Thermo-Economic Systems*, pp. 51–84, Elsevier, 2020, `https://www.sciencedirect.com/science/article/pii/B9780128185940000040`.

46. CERN Collaboration, *class TFractionFitter*, 2020 (accessed in June 25, 2020), `https://root.cern.ch/root/html532/TFractionFitter.html`.

APPENDIX A: DESIGN OF DWC WRITTEN IN OPENSCAD SOFTWARE

```
include <../dimlines/dimlines.scad>
include <variables.txt>

module layer(){
    union(){
  difference() {
    union() {
      cube([P_LENGTH, P_LENGTH, P_Z_C1], center = true);
    }
    union() {
        //active area
      cube([P_WIRE_X, P_WIRE_X, P_Z_C1a], center = true);

      //threads
      translate([ HOLE_X,  HOLE_X, -P_Z_C1/2]) cylinder(h=HOLE_H, r=HOLE_R, center=false , $fn=100);
      translate([-HOLE_X,  HOLE_X, -P_Z_C1/2]) cylinder(h=HOLE_H, r=HOLE_R, center=false , $fn=100);
      translate([ HOLE_X, -HOLE_X, -P_Z_C1/2]) cylinder(h=HOLE_H, r=HOLE_R, center=false , $fn=100);
      translate([-HOLE_X, -HOLE_X, -P_Z_C1/2]) cylinder(h=HOLE_H, r=HOLE_R, center=false , $fn=100);

      // PCB spaces
      translate([0,  P_WIDTH-CONVERTER_PCB_WIDTH/2,  P_Z_ETCH+0.01]) cube([CONVERTER_PCB_LENGTH, CONVERTER_PCB_WIDTH, P_Z_ETCH], center=true);
      translate([0, -(P_WIDTH/2+P_WIRE_X/4),  P_Z_ETCH+0.01]) cube([P_WIRE_X, PCB_WIDTH, P_Z_ETCH], center=true);

      //solder etches
      translate([-(P_WIDTH/2+P_WIRE_X/4),  0, -(P_Z_ETCH+0.01)]) cube([PCB_WIDTH, P_WIRE_X, SOLDER_ETCH], center=true);
      translate([  P_WIDTH/2+P_WIRE_X/4  ,  0, -(P_Z_ETCH+0.01)]) cube([
```

```
    PCB_WIDTH, P_WIRE_X, SOLDER_ETCH], center=true);

    }}}
  {
  translate([0, P_WIDTH-CONVERTER_PCB_WIDTH+CONVERTER_PCB_WIDTH/2,
    P_Z_ETCH+0.01+0.1]) color([1,0,1]) cube([CONVERTER_PCB_LENGTH,
    CONVERTER_PCB_WIDTH2, P_Z_ETCH], center=true);
  translate([0, -(P_WIDTH/2+P_WIRE_X/4), P_Z_ETCH+0.01+0.1]) color
    ([1,0,1])cube([P_WIRE_X, PCB_WIDTH, P_Z_ETCH], center=true);
  }
}

module anode(){
    layer();
    // wires
    for(i = [1:N_ANODE])
        translate([-P_WIRE_X/2+i*GAP_ANODE,P_WIDTH/2+P_WIRE_X/4, P_Z_C1
    +0.1]) rotate([90, 0, 0]) color([0,0,0])cylinder(h=P_WIDTH+P_WIRE_X/2,
     r=R_WIRE, center=false, $fn=100);
}

module cathode(){
    layer();
    // wires
    for(i = [1:N_CATHODE])
        translate([-P_WIRE_X/2+i*GAP_CATHODE,P_WIDTH/2+P_WIRE_X/4, P_Z_C1
    +0.1]) rotate([90, 0, 0]) color([1,0,0])cylinder(h=P_WIDTH+P_WIRE_X/2,
     r=R_WIRE, center=false, $fn=100);
}

//x direction measurement
//cathode1
translate([ 0, 0, P_Z_C1*15]) rotate([0, 0, 0]) cathode();
//anode
translate([ 0, 0, P_Z_C1*10]) rotate([0, 0, 90]) anode();
//cathode2
translate([ 0, 0, P_Z_C1*5]) rotate([0, 0, 0]) cathode();
```

```
56
57 //y direction measurement
58 //cathode1
59 translate([ 0, 0, -P_Z_C1*5]) rotate([0, 0, 90]) cathode();
60 //anode
61 translate([ 0, 0, -P_Z_C1*10]) rotate([0, 0, 0]) anode();
62 //cathode2
63 translate([ 0, 0, -P_Z_C1*15]) rotate([0, 0, 90]) cathode();
```

APPENDIX B: SIMULATION OF DWC USING GARFIELD++ SOFTWARE

```
#include <iostream>
#include <TROOT.h>
#include <TApplication.h>
#include "ViewField.hh"
#include "ViewCell.hh"
#include "ComponentAnalyticField.hh"
#include "MediumMagboltz.hh"
#include "SolidBox.hh"
#include "GeometrySimple.hh"
#include "Sensor.hh"
#include "ViewDrift.hh"
#include "FundamentalConstants.hh"
#include "DriftLineRKF.hh"
#include "ViewMedium.hh"
#include "ViewSignal.hh"
#include "Random.hh"
#include "TrackHeed.hh"
#include "AvalancheMicroscopic.hh"

using namespace Garfield;

double transfer(double t){
  const double tau = 160;
  const double fC_to_mV = 12.7;
  return fC_to_mV*exp(4)*pow((t/tau),4)*exp(-4*t/tau);  //impulse
    response of the PASA
}

int main(int argc, char * argv[]) {
  TApplication app("app", &argc, argv);

  //box dimensions
  const double length = 10; // in cm
```

```
33  const double gap = 0.5; // in cm
34  const double anode_spacing = 0.4; // in cm
35  const double cathode_spacing = 0.2; // in cm
36
37  // Wire diameters
38  const double d_anode = 0.0020; //in cm
39  const double d_cathode = 0.0100; //in cm
40  const double voltage = 2000; // in V
41
42  // Setup the gas
43  const double pressure = 750.; //Torr = 1atm
44  const double temperature = 293.15; //K
45
46  //number of wires
47  int n_anode = length / anode_spacing - 1;
48  int n_cathode = length / cathode_spacing - 1;
49
50
51  // Make a gas medium
52  MediumMagboltz* gas = new MediumMagboltz();
53  // Set the temperature [K] and pressure [Torr]
54  gas->SetTemperature(temperature);
55  gas->SetPressure(pressure);
56  gas->SetComposition("ar", 50., "co2", 50.);
57
58  //Read from .gas file
59  gas->LoadGasFile("ar_50_co2_50.gas");
60  gas->LoadIonMobility("IonMobility_Ar+_Ar.txt");
61
62  // Build the geometry
63  // z=0 anode layer
64  // z=+-gap cathode planes
65  GeometrySimple* geo = new GeometrySimple();
66  SolidBox* box = new SolidBox(0., 0., 0.,gap,length/2,length/2);
67
68  // Add the solid to the geometry, together with the medium inside
69  geo->AddSolid(box, gas);
```

```
70
71  double xmin,ymin,zmin,xmax,ymax,zmax;
72  box->GetBoundingBox(xmin,ymin,zmin,xmax,ymax,zmax);
73
74  std::cout << "minimum and maximum coordinates of the box are: " << std
      ::endl;
75  std::cout << "(" << xmin << " " << ymin << " " << zmin << ")  (" <<
      xmax << " " << ymax << " " << zmax << ")" << std::endl;
76
77  // Setup the electric field
78  ComponentAnalyticField* comp_e = new ComponentAnalyticField();
79
80  //adding anode wires
81  for (int i = 0; i < n_anode; ++i) {
82   double x = 0;
83   double y = (-length/2 + (double)(i+1) * anode_spacing );
84   comp_e->AddWire( x,y , d_anode, voltage, "a");
85   std::cout << i+1 <<"th anode wire added to \tx = " << x << " \ty = "
      << y << std::endl;
86  }
87  comp_e->AddReadout("a");
88
89  comp_e -> AddPlaneX(-gap, 0, "cp-");
90  //at distance gap with potential zero.
91  comp_e -> AddPlaneX(gap, 0., "cp+");
92
93  // parameters: y direction
94  comp_e->AddStripOnPlaneX('y', gap, -length/2.,length/2., "cp+1");
95  //comp_e->AddStripOnPlaneX('y', gap, 0,length/2, "cp+2");
96  //comp_e->AddStripOnPlaneX('y', gap, 5,5.5, "cp+2");
97
98  comp_e->AddReadout("cp-");
99  comp_e->AddReadout("cp+");
100 comp_e->AddReadout("cp+1");
101 //comp_e->AddReadout("cp+2");
102
103 //Add magnetic field
```

```
comp_e->SetMagneticField(0,0,0);
comp_e->SetGeometry(geo);

//create a canvas that will also be used for drift lines plotting
TCanvas* myCanvas = new TCanvas();
ViewCell* cellView = new ViewCell();
cellView->SetComponent(comp_e);
cellView->SetArea(-gap,-length/2,-length/2,gap,length/2,length/2);
cellView->SetCanvas(myCanvas);
cellView->Plot3d();
myCanvas->Update();

// Make a sensor for ions (gating closed)
Sensor* sensor_e = new Sensor();
sensor_e->AddComponent(comp_e);
sensor_e->AddElectrode(comp_e, "a");
sensor_e->AddElectrode(comp_e, "cp-");
sensor_e->AddElectrode(comp_e, "cp+");
sensor_e->AddElectrode(comp_e, "cp+1");
//sensor_e->AddElectrode(comp_e, "cp+2");
sensor_e->SetTimeWindow(0.,100,400); // can be changed for less/better
  resolution in time (effect on convolution can be important)

//Plot drift line
DriftLineRKF* driftline = new DriftLineRKF();
driftline->SetSensor(sensor_e);

const double gain = 1;
double r = gap/2;
double dummy = 0.;
int status=0;
double endpoint = gap;
int plane = 0, cathode= 0, gate = 0, escape = 0; // used to store
  number of ions that drift respectively to plane, cathode, gate or
  drift vol
for(int i=0; i<gain; i++){
  //if(i%100==0)
```

```
    std::cout << i << std::endl;
    driftline->DriftElectron(0,0,0,0);
    std::cout << i << std::endl;
    driftline->GetEndPoint(dummy,endpoint,dummy,dummy,status);
  }

  // Plot isopotential contours
  ViewField* fView = new ViewField;
  fView->SetSensor(sensor_e);
  fView->SetArea(-gap,-length/2,gap,length/2);
  fView->SetVoltageRange(-100., 1000.);
  fView->PlotContour();

  sensor_e->SetTransferFunction(transfer);
  sensor_e->ConvoluteSignal();

  // Plot signal
  ViewSignal* vs1 = new ViewSignal();
  vs1->SetSensor(sensor_e);
  vs1->PlotSignal("a");

  ViewSignal* vs2 = new ViewSignal();
  vs2->SetSensor(sensor_e);
  vs2->PlotSignal("cp+");

  ViewSignal* vs3 = new ViewSignal();
  vs3->SetSensor(sensor_e);
  vs3->PlotSignal("cp-");

  app.Run(kTRUE);
}
```

APPENDIX C: ATLAS TRT CALIBRATION DATA SETS PACKAGES

The following datasets have been used for the calibration of the 2016 data:

- Data:
  - user.dkrasnop.data15_13TeV.279345.physics_Main → μ=10-15
  - user.dkrasnop.data15_13TeV.276329.physics_Main → μ=15-20
- MC15:
  - mc15_13TeV.361036.Pythia8_A2MSTW2008LO_minbias _ inelastic.recon.RDO.e3580_s2726_r6869

To perform the calibration Athena Release 20.1.6.4 is used. The following packages are used:

- TRT_ConditionsServices-01-00-00-08
- TRT_ConditionsData-00-00-51
- TRT_ConditionsAlgs-00-03-09
- TRT_CalibTools-00-01-11
- InDetRecExample-02-05-70
- TRT_CalibAlgs-00-01-08
- TrkRIO_OnTrackCreator-01-02-01

APPENDIX D: TMVA TRAINING CODE

```
#include "TMVA/Factory.h"
#include "TMVA/DataLoader.h"
#include "TMVA/Tools.h"
#include "TMVA/TMVAGui.h"
#include "event.h"

void tmva_analysis1()
{

    TMVA::Tools::Instance();

    auto inputttbarV_ttbarFile = TFile::Open("run_results/from_hanimaga/ttbarV_ttbar_combined_200516_mc_ee.root");
    auto inputZjet_dibosonFile = TFile::Open("run_results/from_hanimaga/Z+jet_diboson_combined_200516_mc_ee.root");

    TTree *BackgroundTree      = (TTree*)inputttbarV_ttbarFile->Get("TmvaEventstree6"  );
    TTree *SignalTree      = (TTree*)inputZjet_dibosonFile->Get("TmvaEventstree6"  );

    TString outfileName( "TMVAoutput.root" );
    TFile* outputFile = TFile::Open( outfileName, "RECREATE" );

    TMVA::Factory factory("TMVAClassification", outputFile,
                          "!V:ROC:!Correlations:!Silent:Color:!DrawProgressBar:AnalysisType=Classification" );

    TMVA::DataLoader loader("dataset");

    loader.AddVariable("LEP0_pt");
    loader.AddVariable("LEP1_pt");

    loader.AddVariable("Z_pt");
    loader.AddVariable("Z_eta");
```

```
31
32      loader.AddVariable("JET0_pt");
33
34      loader.AddVariable("JET0_JET1_mass");
35      loader.AddVariable("ZfarDIJET_mass");
36      loader.AddVariable("DIJET_highpt_mass");
37
38      loader.AddVariable("JET_higheta_pt");
39      loader.AddVariable("JET_higheta_mass");
40
41      loader.AddVariable("MET");
42      loader.AddVariable("fNBtag");
43
44      loader.AddSignalTree(SignalTree,   1);    //signal weight  = 1 -
45      loader.AddBackgroundTree(bBackgroundTree, 1);    //background weight =
        1
46
47      loader.SetWeightExpression("new_weight");
48
49      TCut mycuts, mycutb;
50
51      loader.PrepareTrainingAndTestTree(mycuts, mycutb,
                    "nTrain_Signal=5000:nTrain_Background=5000:SplitMode=
        Random:NormMode=NumEvents:!V" );
52
53      //Multi-Layer Perceptron (Neural Network)
54      factory.BookMethod(&loader, TMVA::Types::kMLP, "MLP", "!H:!V:
        NeuronType=tanh:VarTransform=N:NCycles=500:HiddenLayers=N+5:TestRate
        =5:!UseRegulator:IgnoreNegWeightsInTraining" );
55
56      //Boosted Decision Trees
57      factory.BookMethod(&loader,TMVA::Types::kBDT, "BDT", "!V:NTrees=4000:
        MinNodeSize=2.5%:MaxDepth=4:BoostType=AdaBoost:AdaBoostBeta=0.5:
        UseBaggedBoost:BaggedSampleFraction=0.5:SeparationType=GiniIndex:nCuts
        =20:IgnoreNegWeightsInTraining" );
58
59      //Fisher
```

```
factory.BookMethod(&loader, TMVA::Types::kFisher, "Fisher", "H:!V:Fisher:VarTransform=None:CreateMVAPdfs:PDFInterpolMVAPdf=Spline2:NbinsMVAPdf=50:NsmoothMVAPdf=10");

//kLikelihood
factory.BookMethod(&loader, TMVA::Types::kLikelihood, "Likelihood",
                   "H:!V:TransformOutput:PDFInterpol=Spline2:NSmoothSig[0]=20:NSmoothBkg[0]=20:NSmoothBkg[1]=10:NSmooth=1:NAvEvtPerBin=50");

//PCA-transformed likelihood
factory.BookMethod(&loader, TMVA::Types::kLikelihood, "LikelihoodPCA", "!H:!V:!TransformOutput:PDFInterpol=Spline2:NSmoothSig[0]=20:NSmoothBkg[0]=20:NSmooth=5:NAvEvtPerBin=50:VarTransform=PCA");

// K-Nearest Neighbour classifier (KNN)
factory.BookMethod(&loader, TMVA::Types::kKNN, "KNN", "H:nkNN=20:ScaleFrac=0.8:SigmaFact=1.0:Kernel=Gaus:UseKernel=F:UseWeight=T:!Trim");

// H-Matrix (chi2-squared) method
factory.BookMethod( &loader, TMVA::Types::kHMatrix, "HMatrix", "!H:!V:VarTransform=None");

// Train MVAs using the set of training events
factory.TrainAllMethods();

// Evaluate all MVAs using the set of test events
factory.TestAllMethods();

// Evaluate and compare performance of all configured MVAs
factory.EvaluateAllMethods();

// ----------------------------------------------------------------------

// Save the output
outputFile->Close();
```

```
87
88      std::cout << "==> Wrote root file: " << outputFile->GetName() << std
        ::endl;
89      std::cout << "==> TMVAClassification is done!" << std::endl;
90
91      // Launch the GUI for the root macros
92      if (!gROOT->IsBatch()) TMVA::TMVAGui( outfileName );
93
94  }
```

APPENDIX E: TEMPLETE FIT USING TFRACTIONFITTER

```
void TFraction_templete_fit() {


    gStyle->SetOptFit(0100);
    gStyle->SetOptStat("ne");

    //Reading Files
    TFile *tfile;
    TFile *datafile;
    TFile *zjetsfile;
    TFile *ttbarfile;
    TFile *ttbarVfile;
    TFile *dibosonfile;

    datafile = TFile::Open("TMVEval2.root", "READ");
    if ( datafile->IsOpen() ) cout << "File " << datafile->GetName() << "
    opened successfully" << endl;
    else {cout << "File not FOUND!!!!" << endl;   return; }

    zjetsfile = TFile::Open("TMVEval_Z+jet2.root", "READ");
    if ( zjetsfile->IsOpen() ) cout << "File " << zjetsfile->GetName() <<
    " opened successfully" << endl;
    else {cout << "File not FOUND!!!!" << endl;   return; }

    ttbarfile = TFile::Open("TMVEval_ttbar2.root", "READ");
    if ( ttbarfile->IsOpen() ) cout << "File " << ttbarfile->GetName() <<
    " opened successfully" << endl;
    else {cout << "File not FOUND!!!!" << endl;   return; }

    ttbarVfile = TFile::Open("TMVEval_ttbarV2.root", "READ");
    if ( ttbarVfile->IsOpen() ) cout << "File " << ttbarVfile->GetName()
   << " opened successfully" << endl;
    else {cout << "File not FOUND!!!!" << endl;   return; }
```

```
30
31      dibosonfile = TFile::Open("TMVEval_diboson2.root", "READ");
32      if ( dibosonfile->IsOpen() ) cout << "File " << dibosonfile->GetName
        () << " opened successfully" << endl;
33      else {cout << "File not FOUND!!!!" << endl;    return; }
34
35      //Reading histograms from the files
36      TH1F *hdata  = (TH1F*) datafile->Get("MLPmethod");
37      TH1F *htzjets  = (TH1F*) zjetsfile->Get("MLPmethod");
38      TH1F *htttbar  = (TH1F*) ttbarfile->Get("MLPmethod");
39      TH1F *htttbarV  = (TH1F*) ttbarVfile->Get("MLPmethod");
40      TH1F *htdiboson  = (TH1F*) dibosonfile->Get("MLPmethod");
41
42      TH1F *htttbarV_ttbar = (TH1F*) ttbarVfile->Get("MLPmethod");
43      htttbarV_ttbar->Add(htttbar);
44
45      TH1F *htzjets_diboson = (TH1F*) zjetsfile->Get("MLPmethod");
46      htzjets_diboson->Add(htdiboson);
47
48      hdata->Rebin(2);
49      htzjets_diboson->Rebin(2);
50      htttbarV_ttbar->Rebin(2);
51
52     TObjArray *mc = new TObjArray(2);          // MC histograms are put in
        this array
53     mc->Add(htzjets_diboson);
54     mc->Add(htttbarV_ttbar);
55
56     double frac[2];
57     double frac_err[2];
58     TFractionFitter* fit = new TFractionFitter(hdata, mc, "V"); //
        initialise
59
60     fit->Constrain(0,0.80,1);
61     fit->Constrain(1,0.05,0.1);
62
63     fit->SetRangeX(1,40);
```

```
Int_t status = fit->Fit();
std::cout << "fit status: " << status << std::endl;
if (status == 0) {                          // check on fit status
  TH1F* result = (TH1F*) fit->GetPlot();
  hdata->Draw("E1");
  result->SetLineColor(kBlack);
  result->Draw("same");

 double data_int = hdata->Integral(0,40);

  fit->GetResult(0, frac[0], frac_err[0]);
  htzjets_diboson->Scale(1/(htzjets_diboson->Integral(0,40)));
  htzjets_diboson->Scale(frac[0]*data_int);
  htzjets_diboson->SetLineColor(kMagenta);
  htzjets_diboson->GetXaxis()->SetTitle("MLP response");
  htzjets_diboson->Draw("same");

  fit->GetResult(1, frac[1], frac_err[1]);
  htttbarV_ttbar->Scale(1/(htttbarV_ttbar->Integral(0,40)));
  htttbarV_ttbar->Scale(frac[1]*data_int);
  htttbarV_ttbar->SetLineColor(kRed);
  htttbarV_ttbar->Draw("same");

 auto legend = new TLegend(0.75,0.68,0.98,0.95);
 legend->SetHeader("MVA response",""); // option "C" allows to center the header
 legend->AddEntry(result,"templete fit","l");
 legend->AddEntry(hdata,"data","le1");
 legend->AddEntry(htzjets_diboson,"zjets+diboson","lep");
 legend->AddEntry(htttbarV_ttbar,"ttbarV+ttbar","lep");
 legend->Draw();

 TPaveText *t2=new TPaveText(0.03,0.85,0.4,0.98,"brNDC");
         t2->AddText(Form("Fracitons "));
         t2->AddText(Form("zjets+diboson : %g +- %g ",frac[0],frac_err[0]));
         t2->AddText(Form("ttbarV+ttbar  : %g +- %g ",frac[1],frac_err
```

```
[1]));
            t2->Draw();

        TPaveText *t3=new TPaveText(0.15,0.75,0.35,0.83,"brNDC");
            t3->AddText(Form("Chisquare: %g ",fit->GetChisquare ()));
            t3->AddText(Form("NDF: %d ",fit->GetNDF()));
            t3->Draw();

    cout << "Chisquare: " << fit->GetChisquare () << endl;
    cout << "NDF:        " << fit->GetNDF () << endl;
    cout << endl;
    cout << "Zjets+diboson:" << frac[0] << " +- " << frac_err[0] << "(Real value = 0.914)" << endl;
    cout << "ttbarV+ttbar: " << frac[1] << " +- " << frac_err[1] << "(Real value = 0.086)" << endl;
    cout << endl;

  }

}
```

APPENDIX F: DATASETS AND CUTS USED IN THE ISOSINGLET QUARK SEARCHES BACKGROUND ANALYSIS

The data sets used of the heavy iso-singlet quark searches analysis is used.

F.1. Data

For this analysis, data collected at $\sqrt{s} = 13\,\text{TeV}$ during 2015–2018, corresponding to an integrated luminosity of $139\,\text{fb}^{-1}$, are used. The backgroundevaluation is done with MC samples using full simulation produced in the three relevant simulation campaigns (MC16a, MC16d, and MC16e) and after being processes with the EXOT4 derivation. A complete list of samples is presented in Appendix A. The main backgroundin this analysis is Z+jets. Processes such as $t\bar{t}$ and $t\bar{t}$ produces in associationwith vector bosons are sub-leading backgrounds, while small contributions are expected fromprocesses such as s single top, di-boson and W+jets.

F.2. Z+Jets Background

For the description of the Z boson production plus associated jets,the samples produced bySherpa 2.2.1 using the NNPDF3.0 NNLO PDF set are used. In order to ensure enough statistics in the high P_{T} range, the samples are produced in slices of the max(H_{T}, $p_{\text{T}}(Z)$) and filteringthe heavy flavour composition. Samples produced with MADGRAPH, using the NNPDF3.0 NLO PDF set and interfaced to Pythia 8 with theA14 NNPDF2.3LO tune for showering and are being used to assign a generator uncertanity.These samples are sliced in H_{T}.

F.3. SM $t\bar{t}$ and Single Top Background

The SM $t\bar{t}$ background samples use the POWHEG method implemented in POWHEG-BOX v2 using the NNPDF3.0 NLO PDF set. POWHEG-BOX was interfaced with Pythia 8 with the A14 set of tunable parameters for parton showering and hadronization. The h_{damp} parameter in PowHEG-Box which controls matrix element to parton shower matching in and effectively regulates the high-p_{T} radiation, was set to $1.5m_t$, where $m_t = 172.5\,\text{GeV}$. In this sample non all hadronic final states are considered, since the main contribution for the multileptonic topologies of the analysis comes from the leptonic decays of $t\bar{t}$. As much as possible for systematic uncertanity estimation, alternative generator weights with variations in the factorization and renormalization scales, shower tuning variations, as well as the choice of the PDF set are stored in the sample. For the shower tuning variations, the NLO radiation (scaled from $\times 0.5$ up to $\times 2.0$) as welll as the shower radiation (using the A14 var3c eigentune) and NLO radiation was modified by changing the h_{damp} parameter to $h_{\text{damp}} = 1.5 \times m_t$ and $3 \times m_t$. Extra samples, simulated with AFII, have been used for additional systematics evaluation. Showering uncertanities have been included using samples with the same generator and PDF set as the nominal case by using HERWIG7 with the H7UE tune and for the showering. Generator systematics uncertanities are included using samples generated with aMC@NLO with NNPDF3.0 NLO set and the showering done by Pythia 8 with the A14 NNPDF2.3 LO tune.

The **singletop** background processes have been generated with POWHEG-BOX v1 and interfaced to Pythia 8 with Perugia2012 set of tunable paramaters.

F.4. Di-Boson Background

The contribution from diboson processes (i.e. ZZ, WZ and WW) is evaluated using samples generated by Sherpa 2.2.2 using the NNPDF3.0 NNLO PDF set.

F.5. SM $t\bar{t}$ with Associated Vector Bosons Background

The samples for the production of a top anti-top quark pair in association with vector bosons are generated by a MC@NLO(for $t\bar{t}+W$ and $t\bar{t}+Z$ process) and MAGRAPH (for $t\bar{t}+WW$ processes) interfaced with PYTHIA 8 for hadronization and using the NNPDF23LO PDF ser and the A14 tune. Processes with such as $t\bar{t}+W$, $t\bar{t}+WW$ and $t\bar{t}+Z$ with Z decaying to $\nu\bar{\nu}$, $q\bar{q}$ and ll, where $l=(e,\mu,\tau)$, are considered. Internal generator weights are used for the estimation of the modeling uncertanities.

F.6. Reconstruction Cuts

Table F.1: Electron selection criteria.

Feature	Criterion
Pseudorapidity range Energy calibration Transverse momentum	$(\lvert\eta\rvert < 1.37 \lvert\lvert < 1.52 < \lvert\eta\rvert < 2.47)$ `es2017_R21_PRE` (ESModel) $p_{\mathrm{T}} > 28GeV$
Object quality	Not from a bad calorimeter cluster (`BADCLUSLECTRON`) Remove clusters from regions with EMEC bad HV (2016 data only)
Track to vertex association	$d_0^{\mathrm{BL}}(\sigma) < 5$ $\lvert\Delta z_0^{\mathrm{BL}} \sin\theta\rvert < 0.5\,\mathrm{mm}$
Identification Isolation	(`TightLH`) `None`

Table F.2: Muon selection criteria.

Feature	Criterion
Selection working point	`Medium`
Isolation working point	`FCTightTrackOnly`
Momentum calibration	Sagitta correction used
p_{T} cut	28 GeV
$\lvert\eta\rvert$ cut	< 2.5
d_0 significance cut	3
$\Delta z_0 \sin\theta$ cut	0.5 mm

Table F.3: Jet selection criteria.

Feature	Criterion
R parameter	0.4
Input constituent	EMTopo
Analysis release number	21.2.84
`CalibArea tag`	00-04-82
Calibration configuration	`JES_MC16Recommedation_Consolidated_EMTopo_Apr2019_Rel21`
Calibration sequence (Data)	`JetArea_Residual_EtaJES_GSC_Insitu`
Calibration sequence (MC)	`JetArea_Residual_EtaJES_GSC_Smear`
	Selection requirements
Observable	Requirement
Jet cleaning	`LooseBad`
p_{T}	25 GeV
$\lvert\eta\rvert$	< 4.5
JVT	> 0.59 for $p_{\mathrm{T}} < 60$ GeV, $\lvert\eta\rvert < 0.4$

Table F.4: b-tagging selection criteria.

Feature	Criterion
	EM Topo Jets
Jet collection	`AntiKt4EMTopo`
Jet selection	$p_{\mathrm{T}} > 25\,\mathrm{GeV}$
	$\lvert\eta\rvert < 2.5$
	JVT cut if applicable
Algorithm	`MV2c10`
Operating point	Fixed
	Eff = 77
CDI	`2017-21-13TeV-MC16-CDI-2019-7-25_v1`

Table F.5: Overlap removal criteria.

Reject	Against	Criteria
Electron	Electron	shared track, $p_{\mathrm{T},1} < p_{\mathrm{T},2}$
Muon	Electron	is Calo-Muon and shared ID track
Jet	Electron	$\Delta R < 0.2$
Electron	Jet	$\Delta R < 0.4$
Jet	Muon	`NumTrack < 3 and`
		`(ghost-associated or` $\Delta R < 0.2$`)`
		not a b-jet and `NumTrack < 3 and`
		`(ghost-associated or` $\Delta R < 0.2$`)`
Muon	Jet	$\Delta R < min(0.4, 0.04 + 10GeV/p_{\mathrm{T}}(\mu))$

APPENDIX G: PERMISSIONS OF THE USAGE OF FIGURES

G.1. CERN Resources

Copyright for CERN resources i.e. resources from *http://cds.cern.ch/*.

CERN Accelerating science Sign in Directory

CERN Document Server

Search Submit Help Personalize

Home > Accessing CERN copyrighted material

Accessing CERN copyrighted material

About CERN copyrighted material on the CERN Document Server (CDS)
The CERN Document Server contains multimedia material under CERN copyright. You can freely download and use the high-resolution version of these files, provided you agree and respect the conditions of use.

How to access high-res CERN copyrighted material?
Click on the "high-res" link of a file.
The conditions of use are then displayed. You can agree or disagree to the conditions of use by clicking on the "Agree" or "Disagree" button. If you accept the conditions, the download will start.
Note that if a file is restricted and you are not logged in, you will be redirected to the CERN central login page. Follow the instructions on-screen to login (or request lost password, etc.).

Who can download high-res multimedia files?
Anybody (journalists, physicists, individuals, etc.) who agrees to the conditions of use. Note that for some usages (personal use for computer wallpaper, inclusion in slides, etc.) you might want to download a lower resolution of the file, which remains a good quality enough. The lower resolutions files remains under CERN copyright, and the same conditions of use apply.

What are the conditions of use?
The conditions of use can be found at http://copyright.cern.ch/. There you can also find contact information to request more detailed information.

When I try to download, I get this message "`Redirect Loop`"

Your web browser if most probably configured to use a web proxy to connect to HTTP servers, but not for connecting to (secure) HTTPS servers.
To simplify, this makes you appear as two different users on our side, when you try to login, which we strictly forbid for security reasons on the CERN Document Server.

To solve this problem, you might want to either enable your browser proxy for both HTTP (port 80) and HTTPS (port 443), or to disable it for both protocols.

When I try to download, I get a blank page

You are probably using a browser extension preventing the download to start. For example we have noticed in the past that extension "AdBlock" was preventing users from downloading files

To solve this problem, please temporarily disable any extension blocking the download.

Internet Explorer tells me that the website in encountering problems.
Internet Explorer cannot download files larger than 4 GB. Please use another browser to download large files.

How can I get a better resolution of a document?
The documents on the CERN Document Server are generally already the highest quality available.

What about low resolution multimedia files?
Low-res files are also protected by the CERN copyright, and subject to the same conditions of use as high resolutions files. Though you will not need to login to access them, you agree to the same conditions (including the CERN computing rules) by downloading this material.

Who can I contact in case of question or problem?
You can contact the following services:

- helpdesk@cern.ch for general help.
- http://copyright.cern.ch/contact for questions related to copyright, conditions of use, etc.
- audiovisual.productions.service@cern.ch for questions related to photos.
- audiovisual-support@cern.ch for questions related to videos and audios.
- cds.support@cern.ch for technical help related directly to the CERN Document Server.

CERN Document Server :: Search :: Submit :: Personalize :: Help :: Privacy Notice
Powered by Invenio v1.1.3.1106-62468
Maintained by cds.support@cern.ch

This site is also available in the following languages:
Български Català Deutsch Ελληνικά **English** Español Français Hrvatski Italiano 日本語 ქართული Norsk/Bokmål Polski Português Русский Slovensky Svenska 中文(简) 中文(繁)

Terms of use for CERN audiovisual media

Use of CERN audiovisual media denotes agreement with the following terms:

1. CERN provides the image free of charge for educational and informational use.
2. The image is provided "as-is" and the user shall hold CERN free and harmless in connection with its use.
3. CERN is to be credited as the source of the image.
4. CERN retains copyright in the image. Download and use of the image does not amount to a transfer of intellectual property.
5. The image may not be used in a misleading, inappropriate or offensive manner, in a military context, in advertising or promotion, or in a manner that suggests any kind of endorsement by CERN or its personnel.
6. The image may not be sold, distributed or otherwise made available for use by third parties.
7. The CERN logo is legally protected. CERN's prior written approval shall be obtained for its use or for the use of any image primarily featuring the logo.
8. CERN reserves the right to alter or delete images without notice.

Please contact us by using the contact form (/contact) if you have any questions or comments with respect to CERN content; if you are unsure whether your intended use meets these terms; or, if you seek permission for use of the CERN logo or any other use that does not fall within these terms. CERN appreciates your interest in its work. More information about CERN is available at www.cern.ch.

Copyright abuse should be reported using the contact form (/contact).

G.2. Sauli, F., Gaseous Radiation Detectors

Copyright for Sauli, F., Gaseous Radiation Detectors: Fundamentals and Applications, Cambridge Monographs on Particle Physics, Nuclear Physics and Cosmology, Cambridge University Press, 2014.

PLS Clear

PARTIES:

1. **Cambridge University Press** [CompanyNumber] (Licensor); and
2. **Saime Gürbüz** (Licensee).

Thank you for your recent permission request. Some permission requests for use of material published by the Licensor, such as this one, are now being facilitated by PLSclear.

Set out in this licence cover sheet (the **Licence Cover Sheet**) are the principal commercial terms under which Licensor has agreed to license certain Licensed Material (as defined below) to Licensee. The terms in this Licence Cover Sheet are subject to the attached General Terms and Conditions, which together with this Licence Cover Sheet constitute the licence agreement (the **Licence**) between Licensor and Licensee as regards the Licensed Material. The terms set out in this Licence Cover Sheet take precedence over any conflicting provision in the General Terms and Conditions.

Licence Terms

Licence Date:	17/02/2021
PLSclear Ref No:	47317

The Licensor

Company name:	Cambridge University Press
Address:	University Printing House Shaftesbury Road Cambridge CB2 8BS GB

The Licensee

Licensee Contact Name:	Saime Gürbüz
Licensee Address:	Bogazici University 34470

Licensed Material

title:	Gaseous Radiation Detectors Fundamentals and Applications
ISBN/ISSN:	9781107043015
publisher:	Cambridge University Press

Are you requesting permission to reuse the cover of the publication?	No
Figure number & title	Figure 7.3 Avalanche growth around a thin wire.
Page numbers	185

Are you requesting permission to reuse the cover of the publication?	No
Figure number & title	Figure 7.4
Page numbers	185

Are you requesting permission to reuse the cover of the publication?	No
Figure number & title	Figure 8.1 The first multi-wire proportional chamber,
Page numbers	213

Are you requesting permission to reuse the cover of the publication?	No
Figure number & title	Figure 8.2 Schematics of the MWPC with definitions of the symbols used in
Page numbers	214

Are you requesting permission to reuse the cover of the publication?	No
Figure number & title	Figure 8.3 Field lines and equi-potentials near the anode wires in the MWPC.
Page numbers	214

Are you requesting permission to reuse the cover of the publication?	No
Figure number & title	Figure 8.4 Electric field in the MWPC along the x and y directions.
Page numbers	215

Figure number & title / caption	Table 2.1
Table / chart description	Physical constants for various gases at NTP and approximate values of energy loss and ion-pair production (unit charge minimum ionizing particles).
Page numbers	28

For Use In Licensee's Publication(s)

usage type	Book, Journal, Magazine or Academic Paper-Thesis / Dissertation
Will your dissertation be placed in an online repository?	Yes
Author	Saime Gürbüz
Estimated publication date	01.03.2021
Language	English
Other Territory	Turkey

Title of dissertation/thesis	Construction and Calibration of Gaseous Detectors at KAHVELab and CERN ATLAS Experiment
University or institution	Boğaziçi University
Unlimited circulation?	No

Rights Granted

Exclusivity:	Non-Exclusive
Format:	Thesis/Dissertation
Language:	English
Territory:	Turkey
Duration:	Lifetime of Licensee's edition
Maximum Circulation:	Maximum print circulation: 5 copies
Additional Terms:	Figures 7.4 and 8.1 Are not original to our publication, therefore permission will need to be sought from the original copyright holders for these two figures. Cambridge University Press does not always own the rights in individual figures that appear in our work, they are often acknowledged to an earlier source or third party, to whom you should apply to for permission.

Payment Details

Fee Payable:	£0.00 [+ VAT if applicable]
Payment Terms:	Strictly 30 days from date of Licence

GENERAL TERMS AND CONDITIONS

1. Definitions and Interpretation

1.1 Capitalised words and expressions in these General Terms and Conditions have the meanings given to them in the Licence Cover Sheet.

1.2 In this Licence any references (express or implied) to statutes or provisions are references to those statutes or provisions as amended or re-enacted from time to time. The term **including** will be construed as illustrative, without limiting the sense or scope of the words preceding it. A reference to in **writing** or **written** includes faxes and email. The singular includes the plural and vice versa.

2. Grant of Rights

2.1 Subject to payment by Licensee of the Licence Fee in accordance with paragraph 3 below, Licensor grants to Licensee the non-exclusive right to use the Licensed Material as specified in the Licence Cover Sheet.

2.2 The rights licensed to Licensee under this Licence do not include the right to use any third party copyright material incorporated in the Licensed Material. Licensee should check the Licensed Material carefully and seek permission for the use of any such third party copyright material from the relevant copyright owner(s).

2.3 Unless otherwise stated in the Licence Cover Sheet, the Licensed Material may be:

2.3.1 subjected to minor editing, including for the purposes of creating alternative formats to provide access for a beneficiary person (provided that any such editing does not amount to derogatory treatment); and/or

2.3.2 used for incidental promotional use (such as online retail providers' search facilities).

2.4 Save as expressly permitted in this Licence or as otherwise permitted by law, no use or modification of the Licensed Material may be made by Licensee without Licensor's prior written permission.

3. Payment

3.1 Licensee must pay to Licensor the Licence Fee by means of either credit card or on receipt of an invoice, as selected by Licensee during the licence application process via the PLSclear service.

3.2 If payment is by invoice, Licensee agrees to pay the Licence Fee in full by no later than the payment date specified in the relevant invoice.

4. Copyright Notice and Acknowledgement

4.1 Licensee must ensure that the following notices and acknowledgements are reproduced prominently alongside each reproduction by Licensee of the Licensed Material:

4.1.1 the title and author of the Licensed Material;

4.1.2 the copyright notice included in the Licensed Material; and

4.1.3 the statement "Reproduced with permission of the Licensor through PLSclear."

5. Reversion of Rights

5.1 The rights licensed to Licensee under this Licence will terminate immediately and automatically upon the earliest of the following events to occur:

5.1.1 the Licence Fee not being received by Licensor in full by the payment date specified in the relevant invoice;

5.1.2 the Licensed Material not being used by Licensee within 18 months of the Licence Date;

5.1.3 expiry of the Licence Duration; or

5.1.4 the Maximum Circulation being reached.

6. Miscellaneous

6.1 By using the Licensed Material, Licensee will be deemed to have accepted all the terms and conditions contained in this Licence.

6.2 This Licence contains the entire understanding and agreement of the parties relating to its subject matter and supersedes in all respects any previous or other existing arrangements, agreements or understandings between the parties whether oral or written in relation to its subject matter.

6.3 Licensee may not assign this Licence or any of its rights or obligations hereunder to any third party without Licensor's prior written consent.

6.4 This Licence is governed by and shall be construed in accordance with the laws of England and Wales and the parties hereby irrevocably submit to the non-exclusive jurisdiction of the Courts of England and Wales as regards any claim, dispute or matter arising under or in relation to this Licence.

G.3. Garfield++ Programming Language

Copyright for Schindler, H., Garfield++ User Guide, 2020.

Gmail

saime sarikaya <saimesarikaya@gmail.com>

Use of Images from Garfield++ User Guide

Heinrich Schindler <Heinrich.Schindler@cern.ch> Mon, Feb 15, 2021 at 1:38 PM
To: "saimesarikaya@gmail.com" <saimesarikaya@gmail.com>

Yes, sure, no problem.

> Dear Sir/Madam,
>
> I am a PhD student from Boğaziçi University/Turkey. I am about to finish my studies with the title "Construction and Calibration of Gaseous Detectors at KAHVELab and CERN ATLAS Experiment" submitted to the Institute for Graduate Studies in Science and Engineering.
>
> I am using Garfield++ as a simulation program and need some figures to explain in theory part. I would like to use images/figures from Garfield++ User Guide in my thesis by properly citing.
>
> I kindly request your permission to use the content.
>
> Best regards,
> Saime Gürbüz
>

G.4. The Trigger Chambers of the ATLAS Muon Spectrometer

Copyright for Aloisio, A., et all, "The trigger chambers of the ATLAS muon spectrometer: production and tests", Nuclear Instruments and Methods in Physics Research Section A: Accelerators, Spectrometers, Detectors and Associated Equipment, Vol. 535, No. 1, pp. 265 – 271, 2004

ELSEVIER LICENSE
TERMS AND CONDITIONS

Feb 15, 2021

This Agreement between Mrs. Saime Gürbüz ("You") and Elsevier ("Elsevier") consists of your license details and the terms and conditions provided by Elsevier and Copyright Clearance Center.

License Number	5010191219584
License date	Feb 15, 2021
Licensed Content Publisher	Elsevier
Licensed Content Publication	Nuclear Instruments and Methods in Physics Research Section A: Accelerators, Spectrometers, Detectors and Associated Equipment
Licensed Content Title	The trigger chambers of the ATLAS muon spectrometer: production and tests
Licensed Content Author	A. Aloisio,M. Alviggi,M. Biglietti,V. Canale,M. Caprio,G. Carlino,F. Conventi,R. de Asmundis,M. Della Pietra,D. Della Volpe,P. Iengo,S. Patricelli,G. Sekhniaidze,V. Bocci,A. Di Mattia,L. Luminari,A. Nisati,F. Pastore,S. Falciano,E. Petrolo,R. Vari et al.
Licensed Content Date	Dec 11, 2004
Licensed Content Volume	535
Licensed Content Issue	1-2
Licensed Content Pages	7
Start Page	265
End Page	271

Type of Use	reuse in a thesis/dissertation
Portion	figures/tables/illustrations
Number of figures/tables/illustrations	1
Format	both print and electronic
Are you the author of this Elsevier article?	No
Will you be translating?	No
Title	Construction and Calibration of Gaseous Detectors at KAHVELab and CERN ATLAS Experiment
Institution name	Boğaziçi University
Expected presentation date	Feb 2021
Portions	Schematic view of ATLAS Muon Spectrometer
Requestor Location	Mrs. Saime Gürbüz Boğaziçi Üniversitesi Fizik Bölümü 34342 Kuzey Kampüs, KB Binası Kat 3-4 Istanbul, NRW 34342 Turkey Attn: bogazici university
Publisher Tax ID	GB 494 6272 12
Total	0.00 EUR
Terms and Conditions	

INTRODUCTION

1. The publisher for this copyrighted material is Elsevier. By clicking "accept" in connection with completing this licensing transaction, you agree that the following terms and conditions apply to this transaction (along with the Billing and Payment terms and conditions

established by Copyright Clearance Center, Inc. ("CCC"), at the time that you opened your Rightslink account and that are available at any time at http://myaccount.copyright.com).

GENERAL TERMS

2. Elsevier hereby grants you permission to reproduce the aforementioned material subject to the terms and conditions indicated.

3. Acknowledgement: If any part of the material to be used (for example, figures) has appeared in our publication with credit or acknowledgement to another source, permission must also be sought from that source. If such permission is not obtained then that material may not be included in your publication/copies. Suitable acknowledgement to the source must be made, either as a footnote or in a reference list at the end of your publication, as follows:

"Reprinted from Publication title, Vol /edition number, Author(s), Title of article / title of chapter, Pages No., Copyright (Year), with permission from Elsevier [OR APPLICABLE SOCIETY COPYRIGHT OWNER]." Also Lancet special credit - "Reprinted from The Lancet, Vol. number, Author(s), Title of article, Pages No., Copyright (Year), with permission from Elsevier."

4. Reproduction of this material is confined to the purpose and/or media for which permission is hereby given.

5. Altering/Modifying Material: Not Permitted. However figures and illustrations may be altered/adapted minimally to serve your work. Any other abbreviations, additions, deletions and/or any other alterations shall be made only with prior written authorization of Elsevier Ltd. (Please contact Elsevier's permissions helpdesk here). No modifications can be made to any Lancet figures/tables and they must be reproduced in full.

6. If the permission fee for the requested use of our material is waived in this instance, please be advised that your future requests for Elsevier materials may attract a fee.

7. Reservation of Rights: Publisher reserves all rights not specifically granted in the combination of (i) the license details provided by you and accepted in the course of this licensing transaction, (ii) these terms and conditions and (iii) CCC's Billing and Payment terms and conditions.

8. License Contingent Upon Payment: While you may exercise the rights licensed immediately upon issuance of the license at the end of the licensing process for the transaction, provided that you have disclosed complete and accurate details of your proposed use, no license is finally effective unless and until full payment is received from you (either by publisher or by CCC) as provided in CCC's Billing and Payment terms and conditions. If full payment is not received on a timely basis, then any license preliminarily granted shall be deemed automatically revoked and shall be void as if never granted. Further, in the event that you breach any of these terms and conditions or any of CCC's Billing and Payment terms and conditions, the license is automatically revoked and shall be void as if never granted. Use of materials as described in a revoked license, as well as any use of the materials beyond the scope of an unrevoked license, may constitute copyright infringement and publisher reserves the right to take any and all action to protect its copyright in the materials.

9. Warranties: Publisher makes no representations or warranties with respect to the licensed material.

10. Indemnity: You hereby indemnify and agree to hold harmless publisher and CCC, and their respective officers, directors, employees and agents, from and against any and all claims arising out of your use of the licensed material other than as specifically authorized pursuant to this license.

11. No Transfer of License: This license is personal to you and may not be sublicensed, assigned, or transferred by you to any other person without publisher's written permission.

12. No Amendment Except in Writing: This license may not be amended except in a writing signed by both parties (or, in the case of publisher, by CCC on publisher's behalf).

13. Objection to Contrary Terms: Publisher hereby objects to any terms contained in any purchase order, acknowledgment, check endorsement or other writing prepared by you, which terms are inconsistent with these terms and conditions or CCC's Billing and Payment terms and conditions. These terms and conditions, together with CCC's Billing and Payment terms and conditions (which are incorporated herein), comprise the entire agreement between you and publisher (and CCC) concerning this licensing transaction. In the event of any conflict between your obligations established by these terms and conditions and those established by CCC's Billing and Payment terms and conditions, these terms and conditions shall control.

14. Revocation: Elsevier or Copyright Clearance Center may deny the permissions described in this License at their sole discretion, for any reason or no reason, with a full refund payable to you. Notice of such denial will be made using the contact information provided by you. Failure to receive such notice will not alter or invalidate the denial. In no event will Elsevier or Copyright Clearance Center be responsible or liable for any costs, expenses or damage incurred by you as a result of a denial of your permission request, other than a refund of the amount(s) paid by you to Elsevier and/or Copyright Clearance Center for denied permissions.

LIMITED LICENSE

The following terms and conditions apply only to specific license types:

15. **Translation**: This permission is granted for non-exclusive world **English** rights only unless your license was granted for translation rights. If you licensed translation rights you may only translate this content into the languages you requested. A professional translator must perform all translations and reproduce the content word for word preserving the integrity of the article.

16. **Posting licensed content on any Website**: The following terms and conditions apply as follows: Licensing material from an Elsevier journal: All content posted to the web site must maintain the copyright information line on the bottom of each image; A hyper-text must be included to the Homepage of the journal from which you are licensing at http://www.sciencedirect.com/science/journal/xxxxx or the Elsevier homepage for books at http://www.elsevier.com; Central Storage: This license does not include permission for a scanned version of the material to be stored in a central repository such as that provided by Heron/XanEdu.

Licensing material from an Elsevier book: A hyper-text link must be included to the Elsevier homepage at http://www.elsevier.com . All content posted to the web site must maintain the copyright information line on the bottom of each image.

Posting licensed content on Electronic reserve: In addition to the above the following clauses are applicable: The web site must be password-protected and made available only to bona fide students registered on a relevant course. This permission is granted for 1 year only. You may obtain a new license for future website posting.

17. **For journal authors:** the following clauses are applicable in addition to the above:

Preprints:

A preprint is an author's own write-up of research results and analysis, it has not been peer-reviewed, nor has it had any other value added to it by a publisher (such as formatting, copyright, technical enhancement etc.).

Authors can share their preprints anywhere at any time. Preprints should not be added to or enhanced in any way in order to appear more like, or to substitute for, the final versions of articles however authors can update their preprints on arXiv or RePEc with their Accepted Author Manuscript (see below).

If accepted for publication, we encourage authors to link from the preprint to their formal publication via its DOI. Millions of researchers have access to the formal publications on ScienceDirect, and so links will help users to find, access, cite and use the best available version. Please note that Cell Press, The Lancet and some society-owned have different preprint policies. Information on these policies is available on the journal homepage.

Accepted Author Manuscripts: An accepted author manuscript is the manuscript of an article that has been accepted for publication and which typically includes author-incorporated changes suggested during submission, peer review and editor-author communications.

Authors can share their accepted author manuscript:

- immediately
  - via their non-commercial person homepage or blog
  - by updating a preprint in arXiv or RePEc with the accepted manuscript
  - via their research institute or institutional repository for internal institutional uses or as part of an invitation-only research collaboration work-group
  - directly by providing copies to their students or to research collaborators for their personal use
  - for private scholarly sharing as part of an invitation-only work group on commercial sites with which Elsevier has an agreement
- After the embargo period
  - via non-commercial hosting platforms such as their institutional repository
  - via commercial sites with which Elsevier has an agreement

In all cases accepted manuscripts should:

- link to the formal publication via its DOI
- bear a CC-BY-NC-ND license - this is easy to do
- if aggregated with other manuscripts, for example in a repository or other site, be shared in alignment with our hosting policy not be added to or enhanced in any way to appear more like, or to substitute for, the published journal article.

Published journal article (JPA): A published journal article (PJA) is the definitive final record of published research that appears or will appear in the journal and embodies all value-adding publishing activities including peer review co-ordination, copy-editing, formatting, (if relevant) pagination and online enrichment.

Policies for sharing publishing journal articles differ for subscription and gold open access articles:

Subscription Articles: If you are an author, please share a link to your article rather than the full-text. Millions of researchers have access to the formal publications on ScienceDirect, and so links will help your users to find, access, cite, and use the best available version.

Theses and dissertations which contain embedded PJAs as part of the formal submission can be posted publicly by the awarding institution with DOI links back to the formal publications on ScienceDirect.

If you are affiliated with a library that subscribes to ScienceDirect you have additional private sharing rights for others' research accessed under that agreement. This includes use for classroom teaching and internal training at the institution (including use in course packs and courseware programs), and inclusion of the article for grant funding purposes.

Gold Open Access Articles: May be shared according to the author-selected end-user license and should contain a CrossMark logo, the end user license, and a DOI link to the formal publication on ScienceDirect.

Please refer to Elsevier's posting policy for further information.

18. **For book authors** the following clauses are applicable in addition to the above: Authors are permitted to place a brief summary of their work online only. You are not allowed to download and post the published electronic version of your chapter, nor may you scan the printed edition to create an electronic version. **Posting to a repository:** Authors are permitted to post a summary of their chapter only in their institution's repository.

19. **Thesis/Dissertation**: If your license is for use in a thesis/dissertation your thesis may be submitted to your institution in either print or electronic form. Should your thesis be published commercially, please reapply for permission. These requirements include permission for the Library and Archives of Canada to supply single copies, on demand, of the complete thesis and include permission for Proquest/UMI to supply single copies, on demand, of the complete thesis. Should your thesis be published commercially, please reapply for permission. Theses and dissertations which contain embedded PJAs as part of the formal submission can be posted publicly by the awarding institution with DOI links back to the formal publications on ScienceDirect.

Elsevier Open Access Terms and Conditions

You can publish open access with Elsevier in hundreds of open access journals or in nearly 2000 established subscription journals that support open access publishing. Permitted third party re-use of these open access articles is defined by the author's choice of Creative Commons user license. See our open access license policy for more information.

Terms & Conditions applicable to all Open Access articles published with Elsevier:

Any reuse of the article must not represent the author as endorsing the adaptation of the article nor should the article be modified in such a way as to damage the author's honour or reputation. If any changes have been made, such changes must be clearly indicated.

The author(s) must be appropriately credited and we ask that you include the end user license and a DOI link to the formal publication on ScienceDirect.

If any part of the material to be used (for example, figures) has appeared in our publication with credit or acknowledgement to another source it is the responsibility of the user to ensure their reuse complies with the terms and conditions determined by the rights holder.

Additional Terms & Conditions applicable to each Creative Commons user license:

CC BY: The CC-BY license allows users to copy, to create extracts, abstracts and new works from the Article, to alter and revise the Article and to make commercial use of the Article (including reuse and/or resale of the Article by commercial entities), provided the user gives appropriate credit (with a link to the formal publication through the relevant DOI), provides a link to the license, indicates if changes were made and the licensor is not represented as endorsing the use made of the work. The full details of the license are available at http://creativecommons.org/licenses/by/4.0.

CC BY NC SA: The CC BY-NC-SA license allows users to copy, to create extracts, abstracts and new works from the Article, to alter and revise the Article, provided this is not done for commercial purposes, and that the user gives appropriate credit (with a link to the formal publication through the relevant DOI), provides a link to the license, indicates if changes were made and the licensor is not represented as endorsing the use made of the work. Further, any new works must be made available on the same conditions. The full details of the license are available at http://creativecommons.org/licenses/by-nc-sa/4.0.

CC BY NC ND: The CC BY-NC-ND license allows users to copy and distribute the Article, provided this is not done for commercial purposes and further does not permit distribution of the Article if it is changed or edited in any way, and provided the user gives appropriate credit (with a link to the formal publication through the relevant DOI), provides a link to the license, and that the licensor is not represented as endorsing the use made of the work. The full details of the license are available at http://creativecommons.org/licenses/by-nc-nd/4.0. Any commercial reuse of Open Access articles published with a CC BY NC SA or CC BY NC ND license requires permission from Elsevier and will be subject to a fee.

Commercial reuse includes:

- Associating advertising with the full text of the Article
- Charging fees for document delivery or access
- Article aggregation
- Systematic distribution via e-mail lists or share buttons

Posting or linking by commercial companies for use by customers of those companies.

20. **Other Conditions**:

v1.10

Questions? customercare@copyright.com or +1-855-239-3415 (toll free in the US) or +1-978-646-2777.

G.5. ATLAS Transition Radiation Tracker (TRT)

Copyright for Mindur, B., “ATLAS Transition Radiation Tracker (TRT): Straw tubes for tracking and particle identification at the Large Hadron Colider”, Nuclear Instruments and Methods in Physics Research Section A: Accelerators, Spectrometers, Detectors and Associated Equipment, Vol. 845, pp. 257 – 261, 2017, 92

ELSEVIER LICENSE
TERMS AND CONDITIONS

Feb 15, 2021

This Agreement between Mrs. Saime Gürbüz ("You") and Elsevier ("Elsevier") consists of your license details and the terms and conditions provided by Elsevier and Copyright Clearance Center.

License Number	5010191491957
License date	Feb 15, 2021
Licensed Content Publisher	Elsevier
Licensed Content Publication	Nuclear Instruments and Methods in Physics Research Section A: Accelerators, Spectrometers, Detectors and Associated Equipment
Licensed Content Title	ATLAS Transition Radiation Tracker (TRT): Straw tubes for tracking and particle identification at the Large Hadron Collider
Licensed Content Author	Bartosz Mindur
Licensed Content Date	Feb 11, 2017
Licensed Content Volume	845
Licensed Content Issue	n/a
Licensed Content Pages	5
Start Page	257
End Page	261
Type of Use	reuse in a thesis/dissertation

Portion	figures/tables/illustrations
Number of figures/tables/illustrations	2
Format	both print and electronic
Are you the author of this Elsevier article?	No
Will you be translating?	No
Title	Construction and Calibration of Gaseous Detectors at KAHVELab and CERN ATLAS Experiment
Institution name	Boğaziçi University
Expected presentation date	Feb 2021
Portions	Figure 2
Requestor Location	Mrs. Saime Gürbüz Boğaziçi Üniversitesi Fizik Bölümü 34342 Kuzey Kampüs, KB Binası Kat 3-4 Istanbul, NRW 34342 Turkey Attn: bogazici university
Publisher Tax ID	GB 494 6272 12
Total	0.00 USD

Terms and Conditions

INTRODUCTION

1. The publisher for this copyrighted material is Elsevier. By clicking "accept" in connection with completing this licensing transaction, you agree that the following terms and conditions apply to this transaction (along with the Billing and Payment terms and conditions established by Copyright Clearance Center, Inc. ("CCC"), at the time that you opened your Rightslink account and that are available at any time at http://myaccount.copyright.com).

GENERAL TERMS

2. Elsevier hereby grants you permission to reproduce the aforementioned material subject to the terms and conditions indicated.

3. Acknowledgement: If any part of the material to be used (for example, figures) has appeared in our publication with credit or acknowledgement to another source, permission must also be sought from that source. If such permission is not obtained then that material may not be included in your publication/copies. Suitable acknowledgement to the source must be made, either as a footnote or in a reference list at the end of your publication, as follows:

"Reprinted from Publication title, Vol /edition number, Author(s), Title of article / title of chapter, Pages No., Copyright (Year), with permission from Elsevier [OR APPLICABLE SOCIETY COPYRIGHT OWNER]." Also Lancet special credit - "Reprinted from The Lancet, Vol. number, Author(s), Title of article, Pages No., Copyright (Year), with permission from Elsevier."

4. Reproduction of this material is confined to the purpose and/or media for which permission is hereby given.

5. Altering/Modifying Material: Not Permitted. However figures and illustrations may be altered/adapted minimally to serve your work. Any other abbreviations, additions, deletions and/or any other alterations shall be made only with prior written authorization of Elsevier Ltd. (Please contact Elsevier's permissions helpdesk here). No modifications can be made to any Lancet figures/tables and they must be reproduced in full.

6. If the permission fee for the requested use of our material is waived in this instance, please be advised that your future requests for Elsevier materials may attract a fee.

7. Reservation of Rights: Publisher reserves all rights not specifically granted in the combination of (i) the license details provided by you and accepted in the course of this licensing transaction, (ii) these terms and conditions and (iii) CCC's Billing and Payment terms and conditions.

8. License Contingent Upon Payment: While you may exercise the rights licensed immediately upon issuance of the license at the end of the licensing process for the transaction, provided that you have disclosed complete and accurate details of your proposed use, no license is finally effective unless and until full payment is received from you (either by publisher or by CCC) as provided in CCC's Billing and Payment terms and conditions. If full payment is not received on a timely basis, then any license preliminarily granted shall be deemed automatically revoked and shall be void as if never granted. Further, in the event that you breach any of these terms and conditions or any of CCC's Billing and Payment terms and conditions, the license is automatically revoked and shall be void as if never granted. Use of materials as described in a revoked license, as well as any use of the materials beyond the scope of an unrevoked license, may constitute copyright infringement and publisher reserves the right to take any and all action to protect its copyright in the materials.

9. Warranties: Publisher makes no representations or warranties with respect to the licensed material.

10. Indemnity: You hereby indemnify and agree to hold harmless publisher and CCC, and their respective officers, directors, employees and agents, from and against any and all claims arising out of your use of the licensed material other than as specifically authorized pursuant to this license.

11. No Transfer of License: This license is personal to you and may not be sublicensed, assigned, or transferred by you to any other person without publisher's written permission.

12. No Amendment Except in Writing: This license may not be amended except in a writing signed by both parties (or, in the case of publisher, by CCC on publisher's behalf).

13. Objection to Contrary Terms: Publisher hereby objects to any terms contained in any purchase order, acknowledgment, check endorsement or other writing prepared by you, which terms are inconsistent with these terms and conditions or CCC's Billing and Payment terms and conditions. These terms and conditions, together with CCC's Billing and Payment terms and conditions (which are incorporated herein), comprise the entire agreement between you and publisher (and CCC) concerning this licensing transaction. In the event of any conflict between your obligations established by these terms and conditions and those established by CCC's Billing and Payment terms and conditions, these terms and conditions shall control.

14. Revocation: Elsevier or Copyright Clearance Center may deny the permissions described in this License at their sole discretion, for any reason or no reason, with a full refund payable to you. Notice of such denial will be made using the contact information provided by you. Failure to receive such notice will not alter or invalidate the denial. In no event will Elsevier or Copyright Clearance Center be responsible or liable for any costs, expenses or damage incurred by you as a result of a denial of your permission request, other than a refund of the amount(s) paid by you to Elsevier and/or Copyright Clearance Center for denied permissions.

LIMITED LICENSE

The following terms and conditions apply only to specific license types:

15. **Translation**: This permission is granted for non-exclusive world **English** rights only unless your license was granted for translation rights. If you licensed translation rights you may only translate this content into the languages you requested. A professional translator must perform all translations and reproduce the content word for word preserving the integrity of the article.

16. **Posting licensed content on any Website**: The following terms and conditions apply as follows: Licensing material from an Elsevier journal: All content posted to the web site must maintain the copyright information line on the bottom of each image; A hyper-text must be included to the Homepage of the journal from which you are licensing at http://www.sciencedirect.com/science/journal/xxxxx or the Elsevier homepage for books at http://www.elsevier.com; Central Storage: This license does not include permission for a scanned version of the material to be stored in a central repository such as that provided by Heron/XanEdu.

Licensing material from an Elsevier book: A hyper-text link must be included to the Elsevier homepage at http://www.elsevier.com . All content posted to the web site must maintain the copyright information line on the bottom of each image.

Posting licensed content on Electronic reserve: In addition to the above the following clauses are applicable: The web site must be password-protected and made available only to bona fide students registered on a relevant course. This permission is granted for 1 year only. You may obtain a new license for future website posting.

17. **For journal authors:** the following clauses are applicable in addition to the above:

Preprints:

A preprint is an author's own write-up of research results and analysis, it has not been peer-reviewed, nor has it had any other value added to it by a publisher (such as formatting, copyright, technical enhancement etc.).

Authors can share their preprints anywhere at any time. Preprints should not be added to or enhanced in any way in order to appear more like, or to substitute for, the final versions of articles however authors can update their preprints on arXiv or RePEc with their Accepted Author Manuscript (see below).

If accepted for publication, we encourage authors to link from the preprint to their formal publication via its DOI. Millions of researchers have access to the formal publications on ScienceDirect, and so links will help users to find, access, cite and use the best available version. Please note that Cell Press, The Lancet and some society-owned have different preprint policies. Information on these policies is available on the journal homepage.

Accepted Author Manuscripts: An accepted author manuscript is the manuscript of an article that has been accepted for publication and which typically includes author-incorporated changes suggested during submission, peer review and editor-author communications.

Authors can share their accepted author manuscript:

- immediately
  - via their non-commercial person homepage or blog
  - by updating a preprint in arXiv or RePEc with the accepted manuscript
  - via their research institute or institutional repository for internal institutional uses or as part of an invitation-only research collaboration work-group
  - directly by providing copies to their students or to research collaborators for their personal use
  - for private scholarly sharing as part of an invitation-only work group on commercial sites with which Elsevier has an agreement
- After the embargo period
  - via non-commercial hosting platforms such as their institutional repository
  - via commercial sites with which Elsevier has an agreement

In all cases accepted manuscripts should:

- link to the formal publication via its DOI
- bear a CC-BY-NC-ND license - this is easy to do
- if aggregated with other manuscripts, for example in a repository or other site, be shared in alignment with our hosting policy not be added to or enhanced in any way to appear more like, or to substitute for, the published journal article.

Published journal article (JPA): A published journal article (PJA) is the definitive final record of published research that appears or will appear in the journal and embodies all value-adding publishing activities including peer review co-ordination, copy-editing, formatting, (if relevant) pagination and online enrichment.

Policies for sharing publishing journal articles differ for subscription and gold open access articles:

Subscription Articles: If you are an author, please share a link to your article rather than the full-text. Millions of researchers have access to the formal publications on ScienceDirect, and so links will help your users to find, access, cite, and use the best available version.

Theses and dissertations which contain embedded PJAs as part of the formal submission can be posted publicly by the awarding institution with DOI links back to the formal publications on ScienceDirect.

If you are affiliated with a library that subscribes to ScienceDirect you have additional private sharing rights for others' research accessed under that agreement. This includes use for classroom teaching and internal training at the institution (including use in course packs and courseware programs), and inclusion of the article for grant funding purposes.

Gold Open Access Articles: May be shared according to the author-selected end-user license and should contain a CrossMark logo, the end user license, and a DOI link to the formal publication on ScienceDirect.

Please refer to Elsevier's posting policy for further information.

18. **For book authors** the following clauses are applicable in addition to the above: Authors are permitted to place a brief summary of their work online only. You are not allowed to download and post the published electronic version of your chapter, nor may you scan the printed edition to create an electronic version. **Posting to a repository:** Authors are permitted to post a summary of their chapter only in their institution's repository.

19. **Thesis/Dissertation**: If your license is for use in a thesis/dissertation your thesis may be submitted to your institution in either print or electronic form. Should your thesis be published commercially, please reapply for permission. These requirements include permission for the Library and Archives of Canada to supply single copies, on demand, of the complete thesis and include permission for Proquest/UMI to supply single copies, on demand, of the complete thesis. Should your thesis be published commercially, please reapply for permission. Theses and dissertations which contain embedded PJAs as part of the formal submission can be posted publicly by the awarding institution with DOI links back to the formal publications on ScienceDirect.

Elsevier Open Access Terms and Conditions

You can publish open access with Elsevier in hundreds of open access journals or in nearly 2000 established subscription journals that support open access publishing. Permitted third party re-use of these open access articles is defined by the author's choice of Creative Commons user license. See our open access license policy for more information.

Terms & Conditions applicable to all Open Access articles published with Elsevier:

Any reuse of the article must not represent the author as endorsing the adaptation of the article nor should the article be modified in such a way as to damage the author's honour or reputation. If any changes have been made, such changes must be clearly indicated.

The author(s) must be appropriately credited and we ask that you include the end user license and a DOI link to the formal publication on ScienceDirect.

If any part of the material to be used (for example, figures) has appeared in our publication with credit or acknowledgement to another source it is the responsibility of the user to ensure their reuse complies with the terms and conditions determined by the rights holder.

Additional Terms & Conditions applicable to each Creative Commons user license:

CC BY: The CC-BY license allows users to copy, to create extracts, abstracts and new works from the Article, to alter and revise the Article and to make commercial use of the Article (including reuse and/or resale of the Article by commercial entities), provided the user gives appropriate credit (with a link to the formal publication through the relevant DOI), provides a link to the license, indicates if changes were made and the licensor is not represented as endorsing the use made of the work. The full details of the license are available at http://creativecommons.org/licenses/by/4.0.

CC BY NC SA: The CC BY-NC-SA license allows users to copy, to create extracts, abstracts and new works from the Article, to alter and revise the Article, provided this is not done for commercial purposes, and that the user gives appropriate credit (with a link to the formal publication through the relevant DOI), provides a link to the license, indicates if changes were made and the licensor is not represented as endorsing the use made of the

work. Further, any new works must be made available on the same conditions. The full details of the license are available at http://creativecommons.org/licenses/by-nc-sa/4.0.

CC BY NC ND: The CC BY-NC-ND license allows users to copy and distribute the Article, provided this is not done for commercial purposes and further does not permit distribution of the Article if it is changed or edited in any way, and provided the user gives appropriate credit (with a link to the formal publication through the relevant DOI), provides a link to the license, and that the licensor is not represented as endorsing the use made of the work. The full details of the license are available at http://creativecommons.org/licenses/by-nc-nd/4.0. Any commercial reuse of Open Access articles published with a CC BY NC SA or CC BY NC ND license requires permission from Elsevier and will be subject to a fee.

Commercial reuse includes:

- Associating advertising with the full text of the Article
- Charging fees for document delivery or access
- Article aggregation
- Systematic distribution via e-mail lists or share buttons

Posting or linking by commercial companies for use by customers of those companies.

20. **Other Conditions**:

v1.10

Questions? customercare@copyright.com or +1-855-239-3415 (toll free in the US) or +1-978-646-2777.

G.6. TRT Software Twiki

Copyright for TRT Collaboration, TrtSoftwareDefinitions, 2017,

https://twiki.cern.ch/twiki/bin/viewauth/Atlas/TrtSoftwareDefinitions, accessed at April 2017.

Gmail saime sarikaya <saimesarikaya@gmail.com>

Use of figures in TRT software Twiki

Andrew Beddall <andrew.beddall@cern.ch> Tue, Feb 16, 2021 at 10:07 PM
To: "saimesarikaya@gmail.com" <saimesarikaya@gmail.com>

Hello Saime,

Sorry for the slow reply.
Yes, I think it's fine for you to use the images/figures as long as you give the correct citation.

good luck!
Andrew

From: saime sarikaya [saimesarikaya@gmail.com]
Sent: 15 February 2021 13:49
To: Andrew Beddall
Subject: Use of figures in TRT software Twiki

Dear Andrew,

I am about to finish my PhD and one section of the PhD is my QT studies. In the theory/literature part of this section, I used some plots from the TRT Software Twiki:
https://twiki.cern.ch/twiki/bin/viewauth/Atlas/TrtSoftwareDefinitions

The university asks me to provide a permission for the use of the figures from the people who have copyright or who are responsible.

Could you please confirm that I can use the images or figures from twiki?

Best Regards,
Saime Gürbüz

G.7. TRT Public Results

Copyright for TRT Collaboration, TRT RT dependency for the TRT barrel and end-caps, 2017,

https://twiki.cern.ch/twiki/bin/view/AtlasPublic/TRTPublicResults, accessed at April 2017.

2/18/2021 Gmail - Use of figures in TRT Public Plots

Gmail saime sarikaya <saimesarikaya@gmail.com>

Use of figures in TRT Public Plots

Luehring, Frederick C <luehring@indiana.edu> Mon, Feb 15, 2021 at 5:56 PM
To: saime sarikaya <saimesarikaya@gmail.com>
Cc: Andrew Beddall <andrew.beddall@cern.ch>

Hi Saime,

In rereading this email, I now think you were simply asking me to state if these TRT public plots can be used in your thesis without violating copywrite rules. The answer to that is yes you can and you are expected to use the public plots in documents like your QT write up and thesis. That's what the public figures are: they are public distribution and use. If need more than just a statement from me that it is allowed, let me know.

I cc Andrew.

Thanks!

Fred

--

Fred Luehring Indiana U. HEP mailto:luehring@indiana.edu +1 812 855 1025 IU

http://cern.ch/Fred.Luehring mailto:Fred.Luehring@cern.ch +41 22 767 1166 CERN

From: Frederick Luehring <luehring@indiana.edu>
Date: Monday, February 15, 2021 at 9:45 AM
To: saime sarikaya <saimesarikaya@gmail.com>
Subject: Re: Use of figures in TRT Public Plots

Hi Saime,

I believe these plots are covered by a creative commons license but let me check and get back to you as soon as I can.

Fred

https://mail.google.com/mail/u/0?ik=7cd16836f2&view=pt&search=all&permmsgid=msg-f%3A1691781102999703288&dsqt=1&simpl=msg-f%3A1691781102999… 1/2

--

Fred Luehring Indiana U. HEP mailto:luehring@indiana.edu +1 812 855 1025 IU

http://cern.ch/Fred.Luehring mailto:Fred.Luehring@cern.ch +41 22 767 1166 CERN

From: saime sarikaya <saimesarikaya@gmail.com>
Date: Monday, February 15, 2021 at 7:45 AM
To: Frederick Luehring <luehring@indiana.edu>
Subject: Use of figures in TRT Public Plots

Dear Fred,

I am about to finish my PhD and one section of the PhD is my QT studies. In the theory/literature part of this section, I used some plots from the TRT Public Twiki Page:

https://twiki.cern.ch/twiki/bin/view/AtlasPublic/TRTPublicResults

The university asks me to provide a permission for the use of the figures from the people who have copyright.

Could you please confirm that I can use the images or figures from twiki?

Best Regards,

Saime Gürbüz